New Approaches to Dynamic Equivalent of Active Distribution Network for Transient Analysis

Von der Fakultät für Elektrotechnik und Informationstechnik
der Rheinisch-Westfälischen Technischen Hochschule Aachen
zur Erlangung des akademischen Grades eines Doktors
der Ingenieurwissenschaften genehmigte Dissertation

vorgelegt von

Xiang WU, Master of Science
aus
Jiangxi, VR China

Berichter:
Univ.-Prof. Ph.D. Antonello Monti
Univ.-Prof. Dr.-Ing. Albert Moser

Tag der mündlichen Prüfung: 12. Juli 2016

Bibliographische Information der Deutschen Nationalbibliothek
Die Deutsche Nationalbibliothek verzeichnet diese Publikation in der Deutschen Nationalbibliografie; detaillierte bibliografische Daten sind im Internet über http://dnb-nb.de abrufbar.
D 82 (Diss. RWTH Aachen University, 2016)

Herausgeber:
Univ.-Prof. Dr.ir. Dr.h.c. Rik W. De Doncker
Direktor E.ON Energy Research Center

Institute for Automation of Complex Power Systems (ACS)
E.ON Energy Research Center
Mathieustraße 10
52074 Aachen

E.ON Energy Research Center | 40 Ausgabe der Serie
ACS | Automation of Complex Power Systems

Printed in Germany

ISBN: 978-3-942789-39-4
1. Auflage 2016

Verlag:
E.ON Energy Research Center, RWTH Aachen University
Mathieustraße 10
52074 Aachen
Internet: www.eonerc.rwth-aachen.de
E-Mail: post_erc@eonerc.rwth-aachen.de

Herstellung:
Druckservice Zillekens
Rainweg 19
52224 Stolberg
E-Mail:info@druckservice-zillekens.de

New Approaches to Dynmic Equivalent of Active Distribution Network for Transient Analysis

Xiang Wu

Abstract

With the increasing amount of distributed generators at the distribution level, the dynamic behavior of active distribution networks (ADNs) will have a more significant influence on the overall electrical system. To perform transient analysis of such a large and complex system, it is neither practical nor necessary to apply a fully detailed system model. A technique for obtaining highly accurate yet simple equivalents for ADNs is becoming increasingly important.

In this dissertation, three original equivalent models are proposed to cover the challenges posed by the size and complexity of power system transient analysis.

A fixed-structure dynamic equivalent model (FDEM) is proposed by integrating four individual equivalent models (IEMs), which are derived from approximation of the physical models of electrical equipment. The FDEM appears as a sixth-order state space, which is much less complex than the original systems. It can be easily integrated into different tools as a modular component with to-be-edited parameters. The derivation of the IEMs and FDEM presents the first original contribution.

An adaptive dynamic equivalent model (ADEM) is proposed by formulating an equivalence problem in terms of a Markov decision process problem, which is solved using a machine learning algorithm based on reinforcement learning. The structure of the ADEM is adaptive depending on measured data and it can be directly applied for on-line applications. It keeps not only a simple equivalent model form but also brings flexibility for an equivalent model structure. The transformation of the equivalence problem to Markov decision process problem and the learning skills of the ADEM are the second original contribution.

A random forest-based dynamic equivalent model (RF-DEM) is proposed by introducing randomized learning framework with feedbacks from outputs, which

trains the relationship between inputs and outputs using RF as the supervised learning algorithm. The RF-DEM takes advantage of easy implementation and does not require electrical modeling and approximation knowledge for deriving the equivalent models. The design of the RF-DEM forms the third original contribution.

Acknowledgments

Firstly and foremost, I would like to express my profound gratitude and appreciation to my doctor advisor Professor Antonello Monti, for his kind help and support. His technical guidance, as well as editorial advice are invaluable for my dissertation work. Furthermore, his patience with students and passion to academic work provide me a deep positive impact on my future research career. I would like to express my thanks to Professor Ferdinanda Ponci, for her valuable questions, comments, discussions and suggestions on improving my academic work. I would like also to thank my second supervisor Professor Albert Moser for his critical review and valuable suggestions. I am grateful to Professor Renato Negra and Professor Christoph Jungemann for serving as the chairs of my doctoral examination committee.

Many thanks to all of my present and former colleagues at the Institute for Automation of Complex Power Systems (ACS), for building such an inspiring and nice work environment. Sincere thanks to Sonja Kolen for her great suggestions and support to my work and life. I also appreciate the help from Hong Yang, Timo Isermann, Mohsen Ferdowsi, Fei Ni, Simon Pickartz, secretary office ladies and other colleagues. Very special thanks to Jun Cao for his continuous encouragement and invaluable discussions. His help channels me so much positive energy to my work and life.

I sincerely gratitude to my parents and my wife, for their understanding and support during any situation of my life.

Last but not least, I gratefully acknowledge the financial support from China Scholarship Council for my work at ACS, EON Energy Research Center, RWTH-Aachen University.

Dedication

To my parents and my wife.

Contents

List of Figures

List of Tables

List of Abbreviations

ADEM	adaptive dynamic equivalent model
ADN	active distribution network
ARX	autoregressive model with exogenous
CWTG	full rated converter wind turbine generator
DEM	dynamic equivalent model
DER	distributed energy resource
DFIG	double fed induction generator
DG	distributed generator
DSS	derived state space
EC	electronic converter
EPS	external part of the sub-system
FDEM	fixed-structure dynamic equivalent model
FSIG	fixed speed induction generator
IEM	individual equivalent model
IM	induction machine
M2M	moment matching method
MBA	model-based approach
MDA	modal-based approach
MDP	Markov decision process
MFA	model-free approach
MSE	mean square error
N4SID	subspace state space system identification model
OOB	out-of-bag
PCC	point of common coupling
PL	penetration level

PV	photovoltaic
RF	random forest
RF-DEM	random forest-based dynamic equivalent model
RNN	recurrent neural network
SG	synchronous generator
SM	synchronous machine
SPL	static power load
SS	state space
SVD	singular value decomposition
TL	transmission line

Chapter 1

Introduction

1.1 Background

In the past, the electrical system has been a highly centralized system in which large power plants are interconnected by transmission networks feeding the loads through distribution networks. Thanks to the breakthrough of power electronics technology and driven from the environment concerns, national and international regulation [1], a large amount of power electronics-based distributed energy resources (DERs) have been installed in distribution networks. The DERs are primarily renewable energy sources, such as wind and sun. Most of the DERs are installed in distribution network. This leads to the transition of distribution network from "passive" to "active", namely active distribution network.

For example, the situation in Germany is reported in Fig. 1.1. The renewable energy share of consumption was 16 % in 2010 while in 2014 was more than 26 %. Within 5 years, it increased more than 10 %. The DER share is even higher when it includes the other DERs, such as gas turbines and fuel cells. The trend in using DERs locally is supposed to continue, with a target share of 55 % to 60 % by 2035 [3].

Electrical systems are one of the most complex and largest systems in the world. To manage such a complex electrical system, an adequate model is essential. Traditionally, the power plants and transmission systems are modeled in details, while the distribution networks are represented by simple equivalent load models for dynamic analysis, since the conventional distribution networks are passive.

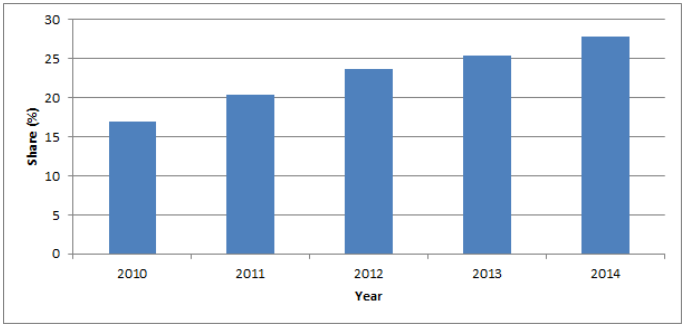

Figure 1.1: Renewable energy share of gross electricity consumption in Germany [1].

With the increasing penetration level of DERs in ADNs, the dynamic behaviors of ADNs will have significant influence on the transmission systems as well. Hence, a simple passive load model is no longer suitable to represent the complex dynamic behaviors of ADNs. On the one hand, the detailed architectures of the ADNs are not always available. On the other hand, online dynamic studies take too much time in a large-scale of electrical system even if the whole grid data is known. Consequently, there is growing interest in dynamic equivalent models for ADNs.

1.2 Transients of Electrical System

According to transient time frames, which covers μs, ms, s, minutes and hours, the transients can be roughly classified as short, middle, and long term transients. Short term transients include electromagnetic transients that are widely used for the determination of component ratings [4], which decay locally. Middle term transients cover electromechanical transients that are relevant to system stability and power system controls [5, 6, 7, 8]. Long term transients mainly involve system regulations. System level transients mainly relate to power system stability, which is mainly in medium-term.

Power system stability is the ability of maintaining the system stable after being subjected to a disturbance. It has been recognized as an important issue of power system operation since the 1920s. A shared global definition of power

system stability is reported in [9]:

> Power system stability is the ability of an electric power system, for a given initial operating condition, to regain a state of operating equilibrium after being subjected to a physical disturbance, with most system variables bounded so that practically the entire system remains intact. [9]

According to this definition, stability is classified as angle stability, voltage stability and frequency stability.

Angle stability

The rotor angle stability is well defined and refers to the ability of a power system to maintain synchronism after being subjected to a large disturbance or a small disturbance. The rotor angle stability under large disturbance is also called transient stability which is the main focus of this dissertation.

Voltage stability

Voltage stability is the ability of the power system to maintain its voltage profile within an acceptable range under full operation scenarios.

Frequency stability

Frequency stability is the ability of the power system to maintain a steady frequency under a significant unbalance between generation and load. The mismatch between generation and load becomes more frequent and significant since a large part of the distributed energy in active distribution networks is coming from wind and solar, which is random and characterized by fast dynamics. Sudden weather changes may cause frequency stability problem as studied in [10].

The impacts of ADNs on transient analysis have always been neglected in the past, while with increasing amounts of distributed energy resource installation, ADNs play an important role in analyzing transient response of disturbances in modern power systems. The work of this dissertation focuses on developing equivalent models for medium-term transient analysis, such as angle (transient) stability and voltage stability under large disturbances.

1.3 Motivations and Challenges

Stability is one of the key technical challenges affected by the increasing penetration of DERs in ADNs and it is also an essential requirement of power system design and operations [1, 11]. When the penetration level of DERs is low, the impacts of the DERs locally installed in distribution networks on the stability of whole system can be neglected. However, with the increasing number of DERs, the impacts are no longer restricted to local distribution networks, but also have significant reflection to the whole electrical system [11]. Before stability analysis or dynamic studies of the whole power system can be done, a good modeling of the whole system is a necessary precondition. However, it is not always feasible and necessary to get the fully detailed model of the whole system because of the complex topology, large size as well as the lack of information. Equivalent technique featuring high accuracy and less complexity is needed to simplify the representation of active distribution network.

1.3.1 Equivalent Motivation and Challenges 1: Provide Reliable Knowledge for Active Distribution Networks

In future smart grid infrastructure, measurement devices are expected to be increasingly installed at the boundary buses and substations. The measured data at the boundary buses between subsystems, as well as substations will be available and can be suitably exploited. For this reason, extracting dynamic behavior information from measured data becomes more interesting. Building an equivalent model for the ADNs by means of measured data is a possible attempt. To obtain dynamic equivalent for stability analysis applications, a strategy could be to record data during disturbances. Then transfer the stored data to management center for building the equivalent model via different communication channels.

In practical applications, the architecture of ADNs is not always visible to distribution system operators and transmission system operators, but there is a need to get the knowledge of the ADNs for transient analysis. To get knowledge of the ADNs, building an equivalent model via measured variables becomes feasible and necessary.

1.3.2 Equivalent Motivation and Challenges 2: Reduce Computation Cost for Fast and Online Stability Analysis

Assuming that power grid data is known and a model of the whole grid is available, it may still be a challenge to perform online stability assessment and real-time operations when the scale of the power system is extremely large [12, 13]. Usually, except communication and control time, only few minutes are allowed for calculation during real-time operations, and the influence of the ADNs with large amount of DERs cannot be neglected. This leads to a heavy computational burden for the computing hardware. Furthermore, the demand of operational flexibility [14] and the trend towards decentralized energy control requires much faster actions from distribution system operators and transmission system operators since the energy generation from RES is volatile and the inertia of the whole grid becomes smaller because of installation of distributed generators (DGs). That is, the whole grid may require stability assessments more often and have more strict time limitation for local real-time control and protection. Under these conditions, an adequate dynamic equivalent model is of urgent need: the equivalent model should accurately represent the dynamic behavior of the ADNs at the boundary buses or substations, but still have limited computation cost. Dynamic equivalent models are of great benefit in providing reliable knowledge of the to-be equivalent power systems and reducing computational cost for simulating large scale power systems.

1.3.3 History of Equivalent Technique in Power System

The main idea behind equivalent model is splitting an original system into two parts. The first part is internal part of the subsystem and the second part is external part of the subsystem. The internal part of the subsystem is the significant area of the original system keeping all the details. The external part of the sub-system (EPS) is the rest of the original system, which is substituted with an equivalent model. Equivalent technique is the method to obtain equivalent model of EPS. The internal part of the subsystem together with the equivalent model composes the equivalent system. Both, original and equivalent system, should behave similar.

The first equivalent method is introduced for power flow calculation in [15]. The general idea is grouping load buses but leaving out generator buses while

assuming that voltage at the boundary buses and the load impedance are constant. An extension for dynamic purpose by linearizing constant power loads around operation point is presented in [16]. Another static equivalent method, namely Radial, Equivalent and Independent, is initially proposed in [17]. It is a loss-less equivalent representation by injecting the same quantity power to internal part of the subsystem. The method is also used for power flow calculation. Later on, coherency equivalent method was proposed in [18, 19, 20]. It involves the identification of coherency generator groups by means of rotor angle swings and the aggregation of identified generators with similar swing features. This method is often used in transmission systems where the large synchronous generators play the major role. To reduce the size of a large linear network but with wide bandwidth response, a Frequency Dependent Network Equivalent is proposed in [21], later a new method of calculating this equivalent is introduced in [22]. Note that Frequency Dependent Network Equivalent is applied for the equivalent model of fast and high frequency transients, such as electromagnetic transients, which often decay soon locally in few milliseconds and will not transfer to the whole system. Hence, the fast dynamics are always neglected in system level transient analysis. Taking advantage of the strengths of each method, several combination methods have also been developed, such as coherency and Radial, Equivalent and Independent in [23], coherency and Frequency Dependent Network Equivalent in [24].

However, there are no coherency features existing in ADNs and the static equivalent is not suitable for dynamic studies. To handle these challenges existing in ADNs, an artificial neutral network-based equivalent method is proposed in [25, 26, 27]. It is a supervised learning method to find the relationships between the inputs and outputs with time serial data. The identification-based equivalent methods: state space (SS), autoregressive model with exogenous (ARX) and subspace state space system identification model (N4SID) can be found in [28, 29, 30]. Linear model reduction methods: singular value decomposition (SVD) and moment matching method (M2M) are applied for dynamic ADNs equivalent in [31, 2]. Note that a linearization of EPS is a precondition. In the recent years, pre-derived equivalent models with unknown parameters: derived state space (DSS) have been introduced in [32, 33, 34]. The further details of equivalent technique for ADNs are described in Chapter 2.

1.4 Contributions

In this dissertation, three new equivalent models are proposed. The three models take advantage of simplicity and practicability by means of measurement data. They only require measurement data at boundary points and they do not need to know the specific topology and parameters of the ADNs.

1.4.1 Contribution 1: Fixed-Structure Dynamic Equivalent Model

A FDEM is proposed in Chapter 3. The FDEM is achieved by integrating four IEMs, which are obtained from approximation of the models of induction machines, synchronous machines, electronic converters and static power loads. In this FDEM model, the input is the voltage value at substations of ADNs, which is feasible and easy to get. The outputs are active and reactive power at secondary side of the substations.

The FDEM is suitable for general applications and in a form of a six-order state space, which is much less complex than the original systems. This model can be easily integrated into different tools as a modular component with to-be-edited parameters.

1.4.2 Contribution 2: Adaptive Dynamic Equivalent Model

An ADEM is presented in Chapter 4, which has a flexible equivalent model structure that is adaptive to the measured data. The ADEM is achieved by formulating an equivalent problem in a form of Markov decision process (MDP) problem. When the dynamics of ADNs are rich and large during disturbance, a higher order equivalent model is identified. Otherwise, if the dynamics of ADNs are poor and small during disturbance, a lower order equivalent model is identified.

This model not only keeps a simple equivalent model form, but also brings flexibility to an equivalent model structure.

1.4.3 Contribution 3: Random Forest-Based Dynamic Equivalent Model

A RF-DEM has been proposed in Chapter 5, which does not require electrical modeling and approximation knowledge for deriving equivalent models. The

random forest (RF) is one kind of supervised learning algorithm, which takes advantage of non-over-fitting. The RF-DEM approach can provide the variable importance that indicates which inputs are the most relevant variables for the training. Furthermore, knowledge of the electrical system is not necessary, which means an engineer without electrical engineering background may also obtain a good equivalent model.

1.5 Dissertation Outline

The organization of this dissertation is shown in Fig. 1.2. The main contributions are presented in Chapters 3, 4 and 5, in which FDEM, ADEM and RF-DEM models are proposed, respectively. More details about the chapters are described as following:

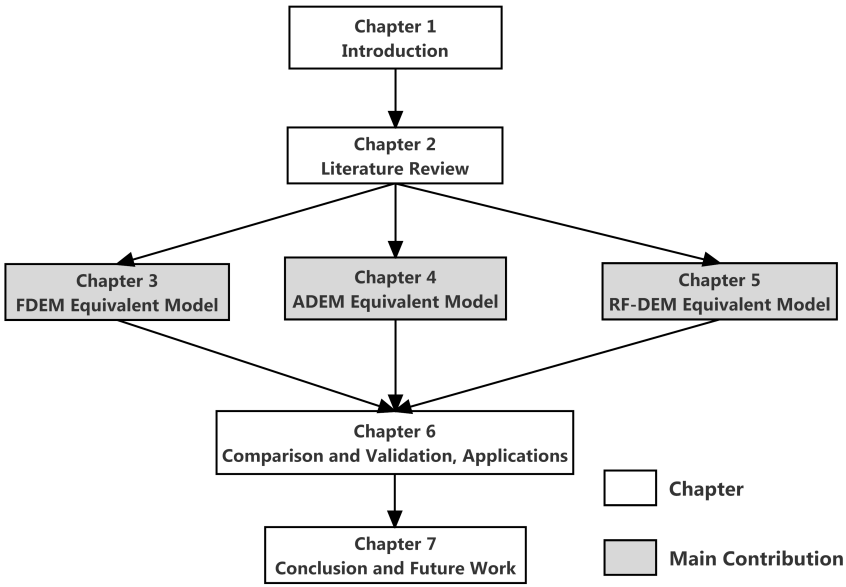

Figure 1.2: The organization of dissertation.

Chapter 2: Equivalent Approaches for Active Distribution Networks After clarifying the general idea of equivalent model, this chapter gives an overview on the development of dynamic equivalent approaches used to derive dynamic equivalent models for ADNs. Their strengths and weaknesses are discussed.

Chapter 3: Fixed-Structure Dynamic Equivalent Approach The chapter proposes a new fixed-structure dynamic equivalent model that is derived from physical models. The procedure of derivation of individual equivalent models as well as the specific optimization algorithm are presented. To prove the applicability of the proposed equivalent model, a set of scenarios are defined. The estimation and validation results of the equivalent model are also provided.

Chapter 4: Adaptive Dynamic Equivalent Approach An adaptive model for dynamic equivalent of ADNs is introduced in this chapter. It is an attempt to apply adaptive idea for dynamic equivalent models by means of reinforcement learning. In the beginning, the connection and fitness between equivalent model and adaptive idea are presented from the theoretical point of view. Then further related adaptive knowledge, MDP, is introduced. Finally, validation results are given.

Chapter 5: Random Forest-Based Dynamic Equivalent Approach This chapter presents a model-free approach for dynamic equivalent of ADNs based on random forest. The drawback of recurrent neural network-based equivalent model is discussed and the strength of random forest-based dynamic equivalent model is pointed out. Then the theoretical background of random forest and the design of random forest-based dynamic equivalent model are addressed. The parameters of RF-DEM is optimized by analyzing the number of trees and subsets of each node, as well as the variable importance and combination of inputs. In the end, the model validation results are presented.

Chapter 6: Comparison and Validations, Applications In this chapter, all the proposed models are validated and compared by setting up different scenarios. Their performances are compared. Their advantage and disadvantage are further discussed and analyzed.

Chapter 7: Conclusion and Future Work The last chapter summarizes the research work along with the conclusions. The following part presents the suggestions for future research and potential applications.

Chapter 2

Equivalent Approaches for Active Distribution Network

2.1 Introduction

The transition of distribution networks from "passive" to "active" and the demand of operational flexibility result in strong motivations for dynamic equivalent technique [14]. Hence, the overview in this chapter focuses on the details of dynamic equivalent technique for ADNs. Generally speaking, all of the equivalent techniques divide the original system into two parts: the internal and external subsystem. The whole architecture is as shown in Fig. 2.1 and can be described as follows:

1. The internal subsystem is the interesting and significant area of the original system, which keeps all of the details.

2. The external subsystem is the rest of the original system which is substituted by an equivalent model. It is of low interest and details are considered not significant.

3. Both sub-systems are connected by boundary buses or substations.

From equivalent model and method point of view, the equivalent technique of ADNs can be categorized in three approaches: modal-based approach (MDA), model-free approach (MFA), and model-based approach (MBA). Each approach has several corresponding methods. MDA achieves the equivalent model by

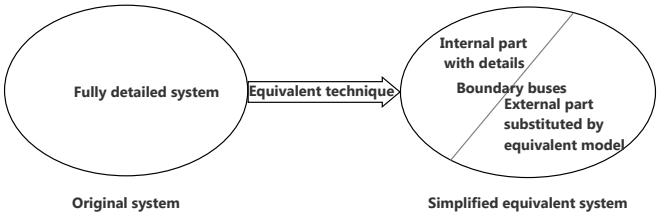

Figure 2.1: The original and equivalent system.

extracting the dominant modes of a linear system with linear model reduction methods which have a strictly mathematical basis. MFA obtains the equivalent model by learning the relationship between inputs and outputs with machine learning methods. MBA represents a pre-defined equivalent model with unknown parameters, which are determined by optimization methods.

2.2 Modal-Based Approach

2.2.1 Introduction

Modal-based approach is based on linearizing the external system at an operation point in the form of state space, and then reducing the linearized EPS with model reduction methods by projection. With the linearized model, it only can apply small disturbances for the transient analysis. That is to say, the disturbances should be small enough and the impedance from the disturbance location to the boundary buses should be large enough [31, 35, 36], i.e, the EPS has linear and time invariant features.

2.2.2 Approach Description

The core of the MDA is to find the projection matrices for model reduction. The linearized full order of the EPS can be described in Equation 2.1 [31, 35, 37]:

$$S : \begin{cases} \dot{X} = AX + BU \\ Y = CX + DU \\ X(0) = X_0 \end{cases} \tag{2.1}$$

where S, in a state space form, represents the linearized EPS. Further, X, U and Y are the vectors of state variables, inputs, and outputs for the system S, respectively. A, B, C, D are the coefficient matrices of the state variables, inputs, and outputs. $X(0)$ is the initial state variable of X. X_0 represents the specific initial state values.

After getting the linearized model of the external system, a theoretical model reduction has to be applied to extract the main modes of the external systems for the final dynamic equivalent model. The general idea of model reduction is to obtain a much lower order linear and time invariant system by projection. The main features of the reduced system $\widetilde{S}$ should be close to the original system S. Two categories of model reduction methods are summarized in [37], namely SVD and M2M reduction. They are applied for dynamic equivalent models in [2, 31].

After applying the model reduction methods, a reduced system model is obtained in Equation 2.2 [31, 35, 37]:

$$\widetilde{S}: \begin{cases} \dot{\widetilde{X}} = \widetilde{A}\widetilde{X} + \widetilde{B}\widetilde{U} \\ \dot{\widetilde{Y}} = \widetilde{C}\widetilde{X} + \widetilde{D}\widetilde{U} \\ \widetilde{X}(0) = \widetilde{X_0} \end{cases} \tag{2.2}$$

where $\widetilde{S}$ represents the reduced system, usually the order of $\widetilde{S}$ is much lower than the original S. $\widetilde{U}$ is the input vector of $\widetilde{S}$, usually is the same as U. $\widetilde{Y}$ is the output vector of $\widetilde{S}$, which should be close to Y. $\widetilde{X}$ is the reduced state variable vector. $\widetilde{A}$, $\widetilde{B}$, $\widetilde{C}$, $\widetilde{D}$ are the coefficient matrices of state variables, inputs, and outputs for $\widetilde{S}$. $\widetilde{X_0}$ is the initial state variable of $\widetilde{X}$.

Singular Value Decomposition Reduction Methods

The SVD methods are based on the modal truncation, which makes $\|S - \widetilde{S}\|$ as small as possible [38]. It keeps the significant Hankel singular values of the linear and time invariant system, but truncates the rest as error [37, 38]. Generally, the original system S is controllable and observable, then the Laypunov equations are represented in Equation 2.3 and 2.4 [37, 38]:

$$AP + PA^T + BB^T = 0 \tag{2.3}$$

$$A^TQ + QA + C^TC = 0 \tag{2.4}$$

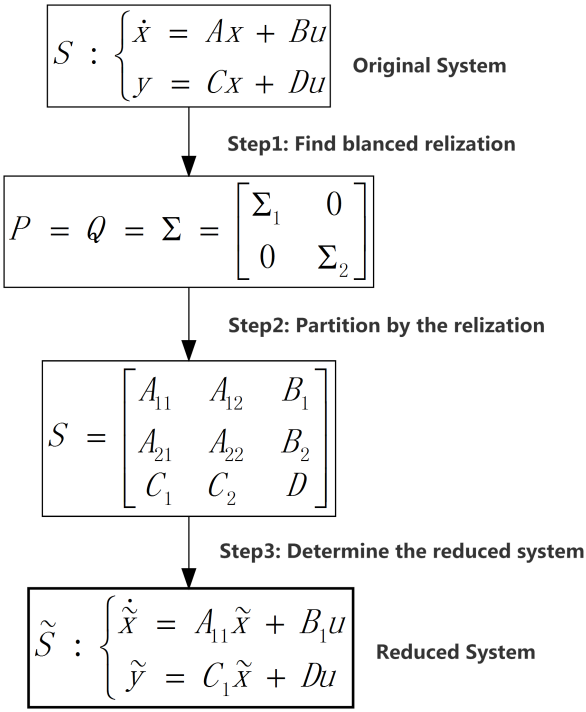

Figure 2.2: The procedure of SVD reduction [31, 39].

The controllability and observability Gramians are the solution matrices P and Q in 2.3 and 2.4, respectively. The procedure of SVD reduction is shown in Fig. 2.2 and divided in the following three steps:

Step 1: Find a balanced realization

The S is in balanced coordinate form when both Gramians are equal and represented as diagonal matrix form with Hankel singular values in Equation 2.5:

$$P = Q = \wedge = diag(\sigma_1, ..., \sigma_n) \tag{2.5}$$

Here it is easy to find a balanced realization for S in Equation 2.6:

$$\sum = \begin{bmatrix} \sum_1 & 0 \\ 0 & \sum_2 \end{bmatrix} \tag{2.6}$$

where $\sum$ is a diagonal matrix with the Hankel singular values on its diagonal. $\sum_1$ and $\sum_2$ are the sub-matrices of $\sum$.

Step 2: Partition A, B, C, D by means of $\sum$

$\sum_1$ contains the Hankel singular values which are preserved, $\sum_2$ includes the small Hankel singular values that are truncated. There are several truncation methods, further details can be found in [37, 38].

Step 3: Determine the reduced $\widetilde{S}$

According to the criterion of required error tolerance, determine the suitable reduced order quantity by comparing the given error tolerance and the native bounded error. The reduced system is obtained when the bounded error has matched the error criterion. If not, then repeat the procedure with a higher order truncation. This step can be integrated into Step 1 after calculating the Hankel singular values.

The calculation processes of the SVD methods are similar, they only differ from realization and truncation approaches. SVD may be very time consuming when a system is too large, since the method requires the calculation of the full Hankel singular values for the original system. However, the reduction error is bounded and the stability of the reduced system is preserved by means of these methods.

Moment Matching Methods

Represent the linear dynamic system S in a transfer function form as in Equation 2.7 [37]:

$$G(s) = C(sI - A)^{-1}B + D \tag{2.7}$$

According to Equation 2.8, the transfer function $G(s)$ can be further expended in Laurent series around the given point s_0 [37].

$$G(s_0 + \sigma) = \eta_0 + \eta_1\sigma + \eta_2\sigma^2 + ... + \eta_i\sigma_i + ... \tag{2.8}$$

The η_i is called the i moment of $s_0 + \sigma$ at s_0. The moment vector is given by $\eta = (\eta_0,..., \eta_i, ...)$. There is a relationship, $\eta_0 = D, \eta_i = CA^{i-1}B, i = 1, 2, 3, ...$, which determines the moments. The goal of moment matching methods is to seek a lower order approximation system $\widetilde{S}$ that has the same moment vectors within an infinite amount of k moments. The corresponding moment form is given in Equation 2.9, where the moment vector is matched per Equation 2.10. The general calculation process is as shown in Fig. 2.3 and divided into three steps.

$$\widetilde{G}(s_0 + \sigma) = \widetilde{\eta}_0 + \widetilde{\eta}_1\sigma + \widetilde{\eta}_2\sigma^2 + ... + \widetilde{\eta}_i\sigma_i + ... \tag{2.9}$$

$$\eta_i = \widetilde{\eta}_i, i = 0, 1, 2, 3, ..., k \tag{2.10}$$

Step1: Select parameters

Select the aimed order k and the initial state s_0. Then perform Laurent series expansion.

Step2: Calculate projection matrices

Use "Lanczos" or "Arnoldi" algorithm [37, 38] to calculate the projection matrices. The matching moments of the "Lanczos" is double size of the "Arnoldi". Further explanation can be found in [37, 38].

Step3: Determine the reduced system

Compare the given error tolerance and the error between the original system and the reduced system. The reduced order is acceptable when the actual error is smaller than the given tolerance, otherwise, select a higher order for Step 1 and repeat the rest steps until it fits the error tolerance.

The moment matching method, also known as Krylov methods, takes advantage of the efficiency of numerical calculation, but brings drawbacks in the possibility of un-bounded error and the fact that the stability may not be preserved.

In the past, the SVD-based Hankel norm approximation has been applied in [31]. It reduces the linearized original system from order 529 to order 26 with reasonable results by means of Hankel norm truncation. The M2M-based Arnoldi-Krylov method has also been used to reduce the same system in [2].

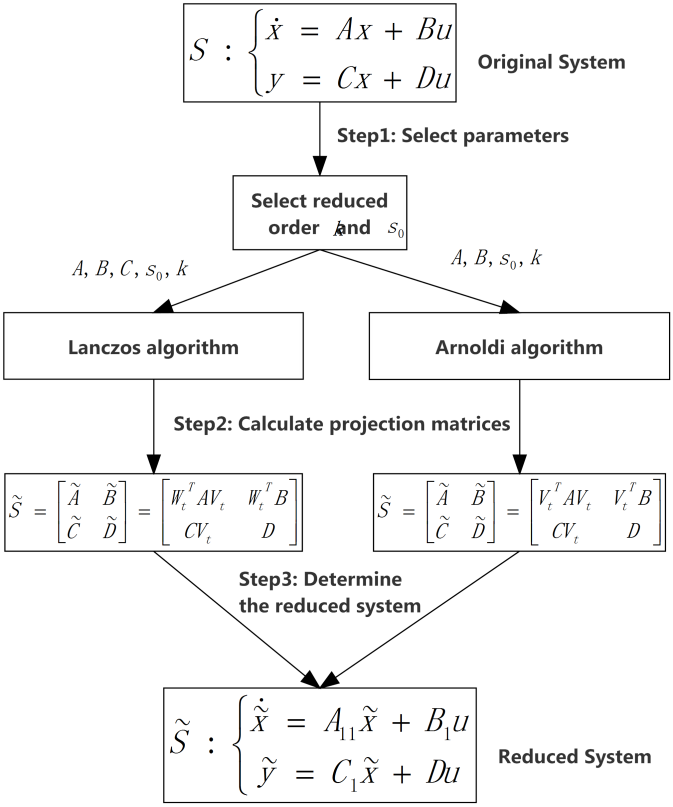

Figure 2.3: The general procedure of moment matching method, adopt from [2].

It brings the original system as low as 27^{th} order. Further studies of both linear model reductions can be found in [36]. From the principle point of view, both proposed methods may not be the most efficient methods to reduce model order. That is because the SVD-based reduction requires much computation time, while M2M-based reduction lacks global error bounds. A SVD-Krylov method could be better combining the theoretical advantages of the SVD and the efficient numerical computation advantage of M2M. Specifically, it takes a two-sided projection, one side reflects the SVD algorithm, the other reflects M2M algorithm. More details can be found in [38, 40].

2.2.3 Advantages and Disadvantages

The MDA methods have clear and strict mathematical deduction and calculation, furthermore, experiment data is not necessary. But the methods need to know the full details of the system and they can only reduce the order of a linear and time invariant systems. Their further advantages and disadvantages are listed as in the following:

Advantages of Modal-Based Approach

- MDA has strict mathematical basis and can extract a reliable equivalent model for the external systems around a given operation point.
- The performance of MDA is independent of the disturbances that happened in original system, it only requires the linearized model of the EPS, while the measured data at the boundary buses is not necessary.
- MDA has good ability to control the order of equivalent model by setting the error tolerance in SVD or predefining the M2M.

Disadvantages of Modal-Based Approach

- The major disadvantage of MDA is its requirement of a fully detailed EPS, including the specific component parameters, the system topologies and operation point. In practical applications, the availability of every detail is quite difficult to achieve in complex and large-scale systems.

- It is also a big challenge to derive a proper linearized model even if the full details of EPS are known. In modern power systems, the high non-linearity of power electronics based component is difficult to linearize.
- MDA works only around an operation point, which is an inherent limitation, since the power systems are always operating in varying conditions.
- MDA works only in linear situations. When the linear approaches cannot properly capture the complex dynamics of the power system, especially during large disturbances, it could face difficulties in reducing the orders of the non-linear models. The derived dynamic equivalent may not be able to retain the non-linear characteristics of the system.
- Concerning the specific reduction methods, it is difficult to calculate the singular values for very large size of linear systems in SVD. Further it may bring instability in the reduced system since the stability is not preserved in the M2M method.

2.3 Model-Free Approach

2.3.1 Introduction

The model-free approach uses supervised machine learning algorithms to train the relationships between inputs and outputs and then predict the responses of new inputs by means of previously trained relationship. It is not necessary to know the detailed topology and parameters of the external system. Only the measured data at the boundary buses are required as inputs and outputs. The input and output variables are defined accordingly in specific applications. The often-used training algorithm for dynamic equivalent model (DEM) are recurrent neural networks (RNNs) [25, 27].

2.3.2 Approach Description

The RNN composes three layers: input layer, hidden layer, and output layer, as shown in Fig. 2.4. Each layer consists of one or more nodes, represented by the small circles. The nodes, called neurons, are interconnected by forward lines and backward lines [25, 27]. Note that the number of hidden layers can be more

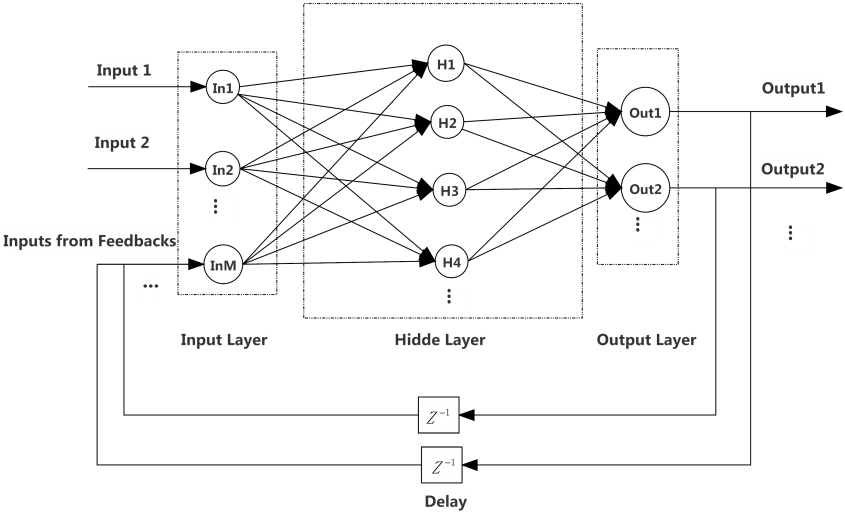

Figure 2.4: Recurrent neural network architecture [41, 42].

than one and the backward lines can be fed into the nodes in preceding layers and also the same nodes. The backward lines enable the dynamic memory of the RNNs. The lines between the nodes indicate the information flow from a node to the next, the information quantity is considered as activation values. The node structure is shown as in Fig. 2.5, it includes k inputs, IP, and its weight coefficient W_i, a bias, b, an activation function Fun, and an output OP. For every node, each of the input IP_i is multiplied by a previously established weight, W_i and are all summed together, resulting in the internal value of an operation. This value is biased by a previously established threshold value b, represents as $x = b + \sum_{i=1}^{k} IP_i W_i$. Then x is sent through an activation function Fun. Finally the result of the neuron is obtained by $OP = Fun(x)$. The activation function is usually an nonlinear function [41]. The final output OP is an input to the next layer or it is a response $Output$ of the neural network when it is the last layer. The process of MFA is described as below:

Step1: Design the RNN-based equivalent model

Define the measured data as inputs and outputs accordingly, then set up the layer and node numbers of the RNN, as well as the backward lines.

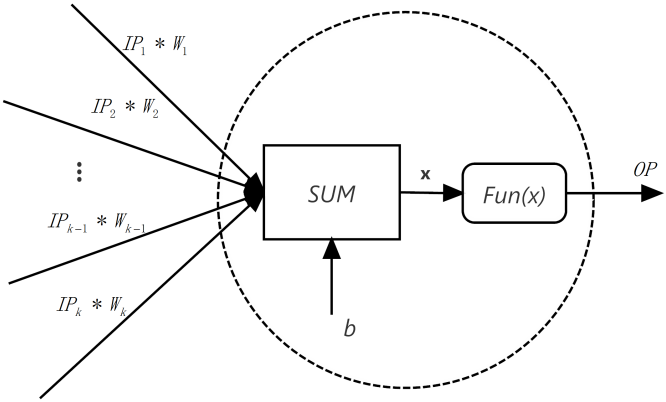

Figure 2.5: Node architecture.

Step2: Training the RNN-based equivalent model

Propagate the input and output data to the equivalent model, then the activation values, weight coefficients are adjusted to minimize the difference between the predicted outputs and the measured outputs. The errors become less in the next iteration with the same inputs, the training process finish when the error is as small as the defined criterion.

Step3: Determine the configuration of RNN

Test the trained RNN models with new sets of data, determine the best configuration of the RNN as the final equivalent model. The RNN is a complete black-box for the designer of the equivalent model, it is difficult to determine the final network of the RNN in the beginning state. An empirical recommendation may be useful [43].

The architectures of RNNs equivalent models are similar in literature [25, 26, 27]. The only difference is the configuration of layer and node and also the definition of inputs and outputs. The definition can be varied for different purposes in power systems. In [25], the author presents a two-step method, firstly, using a "Bottleneck" artificial neural network to extract a reduced state of the external system from inputs. Secondly, using RNN, the dynamic behavior of the external systems is captured and then the new states are used to calculate

the outputs. The inputs are the time series current and voltage measured at the boundary bus, the outputs are the same as inputs but one time step forward. In [26], the author proposes a similar approach except changes inputs and outputs to active and reactive power. This method tries to integrate a differential algebraic equation into the bottleneck and recurrent artificial neural network as equivalent model. It makes the choice of the suitable order of the reduced state more complex and also needs more calculation effort because of the Bottleneck artificial neural network. A further development is represented in [27] where the RNN dynamic equivalent model is comprising two boundary buses. The voltages and feedback currents are defined as inputs, the current deviations at the present time interval are defined as outputs.

2.3.3 Advantages and Disadvantages

The MFA methods are easy to design and implement. They only need experiment data and do not require any detail of the system. But they may not have identical model structure between different trainings, which may increase difficulty for compatibility between different software. Their more specific features are presented as:

Advantages of Model-Free Approach

- It requires only the time series data at the boundary buses by measurement or simulation, the details of internal part of the sub-system and EPS are not necessary.

- It is flexible and easy to design a new dynamic equivalent model for different applications. For example, in some applications, may need voltage and current as inputs, active and reactive power as outputs. In other applications, may need active and reactive power as inputs, voltage and current as outputs. Under such situations, just configure the input and output ports as requested, nothing more has to be changed.

- By applying MFA, the process of training equivalent model is independent from the knowledge of the electrical system. Therefore, developing a good dynamic equivalent model is possible by the other non-electrical engineers.

- Many model-free toolboxes can be downloaded on the Internet. The boxes reduce the cost and save work time on the implementation.

Disadvantages of Model-Free Approach

- The model-free equivalents do not have structural identity between different trainings. The inside of RNNs are black-box to the users. The layers and nodes of RNN may change from different sets of training data.
- There is no good description of the relationship between the RNN parameters and responses, which are hidden in applications.
- RNN-based equivalents may risk in over-fitting problem, which commonly happens in RNN learning.
- There is no general rules to setup a RNN for a model-free equivalent model. Usually the configuration of RNN, such as layers, nodes, are coming from experience, trial and error.
- The RNN may be difficult to integrate directly into the existing power system software, since it is difficult to find a general way to convert the black box RNN.

2.4 Model-Based Approach

2.4.1 Introduction

Model-based approach determines unknown parameters of a pre-defined fixed structure DEM with measured electrical data and suitable optimization algorithms. It does not need any details about EPS, but requires strong electrical system background or experimental experience for deriving the pre-defined equivalent model.

2.4.2 Approach Description

The process of MBA is shown in Fig. 2.6, which can be generalized as three steps: pre-define the equivalent model, optimize the unknown parameters, determine the final equivalent model.

Step1: Pre-define the equivalent model

Firstly, learn from electrical knowledge or from empirical experience, derive a FDEM with unknown parameters and define the measured data as inputs and outputs. The pre-defined FDEM can be represented with state space equations. The form and the order of the FDEM depend on the understanding of the whole power system features. For example, the FDEM is better in high order when the data is measured during large disturbances. It is better in lower order when small disturbances are the focus of the analysis.

Step2: Optimize the unknown parameters

Secondly, there are many kinds of optimization algorithms that can be applied for equivalent solutions. Different optimization algorithms have different efficiency and accuracy level, hence, finding a proper optimization algorithm to determine the unknown parameters is important.

Step3: Determine the final equivalent model

Thirdly, according to the specific criterion and requirements of accuracy, identify a high accuracy and simple equivalent model for validation.

There are also two types of model-based equivalent model. One type is directly deriving from identification technique, for simplification, named as artificial model-based model, such as ARX, SS, N4SID presented in [28, 29, 30]. Another type is deriving from physical modeling of power components, named physic model-based model, such as the models proposed in [32, 34].

A linear ARX and SS model are used in [29]. The ARX model relates a number of the past outputs and inputs and the SS model relates the current inputs and outputs to form the equations. The SS model relates the current inputs and outputs to build the structure. Both, ARX and SS models, only apply in a small disturbance around operation points. In [30], a N4SID is presented, which forms large matrices with the sampled input and output data, then uses singular value decomposition methods to derive the reduced order dynamic equivalent [44]. The identification procedure of N4SID is complex and the method is based on assuming the external system is observable and controllable. Furthermore, the accuracy of these proposed linear models may not be good enough when the measured data contains high dynamics [45]. A DSS model is described

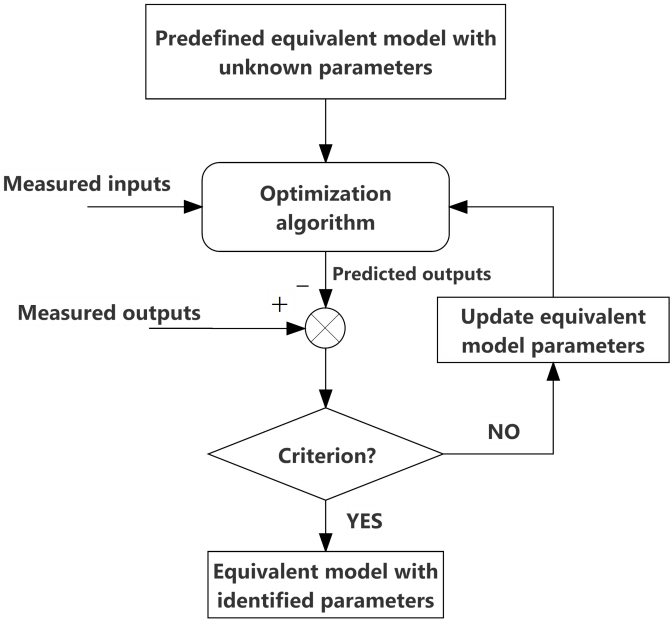

Figure 2.6: The procedure of model-based approach.

in [32, 46], which uses field voltage as input, rotor angle and active output power as outputs for synchronous generators (SGs). This method is not applicable in distribution networks because of the lack of significant SGs. A generic dynamic equivalent model is proposed in [34]. In this paper, the author uses voltage and frequency as inputs, active and reactive power as outputs. However, the frequency does not have significant oscillation in ADN and its dynamics are small for equivalent model. This means that the frequency input can be neglected in dynamic equivalent model, which can be found in [45].

2.4.3 Advantages and Disadvantages

The MBA methods require only experiment data and do not need the system details. Furthermore, they have identical structures that make it easier to integrate between experiment platforms. However, the fixed structure may bring representation constraints when the MBA models do not match well with the experiment data. Their specific advantages and disadvantages are summarized as:

Advantages of Model-Based Approach

- The MBA requires only the measured or recorded data at the boundary buses to derive a dynamic equivalent model. It is independent of the topology, parameters, large scale and complexity of the EPS.

- The dynamic equivalent model is always pre-defined and fixed which means that it is easier to integrate into power system software and management platforms. It can be implemented as a modular block with to-be-edited parameters.

- It can be applied by non-electrical engineers if the external system has the features of observability and controllability under small disturbance. Under this condition, state space model, ARX model and N4SID model can be used.

- The architecture of MBA model is more understandable than the model-free equivalent model.

Disadvantages of Model-Based Approach

- In the MBA, the physic model-based model requires electrical knowledge for deriving its structure and the artificial model-based model has to be learned from experience to set up its structure.
- The MBA approach can be limited in constraints of the equations when the relationship range of the measured input and output data is larger than the representation capacity of the model equations.
- The physic model-based model requires modeling knowledge of power system component and equivalent concept when the dynamic equivalent is derived from the physical power component models, such as the dynamic equivalent model derived in [32, 34].
- Compared to model-free approach, it loses the flexibility for equivalent model design. The artificial model-based and physic model-based models are much more strict for the selection of inputs and outputs. For example, the more dynamic transient signal such as currents or few dynamic behavior such as frequency may be not suitable for inputs and outputs. The previous outputs cannot be fed back as inputs to the equivalent model.

2.5 Summary

This chapter provided an overview of the developed dynamic equivalent model approaches for active distribution networks. The existing three categories of dynamic equivalent technology, MDA, MFA, and MBA, play a significant role in model reduction. Their summarized characteristics are given in Table 2.1, including the specific methods, their theoretical background description and their advantages and disadvantages.

As a conclusion of this chapter, the MDA is not suitable for obtaining equivalent of modern complex power systems. MFA and MBA take advantage of getting measured data easier and many algorithms can be applied for dynamic equivalent technique. Both are a feasible path to a reliable equivalent model. Considering the compatibility of DEM between platforms and the ability of DEM to represent non-linearity, a FDEM based on MBA is proposed in the next chapter.

Table 2.1: Summary of equivalent technique features for ADNs

Approach	Method	Description	Advantage	Disadvantage
Modal-Based	SVD, M2M	Retain significant Hankel singular value, truncate the rest by projections	Strictly mathematical bias, independent of disturbances	Require fully detailed system, cannot represent nonlinear features
Model-Free	RNN	Use measured data to train the relationship of variables, supervised learning	Easy to implement, only need measured data	Over-fitting problem, no explicit identical model between different trainings
Model-Based	ARX, SS, N4SID, DSS	Use measured data to optimize parameters of fixed-structure model	Explicit model structure, only need measured data	Model constraints from its equations

Chapter 3

Fixed-Structure Dynamic Equivalent Approach

3.1 Introduction

According to the characteristics of electrical components, the installed units of ADNs can be classified into active components, passive components, and prosumer components. The active components are distributed generators that convert renewable and fossil energy into electrical energy, such as kinetic energy to electrical energy in wind generators, sunlight radiation energy to electrical energy in photovoltaic generators, etc. The passive components are electrical loads that consume but do not produce electrical energy. They convert electrical energy to other forms of energy, such as electrical energy to heating in ambient heating, water heating devices, electrical energy to mechanical energy in motors, as well as electrical energy to lights in fluorescent, etc. The prosumer components are unit systems that can bidirectionally exchange electrical energy between the grid and themselves. In other words, the prosumer components can consume electrical energy from the grid, and can also feed in electricity backward to the grid. They can be single types of equipment, such as battery systems in households [47]. They can be also the combination of active components and energy storage devices, such as photovoltaic generator together with battery system [48].

The increasing number of active components and prosumer components bring

significant changes to the dynamic behaviors of ADNs and transmission systems. To operate and assess precisely such complex and large-scale systems, suitable dynamic equivalent models with high accuracy but simple forms are urgent. Based on the assumptions:

1. The responses of ADNs to large disturbances depends on the dynamics of significant active components, passive components, and prosumer components, which can be represented by induction machines (IMs), synchronous machines (SMs), electronic converters (ECs), and static power loads (SPLs) [34, 49].

2. The dynamics of frequency at substations in ADNs can be neglected by comparing with the dynamics from voltage since oscillation of frequency in ADN is small and the measured frequency value does not help for identifying equivalent model [45].

The FDEM is proposed in this chapter by the combination of four IEMs. The IEMs are coming from the approximation of IM, SM, EC, and SPL, individually.

3.2 Individual Equivalent Model

Generators and loads play significant roles in the dynamic behaviors of ADNs. They are composed of active components, passive components and prosumer components that are equipped with IMs, SMs, ECs and SPLs.

3.2.1 Induction Machine

The third-order induction model is commonly used to present the dynamics in power system transient analysis [50, 51]. It omits the flux transient and the magnetic saturation. A simplified third-order induction machine model by neglecting stator resistance is represented in Equation 3.1 [50, 51]:

$$\begin{cases} \frac{dE'_q}{dt} = -\frac{X_{im}}{T'_{dim}X'_{im}}E'_q + \frac{X_{im}-X'_{im}}{T'_{dim}X'_{im}}V + (\omega-\omega_s)E'_d \\ \frac{dE'_d}{dt} = -\frac{X_{im}}{T'_{dim}X'_{im}}E'_d - (\omega-\omega_s)E'_q \\ \frac{d\omega_{im}}{dt} = -\frac{VE'_d}{H_{im}X'_{im}} + (-\frac{T_{im}}{H_{im}}) \end{cases} \tag{3.1}$$

where E'_d and E'_q are the rotor voltage behind transient reactance in the direct and quadrature-axis, X_{im} and X'_{im} are the external series steady and transient reactance between the terminals of the IM and its connecting bus, respectively. T'_{dim} is the direct-axis time constant. V is the terminal voltage of IM. ω_s is the synchronous speed of the power grid in electrical radians per second, which is also assumed as constant value, ω_{im} is the shaft speed in electrical radians per second. H_{im} is the inertia constant, T_{im} is the mechanical torque, both values are assumed as constant. The active and reactive power can be represented as in Equation 3.2 [51]:

$$\begin{cases} P_{im} = -\frac{VE'_d}{X'_{im}} \\ Q_{im} = -\frac{VE'_q}{X'_{im}} + \frac{V^2}{X'_{im}} \end{cases} \tag{3.2}$$

The feed direction of IM active power can be introduced in minus or plus to represent loads or generators, respectively. Rewrite the Equation 3.1 and 3.2 into the polar form yields Equation 3.3 and 3.4 [34, 51]:

$$\begin{cases} \frac{dE'_{im}}{dt} = (-\frac{X_{im}}{T'_{dim}X'_{im}})E'_{im} + (\frac{X_{im}-X'_{im}}{T'_{dim}X'_{im}}\cos\delta_{im})V \\ \frac{d\delta_{im}}{dt} = (-\frac{X_{im}-X'_{im}}{T'_{dim}X'_{im}E'_{im}}\sin\delta_{im})V + \omega_{im} - \omega_s \\ \frac{d\omega_{im}}{dt} = (-\frac{V\sin\delta_{im}}{H_{im}X'_{im}})E'_{im} + (-\frac{T_{im}}{H_{im}}) \end{cases} \tag{3.3}$$

$$\begin{cases} P_{im} = (-\frac{V\sin\delta_{im}}{X'_{im}})E'_{im} \\ Q_{im} = (-\frac{V\cos\delta_{im}}{X'_{im}})E'_{im} + (\frac{V}{X'_{im}})V \end{cases} \tag{3.4}$$

where E'_{im} is the voltage behind the transient reactance, δ_{im} is the angle of the rotor flux with respect to the synchronously-rotating reference frame. Similar to [32, 34], omit the constant values, define E'_{im} , δ_{im}, ω_{im} as state variables, V as input, P_{im} and Q_{im} as outputs in Equation 3.4, and the rest as unknown parameters. The approximated equivalent of IM model can be represented by a

state space form, as described in the following Equation 3.5:

$$\begin{cases} \begin{bmatrix} \frac{dE'_{im}}{dt} \\ \frac{\delta_{im}}{dt} \\ \frac{d\omega_{im}}{dt} \end{bmatrix} = \begin{bmatrix} -\frac{X_{im}}{T'_{dim}X'_{im}} & 0 & 0 \\ 0 & 0 & 1 \\ (-\frac{V\sin\delta_{im}}{H_{im}X'_{im}}) & 0 & 0 \end{bmatrix} \begin{bmatrix} E'_{im} \\ \delta_{im} \\ \omega_{im} \end{bmatrix} + \begin{bmatrix} \frac{X_{im}-X'_{im}}{T'_{dim}X'_{im}}\cos\delta_{im} \\ -\frac{X_{im}-X'_{im}}{T'_{dim}X'_{im}E'_{im}}\sin\delta_{im} \\ 0 \end{bmatrix} V \\ \begin{bmatrix} P_{im} \\ Q_{im} \end{bmatrix} = \begin{bmatrix} -\frac{V\sin\delta_{im}}{X'_{im}} & 0 & 0 \\ -\frac{V\cos\delta_{im}}{X'_{im}} & 0 & 0 \end{bmatrix} \begin{bmatrix} E'_{im} \\ \delta_{im} \\ \omega_{im} \end{bmatrix} + \begin{bmatrix} 0 \\ \frac{V}{X'_{im}} \end{bmatrix} V \end{cases} \tag{3.5}$$

To reduce the complexity of the model representation, all of unknown parameters are replaced by p, which is leading to the simplified IM as in Equation 3.6:

$$\begin{cases} \dot{X} = \begin{bmatrix} p & 0 & 0 \\ 0 & 0 & 1 \\ p & 0 & 0 \end{bmatrix} X + \begin{bmatrix} p \\ p \\ 0 \end{bmatrix} U \\ Y = \begin{bmatrix} p & 0 & 0 \\ p & 0 & 0 \end{bmatrix} X + \begin{bmatrix} 0 \\ p \end{bmatrix} U \end{cases} \tag{3.6}$$

In Equation 3.6, $X = \begin{bmatrix} E'_g \\ \delta_g \\ \omega_g \end{bmatrix}$, $U = V$, $Y = \begin{bmatrix} P_{im} \\ Q_{im} \end{bmatrix}$. X and $\dot{X}$ are state variables and their derivative. U and Y are the input and outputs, respectively.

3.2.2 Synchronous Machine

A commonly used third-order synchronous generator model for dynamic analysis is described in [32, 52], which can represent micro-turbines and direct-drive wind turbines that are equipped with SMs. In the third-order model, the sub-transients are neglected because it decays so fast that it is not necessary to use higher order models [52]. The effects of damper windings and the dynamics of the stator are neglected, while the effects of field windings are maintained, which is approximately considered in the rotor damping factor [52]. The dynamic

part of SM can be described by Equation 3.7 [32, 52]:

$$\begin{cases} T'_g \frac{dE'_g}{dt} = E_{FD} - E'_g - (X_d - X'_d) I_d \\ \frac{d\delta_g}{dt} = \omega_g - \omega_s \\ \frac{d\omega_g}{dt} = \frac{1}{2H}(T_m - T_e - D(\omega_g - \omega_s)) \end{cases} \tag{3.7}$$

The output active and reactive power of the SM is described by Equation 3.8 [32, 52]:

$$\begin{cases} P_g = \frac{V}{X'_g} E'_g \sin \delta_g \\ Q_g = -(\frac{V^2}{X'_g} - \frac{V}{X'_g} E'_g \cos \delta_g) \end{cases} \tag{3.8}$$

where E'_g is the voltage behind the transient reactance. X_d and X'_d are the external series steady and transient reactance in direct-axis, respectively. T'_g is the transient time constant. V is the terminal voltage of SM. E_{FD} is the excitation voltage. I_d is the current in d-axis. D is the damping factor, δ_g is the rotor angle with respect to the machine terminals, ω_g is the rotor speed, and ω_s is the nominal synchronous speed that is considered as constant. H is the inertia which value is assumed as constant. T_m is the machine torque that is assumed as constant, and T_e is the electrical torque.

$$\begin{cases} I_d = \frac{E'_g - V \cos \delta_g}{X'_d} \\ I_q = \frac{V \cos \delta_g}{X'_d} \\ V_d = V \cos \delta_g \\ V_q = V \sin \delta_g \\ T_e = V_d I_d + V_q I_q \end{cases} \tag{3.9}$$

where I_d and I_q, V_d and V_q are the current and voltage in direct and quadrature-axis, respectively. By substituting I_d and T_e in Equation 3.7 with their corresponding equivalents in 3.9 [52], the Equation 3.10 and 3.11 can be obtained.

$$\begin{cases} T'_g \frac{dE'_g}{dt} = (-\frac{X_g}{X'_g}) E'_g + [-(\frac{X_g - X'_g}{X'_g}) \cos \delta_g] V + E_{FD} \\ \frac{d\delta_g}{dt} = \omega_g - \omega_s \\ \frac{d\omega_g}{dt} = (-\frac{V \sin \delta_g}{2HX'_g}) E'_g + (-\frac{D}{2H}) \omega_g + \frac{T_m + D\omega_s}{2H} \end{cases} \tag{3.10}$$

$$\begin{cases} P_g = (\frac{V}{X'_g}\sin\delta_g)E'_g \\ Q_g = (\frac{V\cos\delta_g}{X'_g})E'_g - \frac{V}{X'_g}V \end{cases} \tag{3.11}$$

Using the same approximation rule as [32, 34], omit the constant values, define E'_g, δ_g and ω_g as state variables, V as input, P_g and Q_g as outputs, and the rest as unknown parameters. The approximated equivalent of SM can be represented as a state space form by Equation 3.12:

$$\begin{cases} \begin{bmatrix} \frac{dE'_g}{dt} \\ \frac{d\delta_g}{dt} \\ \frac{d\omega_g}{dt} \end{bmatrix} = \begin{bmatrix} (-\frac{X_g}{X'_g T'_g}) & 0 & 0 \\ 0 & 0 & 1 \\ (-\frac{V\sin\delta_g}{2HX'_g}) & 0 & (-\frac{D}{2H}) \end{bmatrix} \begin{bmatrix} E'_g \\ \delta_g \\ \omega_g \end{bmatrix} \\ \quad + \begin{bmatrix} [-(\frac{X_g - X'_g}{X'_g T'_g})\cos\delta_g] \\ 0 \\ 0 \end{bmatrix} V + \begin{bmatrix} \frac{E_{FD}}{T'_g} \\ 0 \\ 0 \end{bmatrix} \\ \begin{bmatrix} P_g \\ Q_g \end{bmatrix} = \begin{bmatrix} (\frac{V}{X'_g}\sin\delta_g) & 0 & 0 \\ (\frac{V\cos\delta_g}{X'_g}) & 0 & 0 \end{bmatrix} \begin{bmatrix} E'_g \\ \delta_g \\ \omega_g \end{bmatrix} + \begin{bmatrix} 0 \\ -\frac{V}{X'_g} \end{bmatrix} V \end{cases} \tag{3.12}$$

Simplify the representation of Equation 3.12 by replacing all of the unknown parameters as p. Separately define the system states, input and outputs as X, U and Y in Equation 3.13:

$$X = \begin{bmatrix} E'_g \\ \delta_g \\ \omega_g \end{bmatrix}, U = V, Y = \begin{bmatrix} P_g \\ Q_g \end{bmatrix} \tag{3.13}$$

Finally, the individual equivalent model of SM can be described as Equation 3.14:

$$\begin{cases} \dot{X} = \begin{bmatrix} p & 0 & 0 \\ 0 & 0 & 1 \\ p & 0 & p \end{bmatrix} X + \begin{bmatrix} p \\ 0 \\ 0 \end{bmatrix} U + \begin{bmatrix} p \\ 0 \\ 0 \end{bmatrix} \\ Y = \begin{bmatrix} p & 0 & 0 \\ p & 0 & 0 \end{bmatrix} X + \begin{bmatrix} 0 \\ p \end{bmatrix} U \end{cases} \tag{3.14}$$

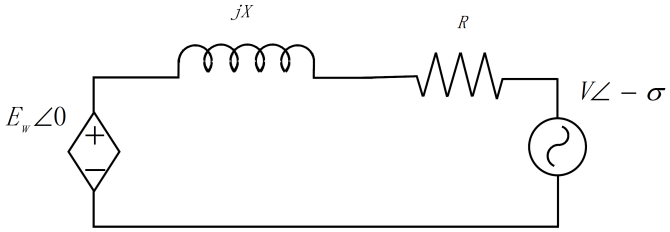

Figure 3.1: Equivalent circuit of ideal power converter.

3.2.3 Electronic Converter

The equivalent circuit of the ideal power converter can be drawn as Fig. 3.1, especially the power converters as an ideal controllable voltage source [49]. It can describe the features of battery systems, photovoltaic systems, and full rated converter wind turbine generators. If their transients are very fast and have enough electricity buffer, the ECs can be considered as ideal voltage sources. In other words, the active and reactive power feeding to the grid by the DG equipped with ideal converters can be represented as in Equation 3.15 [49]:

$$\begin{cases} P_w = \frac{E_w}{R^2+X^2}[R(E_w - V\cos\sigma) + XV\sin\sigma] \\ Q_w = \frac{E_w}{R^2+X^2}[-RV\sin\sigma + X(E_w - V\cos\sigma)] \end{cases} \tag{3.15}$$

where E_w and V are the voltage values of power converter resources and the power grid, respectively. R and X are the resistance and inductance of the connection line, respectively. σ corresponds to the angle difference between the two voltages. P_w and Q_w are the active and reactive power respectively, feeding energy from the power converter resources to the connecting power grid.

Following the similar approximation of IM and SM, define V as the input, P_w and Q_w as the outputs, the rest as unknown parameters. Then, Equation 3.15 can be rewritten as Equation 3.16:

$$\begin{cases} \begin{bmatrix} P_w \\ Q_w \end{bmatrix} = \begin{bmatrix} -\frac{E_w(R\cos\sigma - X\sin\sigma)}{R^2+X^2} \\ -\frac{E_w(R\sin\sigma + X\cos\sigma)}{R^2+X^2} \end{bmatrix} V + \begin{bmatrix} \frac{RE_w^2}{R^2+X^2} \\ \frac{XE_w^2}{R^2+X^2} \end{bmatrix} \end{cases} \tag{3.16}$$

A further simplified representation of Equation 3.16 is given in Equation 3.17,

where p are represented for the unknown parameters, $U = V$ and $Y = \begin{bmatrix} P_w \\ Q_w \end{bmatrix}$.

$$\begin{cases} Y = \begin{bmatrix} p \\ p \end{bmatrix} U + \begin{bmatrix} p \\ p \end{bmatrix} \end{cases} \tag{3.17}$$

3.2.4 Static Power Load

There are also many static power loads installed in ADNs. Generally, they can be classified as constant impedance load, constant current load, constant power load, and combination of the three loads. Learned from an international survey of industry practice on electrical load modeling [53], the SPLs are still popular for power system transient analysis, especially the constant power load model. Therefore, it is considered as one of the major loads in the power system and can be described as Equation 3.18:

$$\begin{cases} P = P_0 \\ Q = Q_0 \end{cases} \tag{3.18}$$

P, Q, P_0, and Q_0 are the active power and reactive power of the loads, respectively. By defining P and Q as outputs of the loads, the equivalent model of the loads can be represented in Equation 3.19:

$$Y = \begin{bmatrix} P_0 \\ Q_0 \end{bmatrix} \tag{3.19}$$

Another commonly used load model is featured with combination of constant impedance, current and power loads. It can be described as Equation 3.20 [54]:

$$\begin{cases} P = P_0[\alpha_1(\frac{V}{V_0})^2 + \alpha_2(\frac{V}{V_0}) + \alpha_3] \\ Q = Q_0[\beta_1(\frac{V}{V_0})^2 + \beta_2(\frac{V}{V_0}) + \beta_3] \end{cases} \tag{3.20}$$

V_0, P_0 and Q_0 are the values at the initial conditions of the loads, α_{1-3} and β_{1-3} are the coefficients of active and reactive power for the three parts of this load, respectively. V is the voltage value of the load. Taking the same approximation rules as the above equivalents, the equivalent of this load can be simplified to Equation 3.21. For the sake of simplicity, the unknown parameters

are represented as p.

$$\begin{cases} Y = \begin{bmatrix} p \\ p \end{bmatrix} U + \begin{bmatrix} p \\ p \end{bmatrix} \end{cases} \tag{3.21}$$

In Equation 3.21, $U = V$ is the input and Y are the outputs.

For another type of popular dynamic load that is composited of IM and passive loads [53], the equivalent of the composited model can be substituted by combination of equivalent models of IM and passive load which have been described in previous sections.

3.3 Fixed-Structure Dynamic Equivalent Model

Considering that the major dynamics come from the behaviors of the generators and loads, the EPSs can be represented by the significant component models with unknown parameters [55, 56].

Based on the assumption that the dynamics from active components, passive components and prosumer components in ADNs are covered by induction machine, synchronous machine, electronic converter and static power load. The detailed models of the four physic components are substituted with the derived IEMs in the previous sections. The FDEM is proposed by combining the equivalent model of the significant individual components with unknown parameters. Note that all of the unknown parameters are represented as p for the purpose of simplicity. The FDEM is described as in Equation 3.22:

$$\begin{cases} \dot{X} = \begin{bmatrix} p & 0 & 0 & 0 & 0 & 0 \\ 0 & 0 & 1 & 0 & 0 & 0 \\ p & 0 & 0 & 0 & 0 & 0 \\ 0 & 0 & 0 & p & 0 & 0 \\ 0 & 0 & 0 & 0 & 0 & 1 \\ 0 & 0 & 0 & p & 0 & p \end{bmatrix} X + \begin{bmatrix} p \\ p \\ 0 \\ p \\ 0 \\ 0 \end{bmatrix} U + \begin{bmatrix} 0 \\ 0 \\ 0 \\ p \\ 0 \\ 0 \end{bmatrix} \\ Y = \begin{bmatrix} p & 0 & 0 & p & 0 & 0 \\ p & 0 & 0 & p & 0 & 0 \end{bmatrix} X + \begin{bmatrix} p \\ p \end{bmatrix} U + \begin{bmatrix} p \\ p \end{bmatrix} \end{cases} \tag{3.22}$$

where p are the unknown parameters. $X = \begin{bmatrix} E'_{im} \\ \delta_{im} \\ \omega_{im} \\ E'_g \\ \delta_g \\ \omega_g \end{bmatrix}$, represents the state variables of the equivalent system. Y is the summation of the active and reactive powers of the individual components.

3.4 Equivalent Identification

Equivalent identification is the process of getting the unknown parameters of the FDEM. The whole procedure includes data preparation, parameter identification and performance evaluation.

3.4.1 Data Preparation

A suitable FDEM structure and a good preparation of the representative training data are the two key points for parameter identification. Depending on the purposes of analysis and also on the architecture of power grids, the experiment should be designed accordingly to get the training data. As claimed in Chapter 1, this dissertation work focuses on the transient studies of the whole system under large disturbances. The transmission systems play significant role for this study and which are kept in details, while the ADNs are not so significant but cannot be neglected, they are replaced by DEMs. The disturbances are often analyzed by means of three-phase short circuit faults [30, 34] that take place at the transmission lines (TLs) of the retained system. All of experiment data are measured at the point of common couplings (PCCs) of the related ADNs.

3.4.2 Parameter Identification

The parameter identification is the adjusting procedure of the unknown parameters for making estimated outputs close to the measured outputs. The FDEM is a state space model with one input and two outputs, but its parameters are unknown. To identify the unknown parameters, as shown in Fig. 3.2, firstly propagate the input data into the proposed equivalent model, and then update

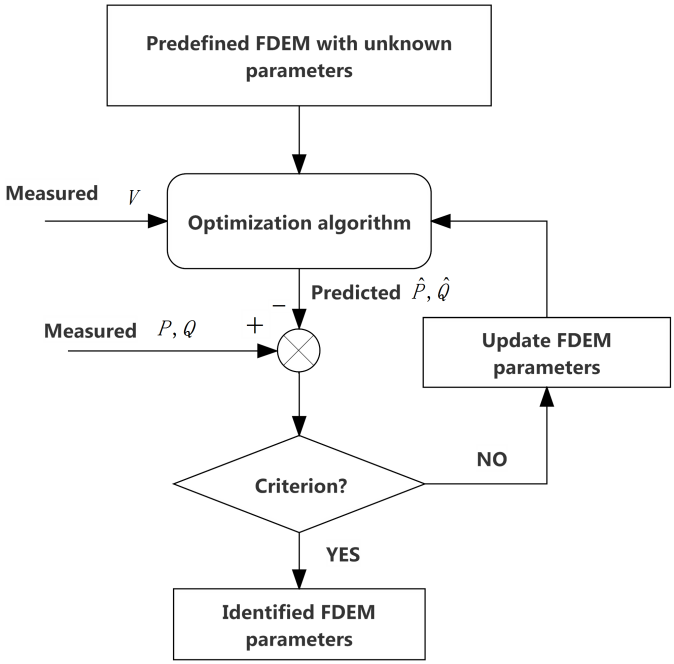

Figure 3.2: Identification flow of FDEM parameters.

the state variables and estimate the sets of outputs. Later compare the estimated and measured results. Repeatedly adjust the parameters under the designed criterion until the estimated outputs are as close as to the measured outputs.

In this research, the input is voltage and the outputs are active and reactive power at PCC. To evaluate the performance of parameter adjustment by means of optimization, a cost function is defined as Equation 3.23:

$$\jmath(p) = \frac{1}{N}[\sum_{i}^{N}(P_i - \hat{P}_i)^2 + \sum_{i}^{N}(Q_i - \hat{Q}_i)^2] \tag{3.23}$$

where, p is the unknown parameter vector, P_i and Q_i are the measured active and reactive power values at time step i, respectively. $\hat{P}_i$ and $\hat{P}_i$ are the estimated active and reactive power values at time step i, respectively. N is the quantity

of time steps.

$\jmath(p)$ can be classified as a least square optimization problem, which can be solved by many algorithms through iterations [57]. Generally, there are two categories of methods available for the problems [58]. One category is given by the methods based on line-search methods [59], such as Gauss-Newton methods, steepest-descent methods, and Levenberg-Marquardt methods. The basic idea is obtaining a search direction in each step and searches along the obtained direction to identify a better iterative point. The other category of methods is based on trust-region-search methods, such as Trust-Region Newton method [58]. The general concept of this method is searching an appropriate neighborhood space around the current point and then obtaining its iterative point. Compared to the line-search methods, the trust region algorithms take advantage of reliability and robustness for solving non-convex models and unbound constraints problems [58, 60]. Hence, the Trust-Region Newton method is chosen to identify the unknown parameters of the proposed FDEM.

The FDEM is implemented as the grey-box model within Matlab [61, 62]. The stop criterion is the difference tolerance and the maximum number of iterations, here the values are set as default to 0.001 and 20, respectively. The parameters after each iteration are identified according to Equation 3.24:

$$\hat{p} = arg \underset{p}{min} \{\frac{1}{N}[\sum_{i}^{N}(P_i - \hat{P}_i)^2 + \sum_{i}^{N}(Q_i - \hat{Q}_i)^2]\} \tag{3.24}$$

$\hat{p}$ is the identified parameter vector that makes the objective function Equation 3.23 has the minimum value.

3.4.3 Performance Estimation

In order to estimate the performance of the identified FDEM, the comparisons of the measured and estimated active and reactive power are separately introduced as $FitnessP$ and $FitnessQ$ in Equation 3.25 and 3.26 [63]:

$$FitnessP = 100 * (1 - \sqrt{\frac{\sum_i^N (P_i - \hat{P}_i)^2)}{\sum_i^N (P_i - \bar{P})^2}}) \tag{3.25}$$

$$FitnessQ = 100 * (1 - \sqrt{\frac{\sum_i^N (Q_i - \hat{Q}_i)^2)}{\sum_i^N (Q_i - \bar{Q})^2}}) \tag{3.26}$$

$FitnessP$ and $FitnessQ$ are the values of the performance criterion for the active and reactive power, respectively. N is the number of measurements, P_i and Q_i are the measured active and reactive power at time step i, $\hat{P}_i$ and $\hat{Q}_i$ are the estimated active and reactive power at time step i, $\bar{P}$ and $\bar{Q}$ are the mean value of the N number of active and reactive power, respectively. The estimated values are calculated from the identified equivalent model Equation 3.22 by giving the same sets of measured inputs.

3.5 Electrical System for Testing and Experiment Platform

The architecture of electrical system for testing consists of an interconnected transmission system and an active distribution network. The transmission system and active distribution network are connected by means of a substation. Furthermore, a certain amount of distributed generators are installed in the active distribution network. In this section, the specific topology and configuration of the electrical system for testing are described. The experiment platform and its setting-up are also introduced.

3.5.1 The Full Test Electrical System

The topology of test system is composed of a standard IEEE 9-buses transmission system and a 16-buses active distribution network: they are connected by a transformer. As shown in Fig. 3.3, the transmission system has three generators equipped with three step up substations. The substations are interconnected by six transmission lines at 230 kV. There are three power loads connected in the transmission systems at the buses B5, B6 and B8. The transformer, $TF4$, is used for the connection of this transmission system and the ADN. The detailed parameter configuration is adopted from [64], as listed in Appendix A.

The ADN is modified from a rural network [65]. It is composed of seven feeders and 16 buses. The electrical parameters of the loads, feeders, and transformers are shown in Table B.1, Table B.2 and Table B.3, respectively. The DGs are installed corresponding with different test scenarios in the ADN. There are totally five types of DGs, including photovoltaics (PVs), double fed induction

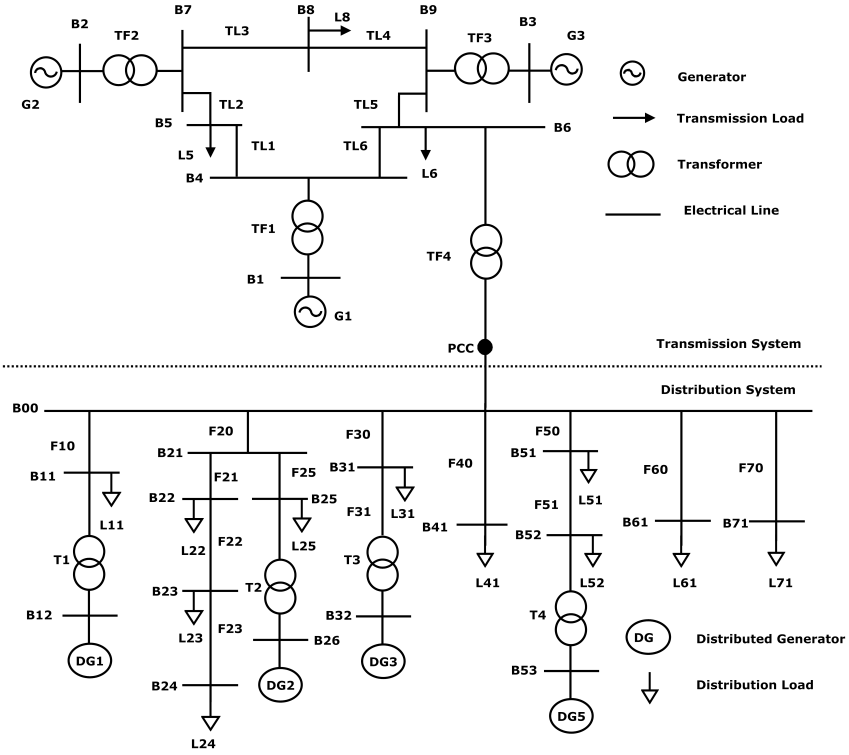

Figure 3.3: The full electrical system.

generators (DFIGs), full rated converter wind turbine generators (CWTGs), fixed speed induction generators (FSIGs), SGs. Their parameters are described in Appendix B.

3.5.2 Equivalent Electrical System

The interested dynamics are medium term transient of power system in this dissertation, the behavior of transmission system are much more significant [9] than the behavior of active distribution network during disturbances. Hence, in the test system, the transmission system is considered as internal part of the sub-system, and the ADN is considered as the external part of the sub-system that is to be simplified. The equivalent system topology is shown in Fig. 3.4. After simplification, the transmission system is keeping all of the details, the ADN is substituted by DEMs.

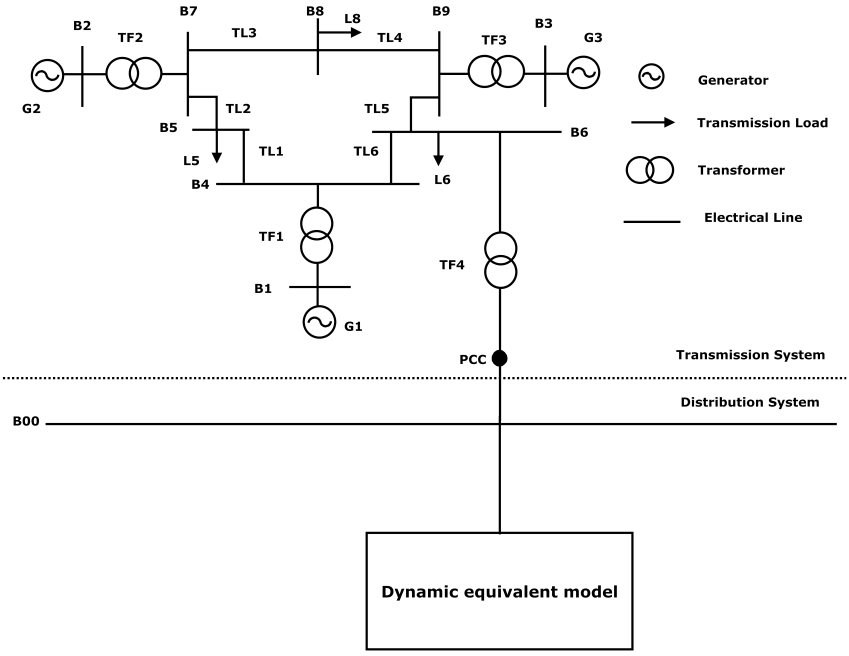

Figure 3.4: Simplified equivalent system.

3.5.3 Experiment Platform

All of the test electrical systems are developed and simulated in PowerFactory [66]. The simulation time is set as 10 second, which is depending on the disturbance type, the infrastructure of the power grid, and the operating point [27, 34]. The time step of the simulation is 0.01 second. The disturbances are setting as three-phase short circuit at the middle of the TLs, which is commonly used for transient analysis [26, 27, 33]. The fault duration is set at 200 ms since most of the allowed fault durations are from 140 ms to 250 ms in the grid codes [67]. The measured points are the PCCs of the power systems, the measured time is 10 second, the same as the simulation time. For the purpose of better visualization, figures are plotted in 6 second. The measured variables are the active and reactive power, voltage, current, frequency, the derivative of voltage and frequency. In this chapter, only the data sets of voltage, active and reactive power value are used.

The optimization and learning algorithms for the FDEM and other proposed equivalent models are implemented in Matlab.

3.6 Test Scenarios

To demonstrate the derived FDEM, three categories of test scenarios are considered: different combinations of DGs, fault locations and penetration levels. Each category includes a numbers of test cases for various situations. Their responses are recorded at the PCCs to identify the unknown parameters of the FDEM. To present the FDEM and results easier, the unknown parameters are specified as $p_1, p_2, ..., p_{17}$. Therefore, the FDEM can be represented in Equation 3.27:

$$\begin{cases} \dot{X} = \begin{bmatrix} p_1 & 0 & 0 & 0 & 0 & 0 \\ 0 & 0 & 1 & 0 & 0 & 0 \\ p_2 & 0 & 0 & 0 & 0 & 0 \\ 0 & 0 & 0 & p_3 & 0 & 0 \\ 0 & 0 & 0 & 0 & 0 & 1 \\ 0 & 0 & 0 & p_4 & 0 & p_5 \end{bmatrix} X + \begin{bmatrix} p_6 \\ p_7 \\ 0 \\ p_8 \\ 0 \\ 0 \end{bmatrix} U + \begin{bmatrix} 0 \\ 0 \\ 0 \\ p_{17} \\ 0 \\ 0 \end{bmatrix} \\ Y = \begin{bmatrix} p_9 & 0 & 0 & p_{11} & 0 & 0 \\ p_{10} & 0 & 0 & p_{12} & 0 & 0 \end{bmatrix} X + \begin{bmatrix} p_{13} \\ p_{14} \end{bmatrix} U + \begin{bmatrix} P_{15} \\ p_{16} \end{bmatrix} \end{cases} \tag{3.27}$$

The procedure adopted for parameters estimation is introduced in Section 3.4.2. As described in Section 3.4.3, the performance of the obtained FDEMs is evaluated by comparing with the new sets of data that are not used in the estimation process. The quantified criterion values are presented as the Fitness value of active and reactive power in Equation 3.25 and 3.26, respectively.

3.6.1 Different DG Combinations

The DG combination scenario is demonstrated by five test groups, CG1, CG2, CG3, CG4, CG5. The DGs in a group are connected to the four buses in the ADN: B12, B26, B32 and B53, respectively. The specific DG locations can be found in Fig. 3.3.

3.6.1.1 DG Combination Setting-Up

The DGs in Fig. 3.3 are marked as DG1, DG2, DG3, DG5. The specific combination information, including DG type and active power size, is shown in the following Table 3.1: the values are the generation of active power from each generator. Note that the DGs and their connecting transformers are composed as pairs accordingly, the specific parameters of the DG transformers are described in Appendix B.3.

3.6.1.2 Test Results

In the DG combination scenario, the measured data sets for training are recorded when the three-phase short circuit disturbances occur at the middle of

Table 3.1: Different DG combinations

	CG1	CG2	CG3	CG4	CG5
B12(DG1)	PV 2.5	PV 2.5	PV 2.0	PV 3.0	FSIG 2.0
B26(DG2)	DFIG 2.5	DFIG 2.5	DFIG 2.5	DFIG 2.0	DFIG 3.5
B32(DG3)	CWTG 1.5	CWTG 1.5	FSIG 2.0	CWTG 1.5	CWTG 1.0
B53(DG5)	SG 2.0	FSIG 2.0	SG 2.0	SG 2.0	SG 2.0
Sum (MW)	8.5	8.5	8.5	8.5	8.5

Table 3.2: Parameters of the identified FDEM in DG combination scenario

Parameters	CG1	CG2	CG3	CG4	CG5
p1	-39.8867	-7.8611	-9.8966	-37.473	-12.3466
p2	0.025	0.025	0.025	0.025	0.025
p3	-6.0815	-7.7468	-9.8497	-4.57	-12.149
p4	-0.08	-0.08	-0.08	-0.08	-0.08
p5	-1.984	-1.984	-1.984	-1.984	-1.984
p6	-7.075	-6.2269	-7.5538	-10.56	-9.152
p7	-8.94	-8.94	-8.94	-8.94	-8.94
p8	-10.1687	-2.0805	-0.8236	-10.138	-1.6092
p9	-1.9533	0.3166	1.8804	-4.16	3.6886
p10	-1.2209	9.2608	11.6636	3.253	12.1588
p11	0.0049	-0.0051	-0.0562	27.733	-0.137
p12	0.0096	-0.2474	-0.3775	-30.8	-0.4694
p13	18.5901	18.4862	23.8606	0.392	24.4972
p14	22.4464	24.3275	27.2215	-18.994	27.8834
p15	-10.0732	-9.7005	-15.0461	28.186	-15.6612
p16	-14.1506	-15.3043	-18.7902	0.392	-19.4318
p17	-222.623	-222.9311	-222.9111	-228.074	-222.8976

TL2, 4, 6, where the fault locations have the long, middle and short distances from the measured point PCC. The faults occur at 1000 MVA level [33, 34, 68].

After preparing the measured data, the data are used for the optimization procedure, and the parameters of FDEMs are obtained. As it can be seen from the Tab. 3.2, the parameters between the test groups are quite different, which make sense since the identification of unknown parameters are numerical solution and there are difference between the training data.

To evaluate the performance of the identified FDEM, the test data is defined as the measured data when the disturbances occur at the middle line of TL3, 5, where the locations are far away and close to the measured point PCC, respectively. These test data are independent from the training data. The test results are shown as in Fig. 3.5.

In the above Fig. 3.5, FDEM-P3 and FDEM-Q3 present the Fitness value of the active and reactive power for the disturbance occurred at TL3. FDEM-P5 and FDEM-Q5 denote the Fitness value of the active and reactive power for the disturbance occurred at TL5. According to the results, the Fitness values of active and reactive power are above 80 %: this can be considered has a good agreement between estimated value and measured value.

The Fig. 3.6, 3.7, 3.8, 3.9, 3.10 show the measured and estimated responses for CG1, CG2, CG3, CG4, CG5, respectively. The MP-3, MQ-3 presents the

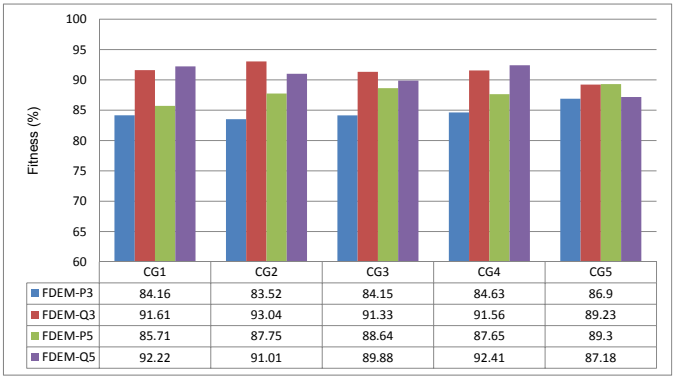

	CG1	CG2	CG3	CG4	CG5
FDEM-P3	84.16	83.52	84.15	84.63	86.9
FDEM-Q3	91.61	93.04	91.33	91.56	89.23
FDEM-P5	85.71	87.75	88.64	87.65	89.3
FDEM-Q5	92.22	91.01	89.88	92.41	87.18

Figure 3.5: Performance of FDEM in different DG combinations.

measured active and reactive power that correspond to the disturbance at the TL3, separately. The EP-3 and EQ-3 are their estimated responses of active and reactive power, in relation to the disturbance at the TL3. The same y-axis definitions of TL3 are applied at TL5 for the measured and estimated responses. As it can be seen from these figures, the measured and estimated responses match well.

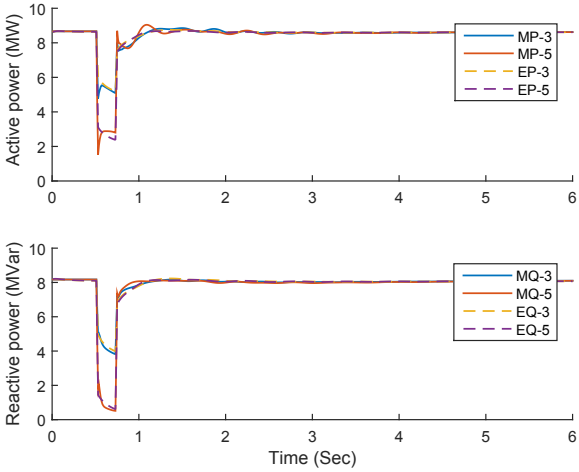

Figure 3.6: Measured and estimated responses of PCC in CG1.

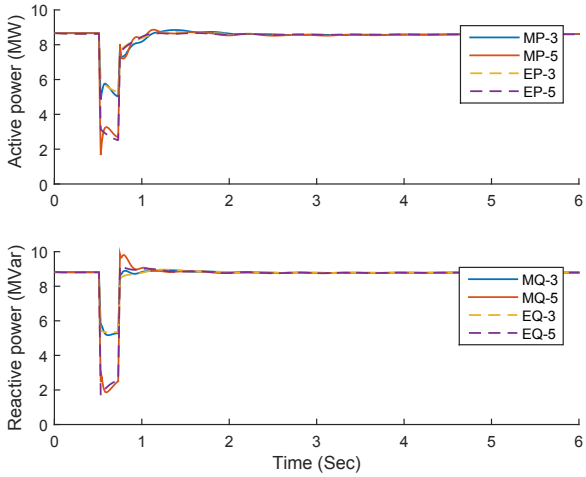

Figure 3.7: Measured and estimated responses of PCC in CG2.

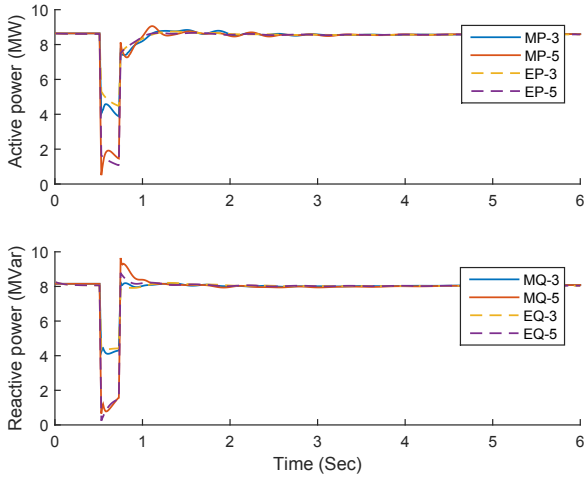

Figure 3.8: Measured and estimated responses of PCC in CG3.

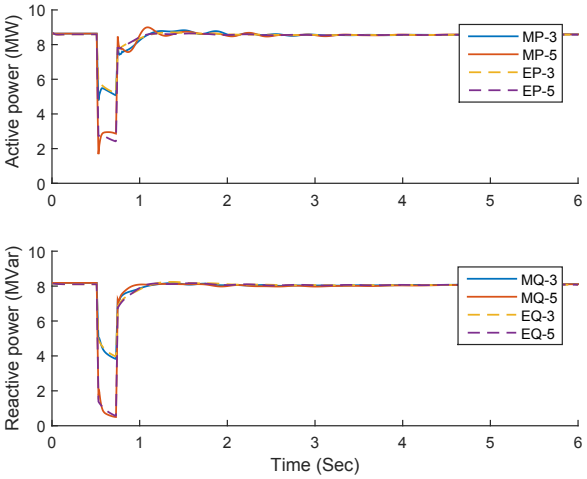

Figure 3.9: Measured and estimated responses of PCC in CG4.

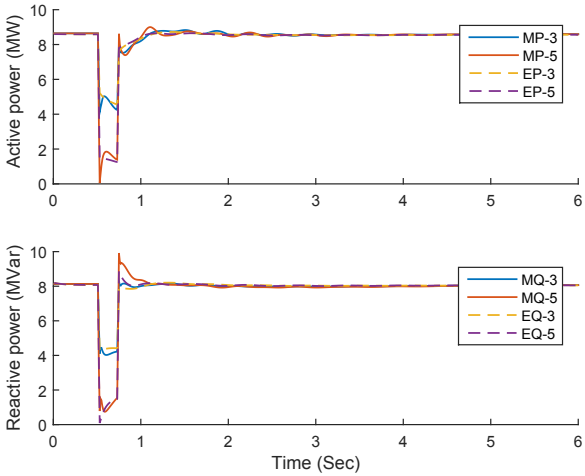

Figure 3.10: Measured and estimated responses of PCC in CG5.

3.6.2 Different Fault Locations

In this section, the fault location scenario has been investigated in five test groups, named FG1, FG2, FG3, FG4, FG5. The FDEM is tested for the various fault locations. The configuration of CG1 is used to represent the original active distribution network since it includes the major and common-used types of DGs in ADNs.

3.6.2.1 Fault Location Setting-Up

A representative equivalent model and a right amount of measured data are the two key ingredients to identify a good DEM. Here "right" means that the measured data include the major and significant dynamic information of original systems. Otherwise, the identification will fail: either the model is not correct, or the data is not enough. In other words, it has no meaning if the measured data is too little. Hence in this test scenario, three sets of data under different disturbance locations are measured for the parameter identification, the other three sets of data are used to test the identified dynamic equivalent model. The

Table 3.3: Different fault locations

	FG1	FG2	FG3	FG4	FG5
Training data	TL4, 5, 6	TL2, 5, 6	TL2, 3, 6	TL1, 3, 5	TL1, 2, 3
Testing data	TL1, 2, 3	TL1, 3, 4	TL1, 4, 5	TL2, 4, 6	TL4, 5, 6

specific fault location is listed in Table 3.3.

The test groups are designed by considering the distance between the fault location and the measure point PCC. In FG1, the disturbance locations (TL4, 5, 6) for the training data are the closest places to the measure point, while the locations (TL1, 2, 3) for the testing data are the farthest to the measure point. The opposite situation exists in FG5. In FG2, the TL2 location is far away from PCC, but the TL5, 6 locations are the closest location to PCC for the training data. The locations for the testing data (TL1, 3, 4) are far away from the measure point. The opposite situation of FG2 is FG3. In FG4, the locations to obtain the training and testing data are cross.

3.6.2.2 Test Results

Processing the training data as described in Section 3.4.2, the identified parameters for each group are shown in Tab. 3.4. The test results are shown in Fig. 3.11, the axes have similar definition as in Fig. 3.5.

According to the results in Fig. 3.11, all the Fitness values are higher than 81 %. This shows that there is a good agreement between the estimated and measured values. The detail views of the responses for FG1 are shown in Fig. 3.12. The measured and estimated results for FG2, 3, 4, 5, are similar as in Fig. 3.12 and will not be presented here, since the training and test data come from three out of the same six disturbances.

Table 3.4: Parameters of the identified FDEM in fault location scenario

Parameters	FG1	FG2	FG3	FG4	FG5
p1	-40.527	-40.4946	-39.7949	-39.6174	-35.3946
p2	0.025	0.025	0.025	0.025	0.025
p3	-3.7198	-3.9766	-6.5821	-5.4486	-23.3468
p4	-0.08	-0.08	-0.08	-0.08	-0.08
p5	-1.984	-1.984	-1.984	-1.984	-1.984
p6	-6.8268	-6.8537	-7.2373	-6.7399	-5.7274
p7	-8.94	-8.94	-8.94	-8.94	-8.94
p8	-10.6632	-10.6227	-10.1474	-10.4404	-9.4044
p9	0.3546	0.0221	-2.3627	-1.5796	6.772
p10	-0.6306	-0.656	-1.3211	-1.2306	0.6269
p11	0.0007	0.0009	0.0063	0.0036	-0.0852
p12	0.0037	0.0041	0.0114	0.0079	0.0079
p13	18.8592	18.7112	18.3826	19.1912	21.0527
p14	22.4635	22.4321	22.3102	22.8057	23.4416
p15	-10.0812	-9.9735	-9.9179	-10.6276	-12.1243
p16	-14.1922	-14.1561	-14.0037	-14.5306	-15.1124
p17	-222.5994	-222.6027	-222.6261	-222.6011	-222.6419

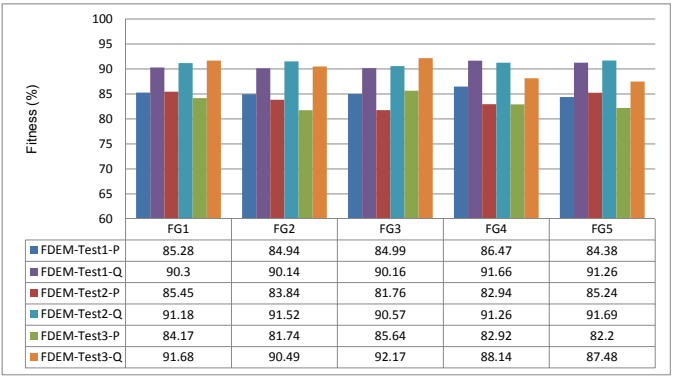

Figure 3.11: Performance of FDEM in different fault locations.

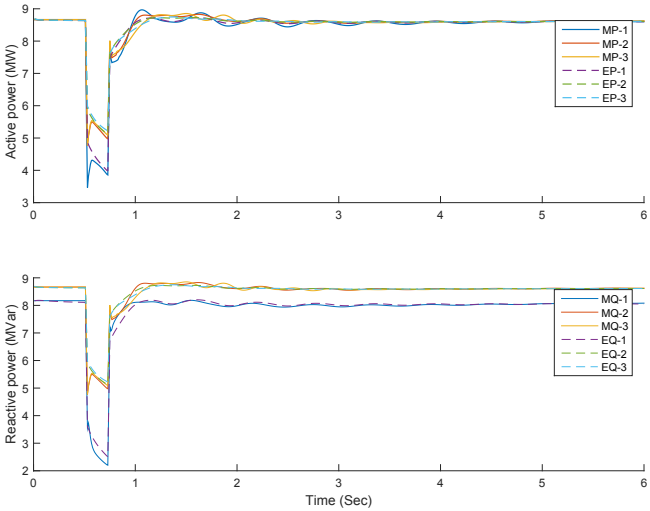

Figure 3.12: Measured and estimated responses of PCC in Test1, 2, 3.

3.6.3 Different Penetration Levels

This scenario is designed to demonstrate the Fitness of FDEM under different penetration levels (PLs) of DGs in ADNs.

3.6.3.1 Penetration Level setting-up

A PL is defined as Equation 3.28 [69]:

$$DG_{PL}\% = \frac{P_{DG}}{P_{DG} + P_{CG}} * 100 \tag{3.28}$$

where P_{DG} and P_{CG} are the amount of total active power generated by DGs and centralized generators respectively. A modified PL for the ADN is defined as Equation 3.29 by assuming that the consumption of the loads equals the total active power produced by DGs and centralized generators.

$$DG_{PL}\% = \frac{P_{DG}}{P_{Load}} * 100 \tag{3.29}$$

Table 3.5: Parameters of the identified FDEM in penetration level scenario

Parameters	10%	30%	50%
p1	-37.19	-35.3913	-39.8867
p2	0.025	0.025	0.025
p3	-25.3596	-33.7175	-6.0815
p4	-0.08	-0.08	-0.08
p5	-1.984	-1.984	-1.984
p6	-5.25	-8.7819	-7.075
p7	-8.94	-8.94	-8.94
p8	-9.4608	-8.9852	-10.1687
p9	2.1018	8.5843	-1.9533
p10	-1.0179	3.0096	-1.2209
p11	-0.0218	-0.2782	0.0049
p12	0.0133	-0.0757	0.0096
p13	27.2645	25.0563	18.5901
p14	15.394	20.647	22.4464
p15	-11.653	-12.8793	-10.0732
p16	-6.9843	-12.5328	-14.1506
p17	-222.6903	-222.6868	-222.623

These tests are performed by using three penetration levels of DGs: 10 %, 30 % and 50 %. The training data is the responses when the disturbances happen in TL2, 4, 6. The testing data is the responses when the disturbances happen in TL3, 5.

3.6.3.2 Test Results

Parameter identification is performed according to the procedure described in Section 3.4.2: the identified parameters for the penetration levels, 10 %, 30 % and 50 %, are presented in Tab. 3.5. The test results are shown in Fig. 3.13, the definition of the axes is the same as in Fig. 3.5.

According to the results in Fig. 3.13, the higher PL of DGs, the smaller Fitness values of active and reactive power. That is because more DGs bring more dynamics to the power grid. However, the values of the Fitness are bigger than 84 %, and then the FDEMs can be still considered a good equivalent model.

Fig. 3.14, 3.15, 3.16 show the specific responses of the different PLs: the definition of their axes are the same as in Fig. 3.6.

According to the test results in PL scenario, the Fitness values become worse

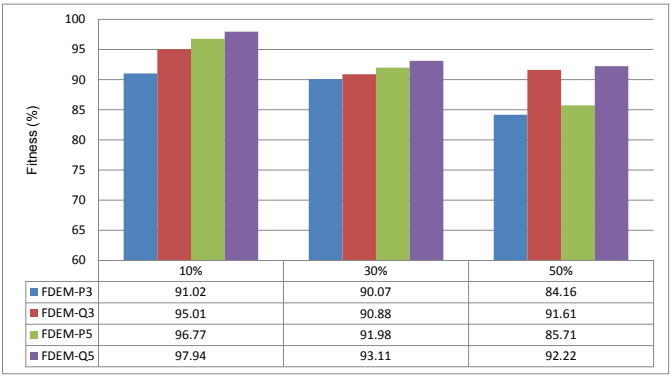

	10%	30%	50%
FDEM-P3	91.02	90.07	84.16
FDEM-Q3	95.01	90.88	91.61
FDEM-P5	96.77	91.98	85.71
FDEM-Q5	97.94	93.11	92.22

Figure 3.13: Performance of FDEM in different penetration levels of DGs.

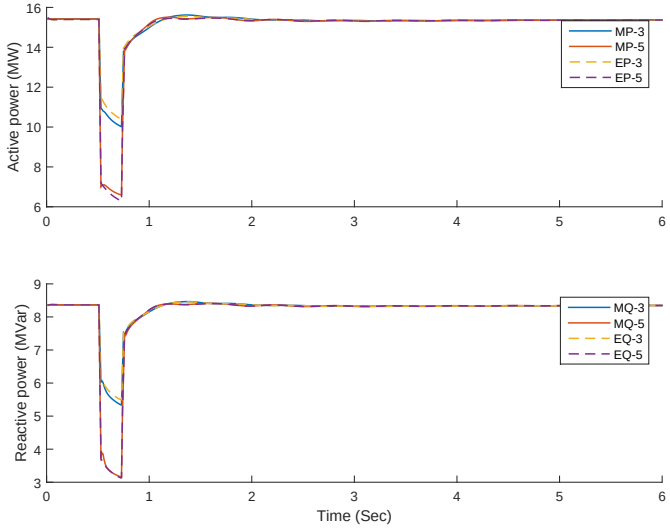

Figure 3.14: Measured and estimated responses of PCC with 10 % penetration of DGs.

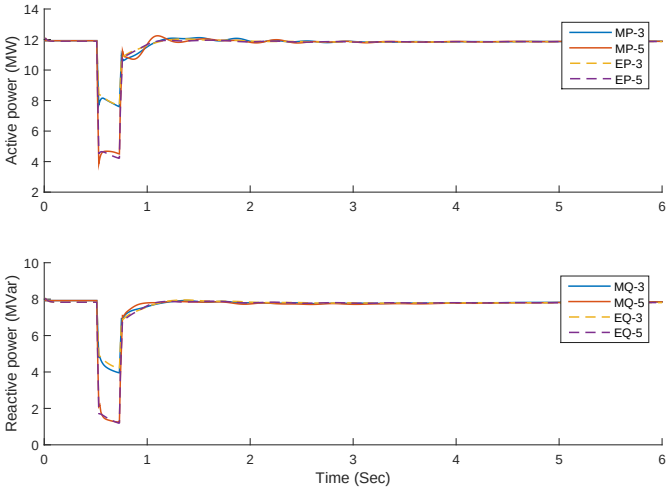

Figure 3.15: Measured and estimated responses of PCC with 30 % penetration of DGs.

with the increasing penetration levels of DG. These results show the more installations of DGs, the more difficult is to catch all the dynamic behaviors.

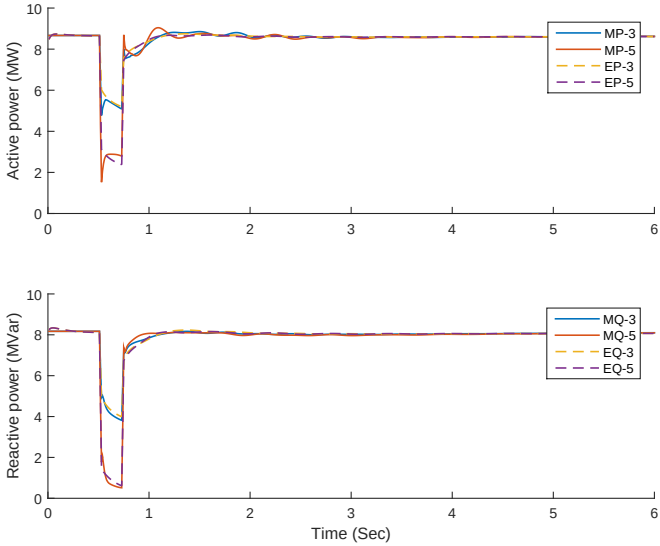

Figure 3.16: Measured and estimated responses of PCC with 50 % penetration of DGs.

3.7 Summary

This chapter proposed an equivalent model FDEM for ADNs. The performance of the FDEMs is evaluated by comparing the measured and estimated active and reactive power in three scenarios, such as different DG combinations, fault locations and penetration levels. It has been found that the measured and estimated results have a good agreement at the PCC under different situations.

While the FDEMs have six orders with 17 parameters, it may also represent a simpler DEMs that has lower order or less unknown parameters when the system has few and smaller dynamics.

Chapter 4

Adaptive Dynamic Equivalent Approach

4.1 Introduction

In practice, the dynamic equivalent models for active distribution networks depend on the system topologies, type of test scenarios and the measurement points [45, 70]. The proposed fixed-structure dynamic equivalent model in Chapter 3 may not be the best for equivalent model representation when the external part of the sub-systems have few and small dynamics. For example, a four order equivalent model has been proposed in [30], which has lower order of equivalent model than FDEM. Considering the simplicity of FDEM and the flexibility of model-free approach, a new adaptive ADEM is proposed for ADNs by combining their strengths. The ADEM is based on Markov decision process, which adapts equivalent models with measured data.

4.2 Adaptive Dynamic Equivalent Model

4.2.1 Low Order Equivalent Model

In the Chapter 3, the FDEM is proposed as a fixed combination of individual equivalent of induction machine, synchronous machine, and electronic converter, static power load in Equation 4.1:

$$Equi = \sum_{i=1}^{4}(M_i) \tag{4.1}$$

Equi is the DEM model, i is the number of individual equivalent models. M_1, M_2, M_3, M_4 present the individual equivalent models of induction machine, synchronous machine, electronic converter, and static constant power load, respectively. Notice that the state variables and parameters of the IEMs are different from each other. When an original system has few and small dynamics, the EPS is represented in an *Equi* with lower order and fewer unknown parameters [45]. In the opposite situations, the *Equi* is represented in a more complex form with higher order and more unknown parameters. In other words, the *Equi* model should be able to adapt with the measured data with flexible order and unknown parameters. To describe this idea better, a representation for ADEM can be formulated in Equation 4.2:

$$Equi = \sum_{i=1}^{4}(c_i M_i) \tag{4.2}$$

Equation 4.2 is similar to the Equation 4.1: the difference is the c_i defining the status of the i^{th} IEM. When $c_i = 1$, the i^{th} IEM includes in the *Equi* model, while $c_i = 0$, this IEM does not include. The *Equi* is to omit the redundant IEM when the to-be equivalent system is fitting in a lower order models. The status c_i and the model M_i are adaptive to experimental data. When the data contains more dynamics, the *Equi* has higher order and more unknown parameters. When the data contains few dynamics, the *Equi* has lower order and less unknown parameters.

To verify the hypothesis, an experiment is proposed to compare two different combinations of IEMs with the same training and testing data. The first one includes four IEM and is represented in Equation 3.27. The second one is represented by the sum of the IEMs of synchronous machine and electronic converter. In the lower order *Equi*, it holds $c = [0110]$ and $Equi = \sum_{i=1}^{4}(c_i M_i) = \sum_{i=2,3}(M_i)$. Its specific equations are introduced in Equation 4.3:

$$\begin{cases} \dot{X} = \begin{bmatrix} p & 0 & 0 \\ 0 & 0 & 1 \\ p & 0 & p \end{bmatrix} X + \begin{bmatrix} p \\ 0 \\ 0 \end{bmatrix} U + \begin{bmatrix} p \\ 0 \\ 0 \end{bmatrix} \\ Y = \begin{bmatrix} p & 0 & 0 \\ p & 0 & 0 \end{bmatrix} X + \begin{bmatrix} p \\ p \end{bmatrix} U + \begin{bmatrix} p \\ p \end{bmatrix} \end{cases} \tag{4.3}$$

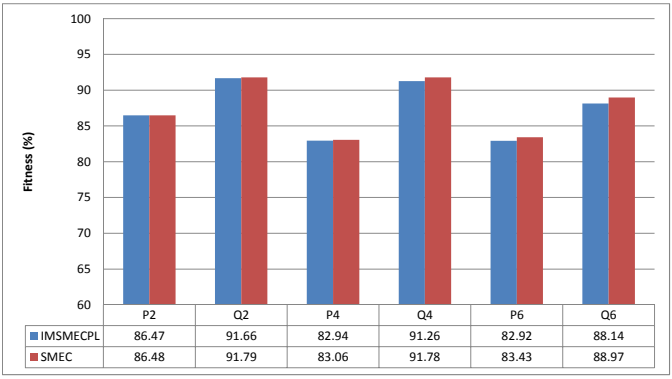

	P2	Q2	P4	Q4	P6	Q6
IMSMECPL	86.47	91.66	82.94	91.26	82.92	88.14
SMEC	86.48	91.79	83.06	91.78	83.43	88.97

Figure 4.1: Comparison between the FDEM and the SM+EC.

The measured data come from the measured data of the test group CG1 in the DG combination scenario. After training and testing, the performances of the FDEM and "SM+EC" models is presented in Fig. 4.1. The results show that the performance of the *Equi* consisted of SM and EC is close to the *Equi* model combining IM, SM, EC and static power load. In other words, it is possible to substitute a high order equivalent model by a lower order equivalent model.

The status of the IEMs depend on the fitting level between the model and measured data. The identification of the right status of IEMs and parameters can be formulated as a decision problem, namely Markov decision process.

4.2.2 Markov Decision Process Basis

A MDP has five tuples [71], (S, A, P, R, γ), where S is a set of states. A is a set of actions which are available at state S. P is the probability, alternatively, $P_a(s, s')$ is the probability that action a in state s leads to a new state s'. $R_a(s, s')$ is the immediate reward received after the transition from the state s to the new state s'. $\gamma \in [0, 1]$ is the discount factor, which represents the weight coefficient between future rewards and present rewards. The goal of MDP is to find a policy, which specifies the actions with specific states that maximize the rewards. In this dissertation, the target is to find the final state and action with minimized punishment (maximized reward) under a given environment (measured data).

4.2.3 MDP Problem Formulation

In this section, the problem of building DEM is formulated into the form of MDP problem.

DEM States

Assuming that there are n numbers of IEM, the first IEM has h numbers of unknown parameters. The i^{th} IEM has k numbers of unknown parameters and the n^{th} IEM has j numbers of unknown parameters. The sets of unknown status and parameters bringing the definition of DEM state, s, is defined in Equation 4.4:

$$s = (\underbrace{c_1, p_1(1), ..., p_1(h)}_{c_1 M_1} ,..., \underbrace{c_i, p_i(1), ..., p_i(k)}_{c_i M_i}, ..., \underbrace{c_n, p_n(1), ..., p_n(j)}_{c_n M_n}) \quad (4.4)$$

Here, c_1 represents the status of IEM-1, $c_1, p_1(1), ..., p_1(h)$ is the state vector of IEM-1, for simplicity, namely $c_1 M_1$. The same definition applies for the other IEMs, $c_k M_k$ are the state vector of the k^{th} IEM, and $c_n M_n$ are the state vector of the n^{th} IEM. For simplicity, the state can be described as in Equation 4.2.

DEM Actions

The change from a state s to another new state s' is defined as an action, the action vector is denoted as a in Equation 4.5:

$$\begin{aligned} a &= s' - s \\ &= (\underbrace{\Delta c_1, \Delta p_1(1), ..., \Delta p_1(h)}_{a_1} ,..., \underbrace{\Delta c_i, \Delta p_i(1), ..., \Delta p_i(k)}_{a_i}, ..., \\ &\qquad \underbrace{\Delta c_n, \Delta p_n(1), ..., \Delta p_n(j)}_{a_n}) \end{aligned} \quad (4.5)$$

The status variable c can only be 0 or 1, which is different from the other unknown parameters. When $\Delta c_i = 0$, the status stays the same. When $\Delta c_i = 1$, the status of IEM switches from 0 to 1, the relevant IEM-i model is included in the *Equi*. When $\Delta c_i = -1$, the status of IEM-i jumps from 1 to 0, then the IEM-i model is neglected in the *Equi*. The change of the other parameters remains as they are. For simplicity, the action is

represented as Equation 4.6:

$$a = (a_1, ..., a_i, ..., a_n) \tag{4.6}$$

DEM Transition

The DEM evolution from a state s to a new state s' is described by the transition function f. The new state s' depends, in addition to the preceding state s, on the action a with a realization of a stochastic process. The general evolution of DEM is thus governed by the relation as Equation 4.7:

$$p(s') = f(s, a) \tag{4.7}$$

DEM Punishment/Reward

In order to evaluate the performance of an action, the reward function, r, is specified as in Equation 4.8. It associates an immediate reward for each transition from a state s to a new state s'.

$$r = \jmath(s) - \jmath(s') \tag{4.8}$$

Here, $r > 0$ and $\jmath$ is the mean square error between estimated and measured outputs, the specific equations are represented in Equation 3.23.

The decision procedure is the path from the initial state to the final state of equivalent model, which have the smallest punishment value. The searching and acting process is called Markov decision process. After intensive learning of a right state and action space, an optimal policy could be achieved, which means the MDP model can select a optimal path to reach the final goals.

A general representation of ADEM can be found in Equation 4.2. The number of IEMs in ADEM can be higher if more IEMs are derived. In this dissertation, the number of IEM is always four, the IEMs are equivalent model of IM, SM, EC and SPL.

4.3 Equivalent Model Identification

So far, the problem of DEM parameter identification is formulated as a MDP decision problem in Section 4.2.3. When transition and reward of MDP are known, a MDP problem can be solved by linear programming and dynamic

programming. However, the specific transition function f is unknown in the defined MDP of the DEM in Section 4.2.3. Hence, reinforcement learning methods, has been proposed to solve the MDP problem since it neither requires explicit transition probability nor explicit reward function [72, 73].

4.3.1 Modified Q-Learning Algorithm

Q-Learning is a simple method to solve MDP problems [74], which is one of the reinforcement learning methods. The updating of Q-value is represented in Equation 4.9:

$$Q(s,a) \leftarrow Q(s,a) + \alpha[r + \gamma * arg \underset{A}{max}\ Q(s',a') - Q(s,a)] \tag{4.9}$$

where $Q(s,a)$ is the action value function of s,a, which quantify how much immediate and future reward, Q-value, can obtain with action a at the state s, the detail explanation can be found in [74]. α is the learning rate, set between 0 and 1, the bigger, the faster to update the Q-value. γ is the discount factor, also set between 0 and 1, the bigger, the more weight on future reward. $arg \underset{A}{max}\ Q(s',a')$ is the maximum Q-value at state s' with action a', A is the available action space for a'.

However, Q-Learning is not efficient in searching a large scale of state and action space [72, 73, 75]. An approximate Q-Learning is proposed in [76], which searches the gradient direction of Q-function. The state-action search of $arg \underset{A}{max}\ Q(s',a')$ is substituted by the gradient of Q-function. A further modification can be done by replacing the gradient of Q-function with gradient of the objective function in Equation 3.23, since the final goal of DEM is to find the state and action [77] with the smallest punishment value. The work flow of the modified Q-Learning is shown in Fig. 4.2. As it can be seen from Fig. 4.2, the work flow mainly has three steps.

1. Initialization
   Initialize the state s_0, the action a_0 and the Q-value $Q(s_0,a_0)$. Set $s = s_0, a = a_0, Q = Q_0$.

2. Iteration
   Iterate the Step2 if the results do not fit the criterion. Update the immediate reward value r according to Equation 4.8. Update the state $s' = s + a$.

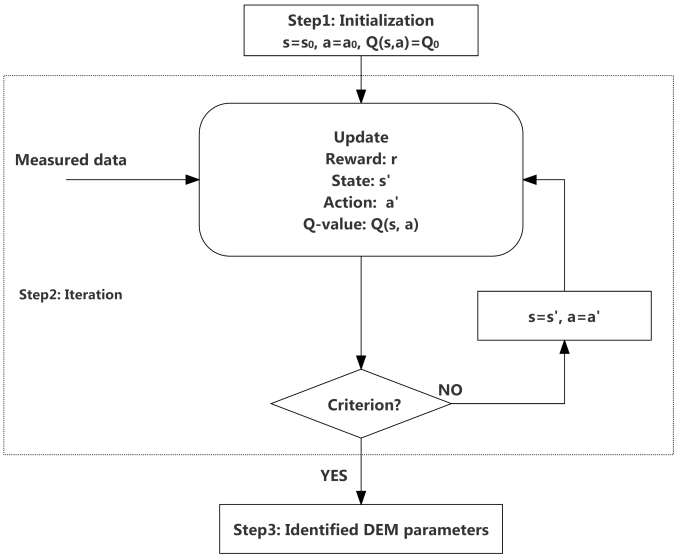

Figure 4.2: Work flow of the modified Q-Learning.

Update the action a' according to $a' = \frac{\partial_J}{\partial p}$, J is given by Equation 3.23, p is the parameter vector of *Equi*. Update the Q-value according to $Q(s,a) = Q(s,a) + \alpha[r + \gamma * Q(s',a') - Q(s,a)]$.

3. Identification
   If the result fits the predefined criterion, then exit work flow with identified DEM, otherwise update the state and action, then go back Step2. The criterion could be the number of updating in Step2 and difference of Q-value between the latest two steps.

4.3.2 Parameter Identification

The procedure of identifying the ADEM is shown in Fig. 4.3, which includes three steps: MDP state space reduction, Iteration, Identification.

In the defined MDP model in Section 4.2.3, there are 21 state variables and large scale of actions. The state status can only be 1 or 0, which is different from the parameters of IEMs and can be further simplified to reduce the state and action space of MDP. Furthermore, in the four individual equivalent models, IM and SM are dynamic individual equivalent model, EC and SPL are static individual equivalent model. The static combination of *Equi* can be neglected for smaller state and action space.

Based on the above considerations, the specific identification of ADEM steps are described as below:

1. Step1: MDP state space reduction
   The complete combination of *Equi* is listed as in Table 4.1. In the status vector of the IEM, when $c_i = 0$, then $M_i = 0$. As it can be seen from Table 4.1, when $c = [0\ 0\ 1\ 1]$, $c = [0\ 0\ 1\ 0]$, $c = [0\ 0\ 0\ 1]$ and $c = [0\ 0\ 0\ 0]$, the *Equi* is static model and it is not necessary to put in state and action space. Furthermore, the *Equi* is equal between $c = [1\ 1\ 1\ 1]$ and $c = [1\ 1\ 1\ 0]$, $c = [0\ 1\ 1\ 1]$ and $c = [0\ 1\ 1\ 0]$, $c = [1\ 0\ 1\ 1]$ and $c = [1\ 0\ 1\ 0]$, respectively, since the equivalent model of static power load is covered by the equivalent model of electronic converter. Hence the final combination of *Equi* is reduced to "IMSMECPL, IMSMPL, IMSM, IMECPL, IMPL, IM, SMECPL, SMPL, SM", which is a large state space reduction. The specific abbreviation meaning of these combinations can be found in Table 4.1.

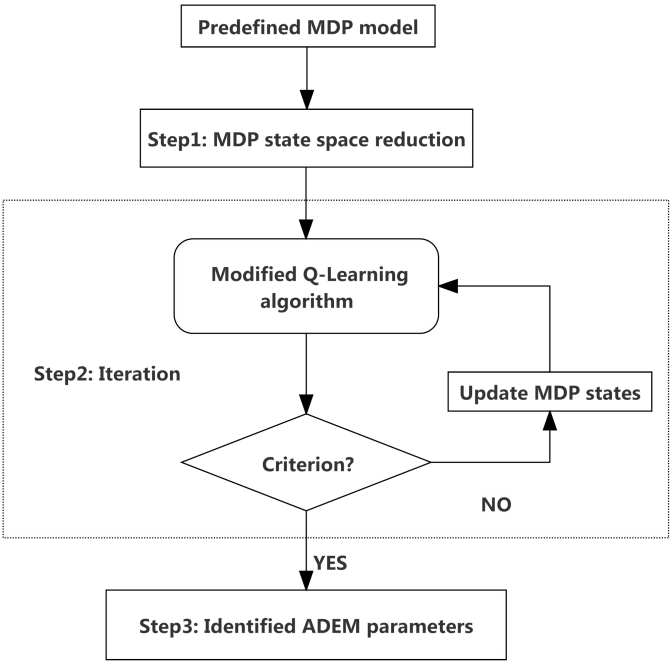

Figure 4.3: Identification flow of ADEM parameters.

Table 4.1: Combination of individual equivalent models

Equi_Nr	Equivalent Model	Status	Description
Equi_1	IMSMECPL	1 1 1 1	Combination of IM, SM, EC, PL
Equi_2	IMSMEC	1 1 1 0	Combination of IM, SM, EC
Equi_3	IMSMPL	1 1 0 1	Combination of IM, SM, PL
Equi_4	IMSM	1 1 0 0	Combination of IM, SM
Equi_5	IMECPL	1 0 1 1	Combination of IM, EC, PL
Equi_6	IMEC	1 0 1 0	Combination of IM, EC
Equi_7	IMPL	1 0 0 1	Combination of IM, PL
Equi_8	IM	1 0 0 0	Combination of IM
Equi_9	SMECPL	0 1 1 1	Combination of SM, EC, PL
Equi_10	SMEC	0 1 1 0	Combination of SM, EC
Equi_11	SMPL	0 1 0 1	Combination of SM, PL
Equi_12	SM	0 1 0 0	Combination of SM
Equi_13	ECPL	0 0 1 1	Combination of EC, PL
Equi_14	EC	0 0 1 0	Combination of EC
Equi_15	PL	0 0 0 1	Combination of PL

2. Step2: Iteration
   Iterate the Step2 if the results do not fit the criterion. Update all the parameters of Q-Learning. Update the state of MDP model.

3. Step3: ADEM Identification
   If the results fit the predefined criterion, then exit work flow with identified ADEM, otherwise update the state of MDP, then go back to Step2. The criterion can be set as the performance of the identified DEM in Step2 with threshold value.

4.4 Test Results

The test electrical systems are the CG1 and CG3 which are described in Section 3.6.1.1. The training and testing data are the responses of disturbances occurred at TL2, 4, 6, and TL3, 5, respectively.

Table 4.2: Parameters of the identified ADEM in CG1

Equi	IMSMECPL	IMSMPL	IMSM	IMECPL	IMPL	IM	SMECPL	SMPL	SM
Punishment	0.0348	0.1035	0.1121	0.033	0.2295	0.7798	0.0324	0.089	0.7845
Status	1 1 1 1	1 1 0 1	1 1 0 0	1 0 1 1	1 0 0 1	1 0 0 0	0 1 1 1	0 1 0 1	0 1 0 0
p1	-39.8867	-150.115	-260.145	-19.765	-262.13	-321.26	0	0	0
p2	0.025	0.025	0.025	0.025	0.025	0.025	0	0	0
p3	-6.0815	-126.001	-226.058	0	0	0	-1.3309	-511.797	-220.423
p4	-0.08	-0.08	-0.08	0	0	0	-0.08	-0.08	-0.08
p5	-1.984	-1.984	-1.984	0	0	0	-1.984	-1.984	-1.984
p6	-7.075	-52.1297	-79.065	-7.3959	-52.001	-52.442	0	0	0
p7	-8.94	-8.94	-8.94	-8.94	-8.94	-8.94	0	0	0
p8	-10.1687	-8.4719	-15.1486	0	0	0	-10.5913	204.8619	-257.395
p9	-1.9533	-53.5885	-63.2293	0.7806	-52.357	-52.507	0	0	0
p10	-1.2209	9.0614	-48.3798	0.7105	0.0628	4.0762	0	0	0
p11	0.0049	9.5229	9.9933	0	0	0	0	45.3616	-7.0499
p12	0.0096	-1.6808	14.1577	0	0	0	0.0009	-3.1237	3.5689
p13	18.5901	0	0	19.1171	0	0	18.8983	0	0
p14	22.4464	25.3347	8.3706	22.7907	22.654	8.6503	22.8074	23.8398	12.248
p15	-10.0732	7.6049	0	-10.1555	-1.8056	28.186	-10.2203	8.7065	0
p16	-14.1506	-17.1414	0	-14.3826	-14.494	0	-14.5178	-15.6977	0
p17	-222.623	-223.054	-223.142	0	0	0	-222.589	-205.361	-8.4786

4.4.1 Testing in CG1

After processing the measured training data of CG1 into Q-Learning identification flow as in Section 4.3.2, the best states of each *Equi* in CG1 are shown in Table 4.2. The best states have the smallest punishment value in the combinations, separately in each combination.

As can be seen from Table 4.2, the combination of "SMECPL" has the smallest punishment value, therefore, it is considered as the ADEM. "IMSMECPL" and "IMECPL" have a punishment value close to the one of "SMECPL", which means they may also be the dynamic equivalent models. "IM" and "SM" have the largest punishment value, which means their performance are the worst. The punishment value of the other combinations of IEMs are in the middle of the largest value and smallest value. In the environment of CG1, the punishment values are small when the *Equi* includes the equivalent model of EC, otherwise, the punishment values become much bigger. The combination of "XX+EC" is the preferred one, where "XX" means dynamic individual equivalent models.

The identified *Equi* are tested with the measured data when the disturbances occur at TL3, 5, respectively. The performance of each *Equi* is shown in Fig. 4.4.

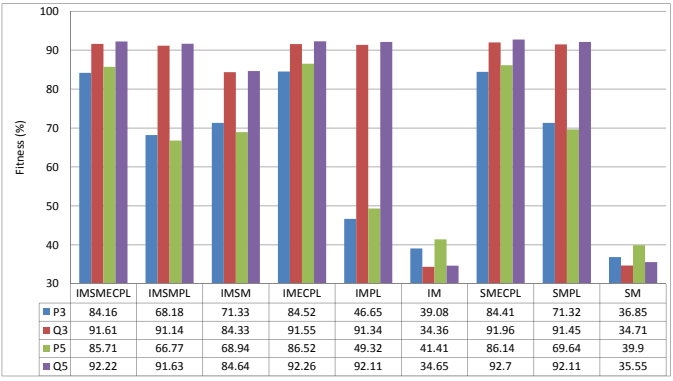

	IMSMECPL	IMSMPL	IMSM	IMECPL	IMPL	IM	SMECPL	SMPL	SM
P3	84.16	68.18	71.33	84.52	46.65	39.08	84.41	71.32	36.85
Q3	91.61	91.14	84.33	91.55	91.34	34.36	91.96	91.45	34.71
P5	85.71	66.77	68.94	86.52	49.32	41.41	86.14	69.64	39.9
Q5	92.22	91.63	84.64	92.26	92.11	34.65	92.7	92.11	35.55

Figure 4.4: Performance of ADEM in CG1.

"P3" and "Q3" denote active and reactive power Fitness value under disturbance at TL3, respectively. "P5" and "Q5" denote active and reactive power Fitness value under disturbance at TL5, respectively.

As it can be seen in Fig. 4.4, the combination of the "IMSMECPL","IMECPL", and "SMECPL" have better performance. The Fitness value of the identified ADEM, "SMECPL", are 84.41 % and 91.96 % for active and reactive power under disturbance at TL3, 86.14 % and 92.7 % for active power and reactive power under disturbance at TL5, respectively. The measured and estimated values have a good agreement. The combinations of "IMSMECPL" and "IMECPL" have similar performance to the "SMECPL", while the combination of "IM" and "SM" has a poor performance. In the rest of combinations, "IMSMPL", "IMSM", "IMPL", and "SMPL" have good performance for reactive power, but weak performance for active power. The reason is $p_{13} = 0$, which is an important coefficient of the input variable for the value of active power.

The specific responses of PCC are shown in Fig. 4.5. The MP-3, MQ-3 presents the measured active and reactive power that corresponds to the disturbance at the TL3, separately. The EP-3 and EQ-3 are their estimated responses for active and reactive power, in relation to the disturbance at the TL3. The same y-axis definitions of TL3 are applied at TL5 for the measured and estimated responses. As it can be seen in Fig. 4.5, the estimated responses are close to the measured ones.

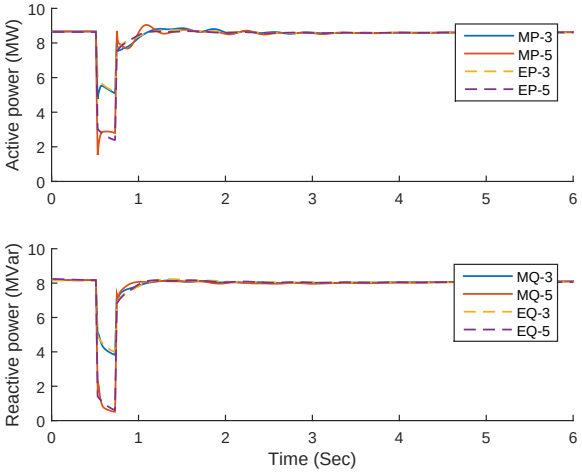

Figure 4.5: Measured and estimated responses of PCC with ADEM in CG1.

4.4.2 Testing in CG3

After processing the measured training data of CG3 into ADEM identification flow as in Section 4.3.2, the best states of each *Equi* in CG3 are shown in Table 4.3, which have the smallest punishment value, respectively.

As it can be seen from Table 4.3, the model of "IMSMECPL" has the smallest punishment value, which is considered as the ADEM. Different from the results in CG1, "IMSMECPL" is the only one with a small punishment value: the punishment value of the other combinations is at least two times larger than the punishment value of the "IMSMECPL". "IM" and "SM" have a similar situation as in CG1: they both have the largest punishment value. From the punishment value point of view, a conclusion for the CG3 environment can be that the higher the number of individual equivalent models which are included in the *Equi*, the better performance of the dynamic equivalent model. The lower the number of individual equivalent models which are combined in the *Equi*, the worse is the performance of the dynamic equivalent model.

With testing data from disturbances occur at TL3, 5, the performance of each combination of *Equi* is shown in Fig. 4.6. "P3" and "Q3" denote active and

Table 4.3: Parameters of the identified ADEM in CG3

Equi	IMSMECPL	IMSMPL	IMSM	IMECPL	IMPL	IM	SMECPL	SMPL	SM
Punishment	0.0421	0.1918	0.222	0.1035	0.3774	1.0055	0.1083	0.165	0.8961
Status	1 1 1 1	1 1 0 1	1 1 0 0	1 0 1 1	1 0 0 1	1 0 0 0	0 1 1 1	0 1 0 1	0 1 0 0
p1	-9.8966	-95.9433	-250.977	-12.6462	-12.646	-301.43	0	0	0
p2	0.025	0.025	0.025	0.025	0.025	0.025	0	0	0
p3	-9.8497	-85.7722	-202.044	0	0	0	-12.6847	-649.192	-129.228
p4	-0.08	-0.08	-0.08	0	0	0	-0.08	-0.08	-0.08
p5	-1.984	-1.984	-1.984	0	0	0	-1.984	-1.984	-1.984
p6	-7.5538	-47.8462	-82.0842	-7.3905	-7.3905	-50.73	0	0	0
p7	-8.94	-8.94	-8.94	-8.94	-8.94	-8.94	0	0	0
p8	-0.8236	5.3935	-26.669	0	0	0	-260.56	195.1385	-288.542
p9	1.8804	-42.7849	-73.7641	0.2878	0.2878	-50.55	0	0	0
p10	11.6636	32.6381	-36.5265	1.4789	1.4789	6.5331	0	0	0
p11	-0.0562	8.0907	12.5645	0	0	0	0	74.0219	-5.1819
p12	-0.3775	-6.1197	10.3334	0	0	0	0.0215	-45.8235	1.5809
p13	23.8606	0	0	23.0174	0	0	22.9691	0	0
p14	27.2215	37.1822	8.9003	21.8415	21.8415	9.1003	21.5594	34.8542	10.5707
p15	-15.0461	7.8831	0	-14.1924	-14.192	28.186	-14.1938	8.6106	0
p16	-18.7902	-28.3299	0	-12.8404	-12.84	0	-12.891	-26.679	0
p17	-222.9111	-223.355	-222.022	0	0	0	-50.2547	-194.787	76.6835

reactive power Fitness value under disturbance at TL3, respectively. “P5” and “Q5” represent active and reactive power Fitness value under disturbance at TL5, respectively.

As it can be seen in Fig. 4.6, the combination of “IMSMECPL” has the best performance and it is the identified ADEM. The “IM” and “SM” have the worst performance as each Fitness value of active and reactive power is less than 50 %. “IMECPL” and “SMECPL” have better performance, but the Fitness value of their reactive power is less than 80 %. The performance of the other combinations, “IMSMPL”, “IMSM”, “IMPL”, and “SMPL”, is in the middle, with a Fitness value of active and reactive power between 46.02 % and 79.9 %. The test results in Fig. 4.6 match with the conclusion that the more combination of IEMs, the better performance of the *Equi* model.

The specific responses are shown in Fig. 4.7. “MP-3,5, EP-3,5, MQ-3,5, EQ-3,5” have the same denotations as Fig. 4.5. Fig. 4.7 shows the estimated active and reactive power match well with the measured ones, respectively.

There are three *Equi* DEMs that have good performance in CG1, but only one *Equi* DEM has good performance in CG3. The difference of equivalence results between CG1 and CG3 comes from the different topologies of the two ADNs.

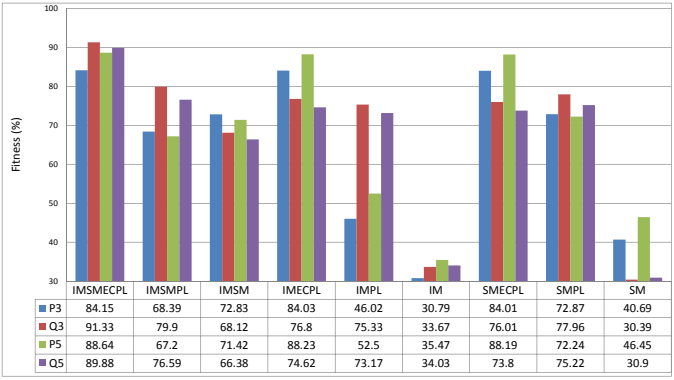

	IMSMECPL	IMSMPL	IMSM	IMECPL	IMPL	IM	SMECPL	SMPL	SM
P3	84.15	68.39	72.83	84.03	46.02	30.79	84.01	72.87	40.69
Q3	91.33	79.9	68.12	76.8	75.33	33.67	76.01	77.96	30.39
P5	88.64	67.2	71.42	88.23	52.5	35.47	88.19	72.24	46.45
Q5	89.88	76.59	66.38	74.62	73.17	34.03	73.8	75.22	30.9

Figure 4.6: Performance of ADEM in CG3.

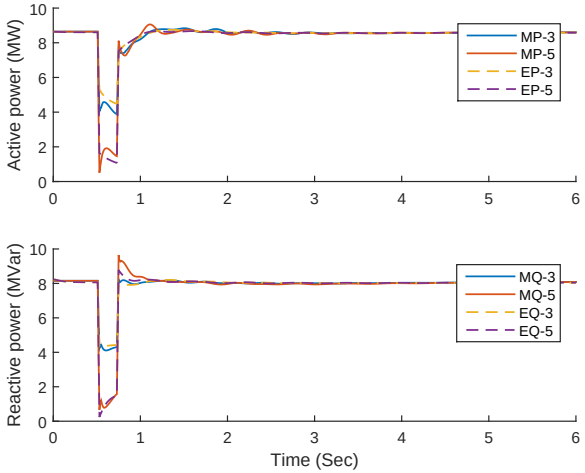

Figure 4.7: Measured and estimated responses of PCC with ADEM in CG3.

Their specific topologies and parameters can be found in Fig. 3.3 and Table 3.1. In conclusion, different topologies of ADNs may have different order ADEMs that can be identified by an adaptive structure dynamic equivalent approach.

4.5 Summary

After discussing the available lower order dynamic equivalent models for active distribution networks, an equivalence problem is formulated into the form of Markov decision process problem in this chapter. The related MDP knowledge is introduced, such as states, actions, and reward function. Then the MDP problem is solved by modified Q-Learning, which is based on reinforcement learning. To reduce the exploration time, the state and action space is reduced, the Q-value is updated by calculating the gradient value of the objective function. The statuses are identified and then the internal unknown parameters of the equivalent models are tuned from the environment (i.e. the measured data). Finally the suitable equivalent models are identified according to punishment value.

The ADEM approach uses the approximation equations of the physical models as equivalent model, and also the knowledge of MDP and Q-Learning for parameter identification. It can be directly applied to online applications while keeping not only a simple equivalent model form but also flexible model structure.

Chapter 5

Random Forest-Based Dynamic Equivalent Approach

5.1 Introduction

As presented in Section 2.4, a physical-based model approach is impossible to derive when proper data about the actual structure are missing. Furthermore, an artificial model-based approach may suffer from accuracy problems during identification when the measured data includes strong behaviors. In this situation, a model-free approach may be advantageous.

As presented in Section 2.3, the RNN models are prone to over-fitting [78] and the setting of RNN configurations, such as the number of hidden layers, the type of activation functions and the number of nodes, are difficult [78]. In addition to that, RNNs do not quantify the input importance for the training result. The RNN methods may contain sets of unimportant inputs, which are not necessary but still consume computation capacity in the training.

To overcome the above limitations, a random forest-based dynamic equivalent model is proposed in this chapter. It is a new type of MFA model which is based on random forest algorithm [79].

5.2 Random Forest Basis

The RF is a combination of independent decision tree predictors [80], which grow in randomly selected training sets and have the same distribution for each

tree. Initially, it was proposed for classification and regression in [79]. In this paper, a classic definition of RF is introduced as:

> A random forest is a classifier consisting of a collection of tree-structured classifiers $h(x,\Theta k), k = 1, ...,$ where the Θk are independent identically distributed random vectors and each tree casts a unit vote for the most popular class at input x. [79]

5.2.1 Random Forest Algorithm

The architecture of the RF is shown in Fig. 5.1. On the top, there is a root node that contains all the measured data. In the middle, there are many nodes that consist of number of independent trees. The individual trees select the training data from measured data with randomness of Bagging [79, 81]. The nodes randomly sample a certain number of variable subsets from the selected training data of the individual trees, separately. At the end terminal, the RF output is an average value of the predicted outputs from the individual trees.

The individual trees are growing by splitting nodes from top to bottom [82]. The splitting is started at the root node. Then it distributes the measured data to the individual trees with the Bagging approach. Later, the nodes split repeatedly until the specific stop criterion is met. The specific work flow is shown in Fig. 5.2. It has six steps in the work flow of the individual tree. For a better description, it is assumed that there are N number of measured pairs of inputs and outputs, n number of trees in the RF, and each node selects m number of subsets.

Step1: Bagging selection

In RF, the measured data is divided into groups for each tree: training and testing data group, also named in-bag and out-of-bag (OOB) data in Bagging [79]. The training data is used to train the RF model, the testing data is used to internally evaluate the performance of the trained model. The selection of the two data groups is based on Bagging, which enhances predicting accuracy and gives ongoing estimates of the generalization error for improving the RF [79]. It randomly takes a sample from the measured data and puts it back, then repeats the process again and again until the sample number equals the measured number, N. If the sample number is

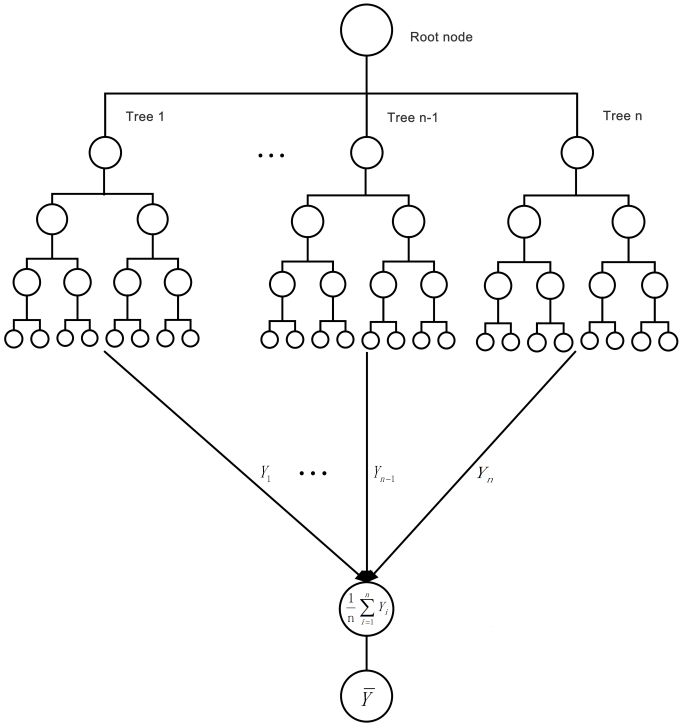

Figure 5.1: Random forest architecture.

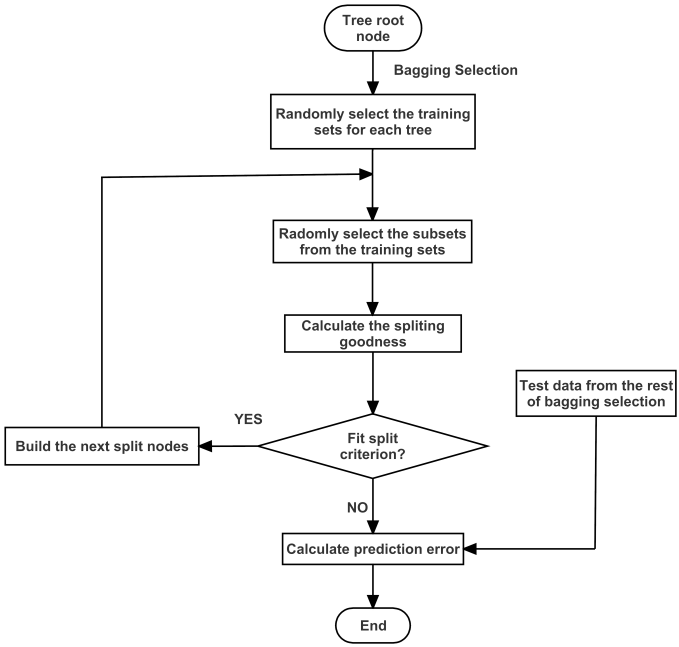

Figure 5.2: Work flow of individual tree.

big enough, the selected samples are around two-thirds of the measured data, the unselected is one-third since there is $\lim_{N\to\infty}(1-\frac{1}{N})^N \approx \frac{1}{3}$. N is the defined sample number of measured data. Note that a sample is a pair of inputs and outputs for supervised learning.

Step2: Subset selection

Randomly select m types of inputs and their corresponding outputs from the training sets for a tree node.

Step3: Calculate splitting goodness

Calculate splitting goodness of each input variable with the selected subsets, define splitting threshold, then choose the best split variable to be split. In principle, sets of methods can be used for the goodness calculation [82, 83]. In RF, the Gini method is used for the calculation [79, 84]. Gini index measures the divergence between the probability distributions of the target splitting inputs' values. The evaluation criteria for selecting the splitting input is defined as Gini gain [82].

Step4: Decide to split or not

According to the calculated splitting goodness, check whether the best splitting input variable fits for the criterion. If yes, then split it and go to next splitting loop until the end of the growing of the tree. Otherwise, evaluate the node performance by calculating the prediction error with the testing data.

Note that each node chooses one input variable to split and the splitting is dividing the training sets, not the types of input and output pairs. The more splitting, the less quantity of training sets for the next splitting is provided. Each tree takes the same procedure, in the end, using the average of the individual tree's outputs as the final RF output. After training, only the splitting of variable type and threshold value is kept at each node. During the testing, with these trained variable type and threshold value, each node will guide the testing inputs to the terminal nodes for outputs.

5.2.2 Important Features

There are three important features for the RF: non-over-fitting, out-of-bag error estimation, and variable importance.

Non-Over-Fitting

Over-fitting is a situation in which the trained model is much more complex than the real relationship between input and output training data. The over-fitting usually occurs when there are many noises and outliers in the training data. Then the model begins to memorize the noises and outliers rather than learn the real input-output relationship. RF avoids the over-fitting problem because of the Strong Law of Large Numbers and the random selection of the training sets [79]. The randomness is required for the selection of training sets for the individual trees and the sub-training sets for the nodes.

OOB Error Estimation

The OOB error estimation is used to evaluate the performance of the trained RF model. As described in Section 5.2.1, one-third of measured pairs that are not selected during Bagging selection are used to test the trained RF model. The OOB input vector X is propagated to the trained RF to get the estimated output, $\hat{Y}$. The mean square error (MSE) is calculated as OOB error of the RF model, represents as Equation 5.1 [79]:

$$OOB_{error} = \frac{1}{k}\sum_{i=1}^{k}(\hat{Y}_i - Y_i)^2 \tag{5.1}$$

Here, Y_i and $\hat{Y}_i$ are the i^{th} measured and estimated output value in OOB data, respectively. k is the number of OOB data of the RF. To estimate the performance of individual tree and the dependence between the trees, the strength and correlation is also introduced [79].

Variable Importance

The variable importance indicates which inputs are the most relevant variables for the training. It permutes one variable of the inputs in OOB data, the rest of inputs stay the same. Then, the changed sets of data propagate on the trained RF. Later, the difference for each tree between the MSEs that are triggered from the original and permuted inputs is calculated. Finally, the differences of the individual trees are averaged. The specific

criterion of variable importance is defined in Equation 5.2 [79, 85, 86]:

$$VI = \frac{1}{n}\sum_{j=1}^{n}(OOB_{error\,j}(X_h, permuted) - OOB_{error\,j}) \tag{5.2}$$

Here VI is the importance value of variable X_h which is permuted and n is the number of individual trees. $OOB_{error\,j}(X_h, permuted)$ is the MSE value triggered by the permuted OOB input data of tree j. $OOB_{error\,j}$ is the MSE value triggered by the original OOB input data of tree j. The specific $OBB_{error\,j}(X_h, permuted)$ is represented as in Equation 5.3, where kk is the number of OOB data in tree j.

$$OBB_{error\,j}(X_h, permuted) = \frac{1}{kk}\sum_{z=1}^{kk}(\hat{Y_z}(X_h, permuted) - Y_z)^2 \tag{5.3}$$

The variable importance of other variables can be obtained by repeating the above process. When the value of variable importance is bigger than the others, it can be considered more influential for the training.

5.3 Random Forest-Based Dynamic Equivalent Model

5.3.1 Architecture

Based on the theoretical analysis of RF features in the above, a general RF-DEM is designed as in Fig. 5.3. The inputs are composed of the measured input variables and the feedback variables from the predicted outputs. The feedback variables are used for capturing the dynamics of the external part of the sub-system. The model constructs from finite number of trees, each tree is independent and composed of number of nodes. In the above RF model, the only two parameters are required:

1. The number of trees, n, as defined in Section 5.2.1.

2. The number of subsets for each node, m, as defined in Section 5.2.1.

From experiment experience, n is selected in the range between 5 and 225, m is selected in the range between 1 and 7. 7 is the maximum number of input variables that measured from experiment. The range values are set to find an

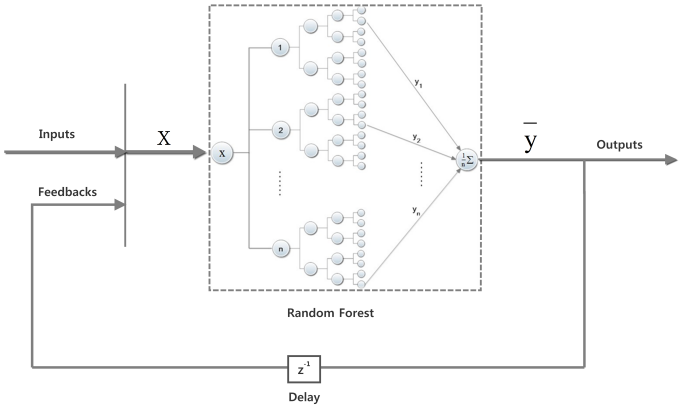

Figure 5.3: Random forest-based dynamic equivalent model.

optimal RF model in the further impacts analysis of number of trees, number of subsets, and variable importance in Sections 5.4.1, 5.4.2, and 5.4.3, respectively.

In the experiment of this chapter, the transmission system remains the same as in Section 3.5.1, the active distribution network is the electrical system of CG1 in Section 3.6.1. For training, the input of the RF-DEM consists of the measured inputs and the feedback variables of the outputs. In detail, the measured inputs are voltage and current magnitude per unit, electrical frequency per unit, and differential value of voltage and frequency. The output of the RF-DEM consists of active and reactive power at PCC. The active and reactive power in a previous time-step are also used as one part of inputs. The variables are described in Table 5.1.

Table 5.1: Variables of input and output vector

Nr.	Variable	Description
1	V	Voltage magnitude in p.u.
2	I	Current magnitude in p.u.
3	dv	Voltage differential value
4	f	Electrical frequency in p.u.
5	df/dt	Frequency differential value
6	P0	Active power at previous time-step
7	Q0	Reactive power at previous time-step
8	P	Active power
9	Q	Reactive power

5.3.2 Equivalent Training

The procedure of training the RF model is shown in Fig. 5.4. The training sets are composed of inputs and corresponding outputs at the PCC. According to the pre-defined test parameter ranges, the configuration of the input vector and the number of trees and subsets are repeatedly updated until there are no new configurations. The toolbox of RF for implementation is adopted from [87]. The number of trees are set as 5, 25, 50, 75, 100, 125, 150, 175, 200 and 225, the number of subsets are set as 1, 2, 3, 4, 5, 6, and 7. The input vectors are updated by the different combinations of measured input variables and the feedbacks of active and reactive power.

The complete RF-DEM training includes four steps: the optimization of the number of trees and subsets, the analysis of the variable importance, as well as the reduction of the input variables. Each step requires the RF process presented in Section 5.2.1. During the training procedure there are two kinds of randomness: one from the selection of training data for the individual trees and the other from the selection of subsets for each node. To reduce the randomness influence for the results, all the parameters to be investigated are repeated a certain number of times, separately. Later their average results are compared. The specific steps are described as:

Step1: Optimize the number of trees

Firstly set up the to-be-investigated number of the trees for RF-DEM. As shown in Fig. 5.4, then repeat "RF algorithm" certain times for each

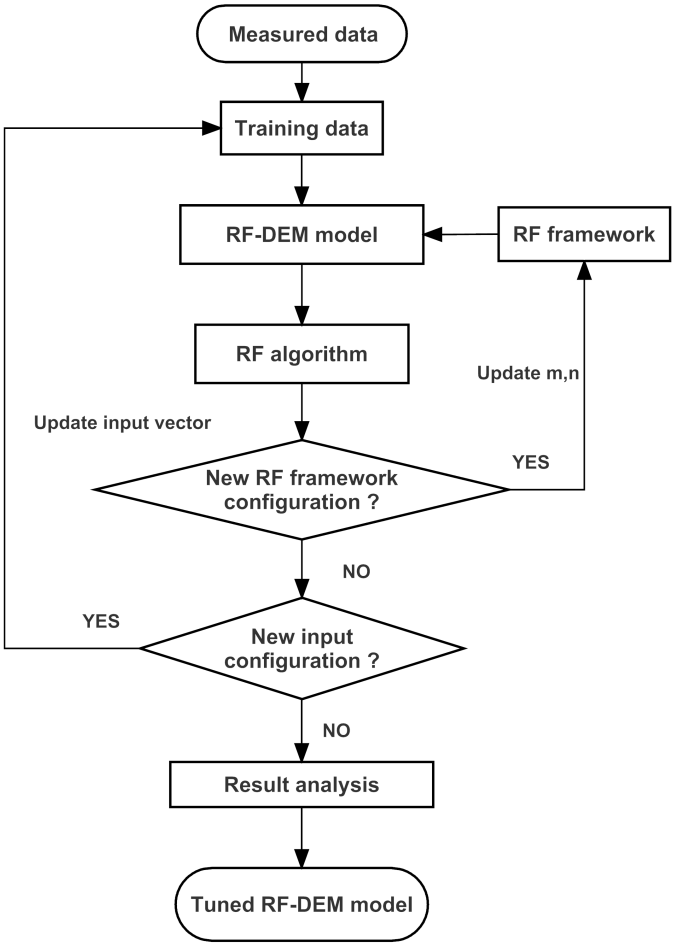

Figure 5.4: The training flow of RF-DEM.

investigated number of trees for reducing the randomness influence to the results. The "RF algorithm" details are described in Section 5.2.1. Finally compare the average of MSE value of the investigated RF model, the RF model with the smallest MSE value has the best number of trees.

Step2: Optimize the number of subsets

In the beginning, set up the to-be-investigated number of the subsets for RF-DEM. Later repeat the "RF algorithm" certain times for each investigated number of subsets to reduce the randomness influence to the results. In the end, compare the average MSE value of the outputs of the investigated RF model, the RF model with the smallest MSE value has the best number of subsets.

Step3: Variable importance analysis

Analyze the importance value of individual variables. Keep the most important variables and leave out the non-significant variables as inputs for further training.

Step4: Optimize the input variables

The variables that have similar importance value may be coupled. They should be separated and combined together as inputs for further analysis. Set the variables with similar importance values as inputs for training, individually. Again set the combinations of different variables which have similar importance value for training. If the separated and combined training have very similar results, which means these variables are coupled, then keep one of the variables and leave out the others. Repeat the similarity checking for the other variables until get the smallest size of uncoupled input variable vector but with the same accuracy level results.

5.4 Analysis and Test Results

The goal of RF analysis is to find an optimal configuration of the RF model. The good choice is fewer input vectors, lower correlation between trees but stronger strength of individual trees [79]. The training and testing data are the responses of disturbances occurred at TL2, 4, 6 and TL3, 5, respectively. The impact of number of trees and subsets as well as the effect of input vectors on

the trained results are analyzed. According to the analysis results, an optimal RF-DEM is obtained for further comparison with new sets of test data.

5.4.1 Impact of Number of Trees

The size of a forest means the number of trees n in the RF, which has significant influence on the training results [79]. Generally, an increasing number of trees improves the accuracy of the RF model. However, with large number of trees, the correlation between trees will be also high, which can decrease the accuracy of the results. Furthermore, the RF model will become too large and complex when the trees are infinitely growing and the growing size of RF takes the cost of increasing the training and testing time.

In order to identify the optimal number of random trees (n) in the forest, n is varying from 5 to 225 in this experiment and m is set to 3 by the suggestion of [79, 81]: $m < 1/3\ M$ where M is the total number of the input types. To reduce the randomness influence of the random selection of the training sets and subsets, all the summarized results are averaged over one hundred training results for the analysis. The results are shown in Fig. 5.5, the horizontal axis are the number of trees, the vertical axis is the MSE error value, "MSE-P" and "MSE-Q" are the MSE error values of active and reactive power, respectively.

As it can be seen in Fig. 5.5, the number of 150 and 225 trees have good results for active and reactive power MSE error. But considering the size of RF model, the number of 150 trees is selected as the best number of trees.

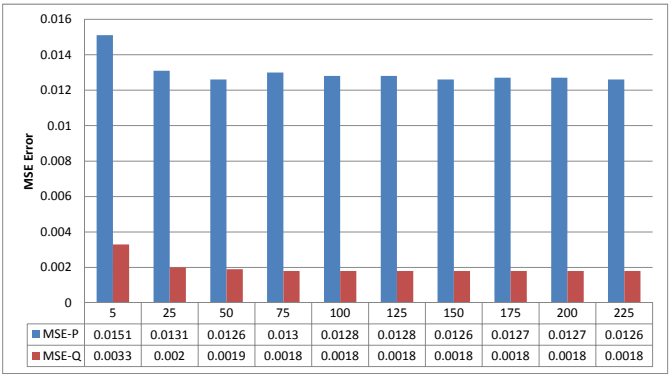

	5	25	50	75	100	125	150	175	200	225
MSE-P	0.0151	0.0131	0.0126	0.013	0.0128	0.0128	0.0126	0.0127	0.0127	0.0126
MSE-Q	0.0033	0.002	0.0019	0.0018	0.0018	0.0018	0.0018	0.0018	0.0018	0.0018

Figure 5.5: Impact of number of trees.

5.4.2 Impact of Number of Subsets

As one of the only two setting parameters in RF, the number of subsets at each node, m, also has big impacts on the training results [79]. When the number of subsets is too large, strength of individual trees increases, but correlation between trees also increases, which can decrease the accuracy of training results. The strength represents prediction-ability of individual trees, the stronger strength, the more accuracy a RF model. The correlation represents similarity between trees, the higher correlation, the less accuracy a RF model. When the number of subsets becomes too small, correlation between trees decreases, but strength of individual trees decreases, which can decrease the accuracy of training results. In another words, the stronger strength and weaker correlation, the better a RF model, a right number of subsets is important for the RF model.

The results are shown in Fig. 5.6, the horizontal axis is the number of the subsets for each node, and the others are defined the same as in Fig 5.5.

According to the results in Fig. 5.6, the number of 1 subset has the best performance. In the test cases, there are only seven inputs that may have strong coupling relationships. Hence, the number of the subsets cannot be bigger, otherwise the correlation between trees become high, which impacts on the accuracy of outputs. The RF model with one subset has strong strength and low correlation, therefore, one has selected as the best number of subsets.

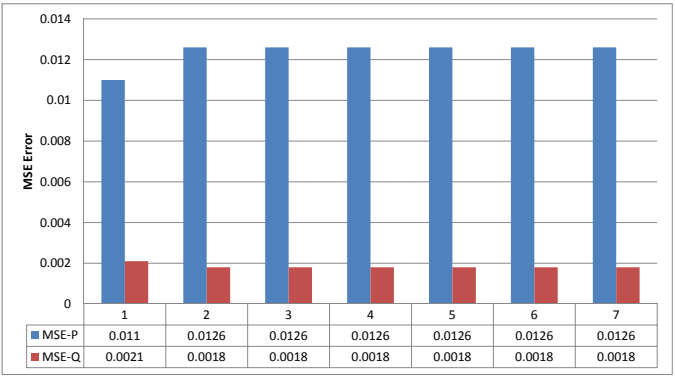

Figure 5.6: Impact of number of variable subsets.

5.4.3 Impact of Variable Importance

Variable importance is an index that quantifies the relationship between input and output variables. The index plays a significant role in reduction of input variables, which keeps the important but deletes the non-significant input variables. The reduction of input variables simplifies RF model architecture and reduces computation time.

The results are shown in Fig. 5.7, the horizontal axis are the input variables, such as the voltage and current magnitude in per unit, electrical frequency in per unit, differential value of voltage and frequency, active and reactive power value at one previous time step. The vertical axis is the importance value as defined in Section 5.2.2. VI-P and VI-Q are the variable importance of active and reactive power, respectively. As it can be seen from the results, the variables of voltage and current magnitude, the differential value of voltage and the feedback of active power have important influence on the predicted outputs. The impacts on reactive power are more than on active power. However, there are strong coupling correlations between the electrical variables. Hence, further analysis of variable combinations and test cases are considered in the next section.

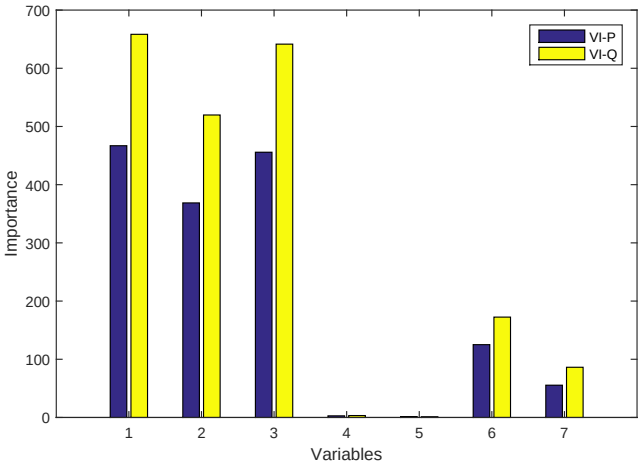

Figure 5.7: Impact of variable importance.

5.4.4 Impact of Combination of Input Variables

In this case, seven RF models are built by means of different combinations of input variables and the feedback from active and reactive power. The results are shown in Fig. 5.8, the horizontal axis is the different combinations of the variables as the inputs of the RF models, the vertical axis is MSE error of active and reactive power, respectively. As it can be seen in Fig. 5.8, the combinations with current have a good performance in active power: 2-6-7, 1-2-6-7, etc. These combinations with voltage or voltage differential value have a good performance in reactive power: 1-6-7, 3-6-7, etc. The performance between 1-6-7 and 3-6-7 as well as between 1-2-6-7 and 2-3-6-7 are similar, which are caused by the strong correlation of the voltage and its derivative. Considering the voltage differential value is not commonly measured and the current is prone to have more noise and dynamics, therefore, voltage and feedbacks of active and reactive power are selected as the input vector.

According to the above analysis, an optimized RF-DEM is obtained: $n = 150$, $m = 1$, voltage and feedbacks of active and reactive power as the input variables.

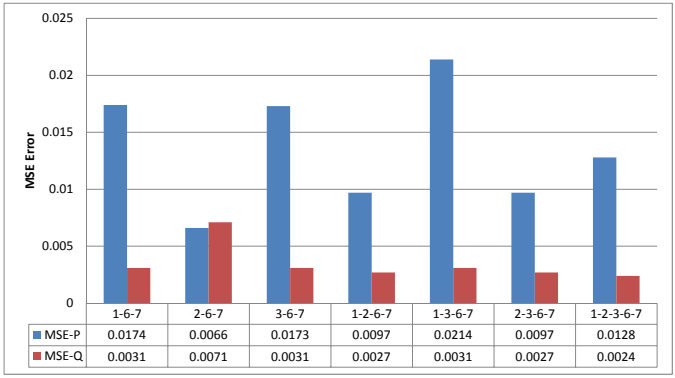

Figure 5.8: Impact of combination of input variables.

5.4.5 Test Results

To test the trained RF-DEM model, the measured data from disturbances occurred at TL3, 5 is applied to evaluate the performance of the trained model. The results are shown in Fig. 5.9, MP-3 and EP-3 are the measured and estimated active power corresponding to the disturbance occurred at TL3, MQ-3 and EQ-3 are the measured and estimated reactive power corresponding to the disturbance occurred at TL3, respectively. Similar definition applies for MP-5, EP-5, MQ-5 and EQ-5 to compare the responses of disturbance occurred at TL5. As it can be seen from the curves in Fig 5.9, there is a good agreement between the measured and estimated values for both disturbances. The specific quantities of MSE, which are defined in Section 5.2.2, are 0.0121, 0.0021 for the active and reactive power under disturbance occurred at TL3, respectively. The MSE of active and reactive power under disturbance occurred at TL5 are 0.0226 and 0.0028, respectively.

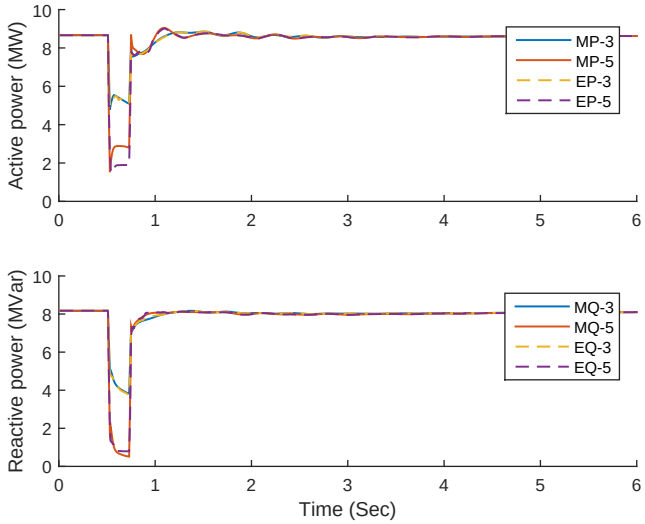

Figure 5.9: Measured and estimated responses of PCC with RF-DEM in CG1.

5.5 Summary

In this chapter, four cases are studied to analyze the impacts of the number of trees and subsets, the variable importance and the combination of input variables. The four features have significant influence on the performance of the RF-DEM model. There are two important parameters in the internal framework of the RF model: the number of trees, n, and number of subsets at each node, m. The optimal number of trees and subsets are identified for this example: 150 and 1, respectively. For further simplification of the RF-DEM model, the variable importance takes big roles in the selection of input variables. Voltage, current, voltage derivative and feedbacks from outputs are the most important variables. To reduce the coupling relationship influence of the electrical variables, the combinations of input variables for training are also studied. Considering practical applications, voltage and feedbacks of the outputs are selected for input vector.

As a conclusion, $n = 150$, $m = 1$, the combination of voltage, feedbacks of

active and reactive power as input variables, are the best parameters for the RF-DEM.

Chapter 6

Comparison and Validations, Applications

6.1 Introduction

This chapter tests the proposed dynamic equivalent models under different scenarios, such as distributed generator combinations, fault locations and penetration levels. The indicators for validation include different fault durations, system operation points and fault levels.

6.2 Test Scenarios

In this section, three test scenarios are set up to compare the performance of the three proposed models: fixed-structure dynamic equivalent model, adaptive dynamic equivalent model, and random forest-based dynamic equivalent model. The scenarios include DG combinations, fault locations and penetration levels of DGs.

6.2.1 Different DG Combinations

In the DG combination scenario, the measured data for training are recorded when disturbances occur at the middle of TL1, 3, 5, where the fault locations have the long, middle and short distances from the measured point of common coupling. Testing data are defined as response data of the disturbances occurred

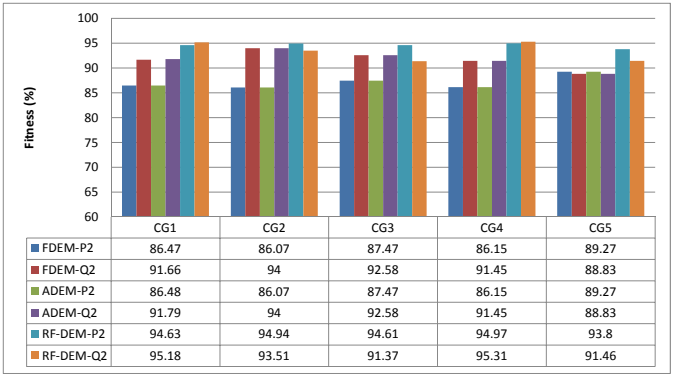

	CG1	CG2	CG3	CG4	CG5
FDEM-P2	86.47	86.07	87.47	86.15	89.27
FDEM-Q2	91.66	94	92.58	91.45	88.83
ADEM-P2	86.48	86.07	87.47	86.15	89.27
ADEM-Q2	91.79	94	92.58	91.45	88.83
RF-DEM-P2	94.63	94.94	94.61	94.97	93.8
RF-DEM-Q2	95.18	93.51	91.37	95.31	91.46

Figure 6.1: Performance of the proposed models in DG combination scenario with fault at TL2.

at the middle of TL2, 6, where the locations are far away and close to the measured PCC, respectively. These disturbance locations for the training and testing data are opposite to the test scenario in Section 3.6.1.1.

After processing the proposed equivalent models and training data as described in Section 3.4.2, 4.3.2 and 5.3.2, the testing data are used to compare the identified models. The performance of proposed FDEM, ADEM and RF-DEM are shown in Fig. 6.1 and 6.2 for faults occurred TL2, 6. These results are presented in the bar charts and their relevant values are listed at the bottom. The vertical axis is the Fitness value of active and reactive power. The horizontal axis is the five groups of DG combinations, which details are in Section 3.6.1.1.

According to the results in Fig. 6.1 and 6.2, all the Fitness values are above 80 %, which can be considered has a good agreement between estimated and measured values. In CG2, CG3, CG4, CG5, the Fitness value for the FDEM and ADEM are the same since the ADEM approach made decision of selecting the same model as FDEM. While in CG1, the ADEM selects the combination of SM, EC and SPL.

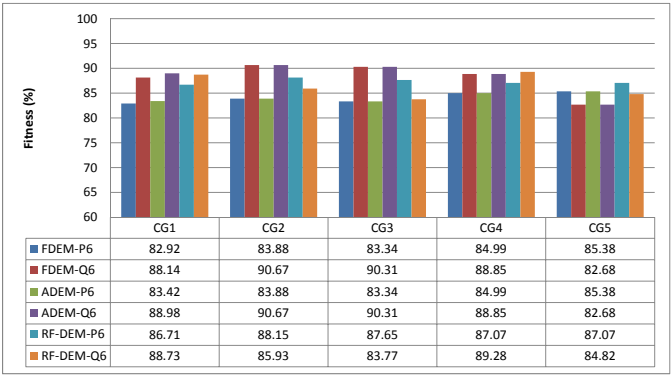

	CG1	CG2	CG3	CG4	CG5
FDEM-P6	82.92	83.88	83.34	84.99	85.38
FDEM-Q6	88.14	90.67	90.31	88.85	82.68
ADEM-P6	83.42	83.88	83.34	84.99	85.38
ADEM-Q6	88.98	90.67	90.31	88.85	82.68
RF-DEM-P6	86.71	88.15	87.65	87.07	87.07
RF-DEM-Q6	88.73	85.93	83.77	89.28	84.82

Figure 6.2: Performance of the proposed models in DG combination scenario with fault at TL6.

6.2.2 Different Fault Locations

In the fault location scenario, the original ADN for testing equivalent models stays the same as CG1, which details are in Section 3.6.1.1, the ADEM is identified as the combination of SM, EC and SPL. The fault locations are the same as in Section 3.6.2. However, the training and testing data are exchanged, which means the previous training and testing data of Section 3.6.2 is used for testing and training, respectively. The specific fault locations for training and testing models are listed in Table 6.1.

The performance of the identified FDEM, ADEM and RF-DEM is shown in Fig. 6.3, 6.4 and 6.5. Test1 is the test with the measured data from disturbances at TL4, TL2, TL2, TL1, TL1 for FG1, FG2, FG3, FG4, FG5, respectively. Test2 is the test with the measured data from disturbances at TL5, TL5, TL3, TL3, TL2 for FG1, FG2, FG3, FG4, FG5, respectively. Test3 is the test with the

Table 6.1: Different fault locations

	FG1	FG2	FG3	FG4	FG5
Training data	TL1, 2, 3	TL1, 3, 4	TL1, 4, 5	TL2, 4, 6	TL4, 5, 6
Testing data	TL4, 5, 6	TL2, 5, 6	TL2, 3, 6	TL1, 3, 5	TL1, 2, 3

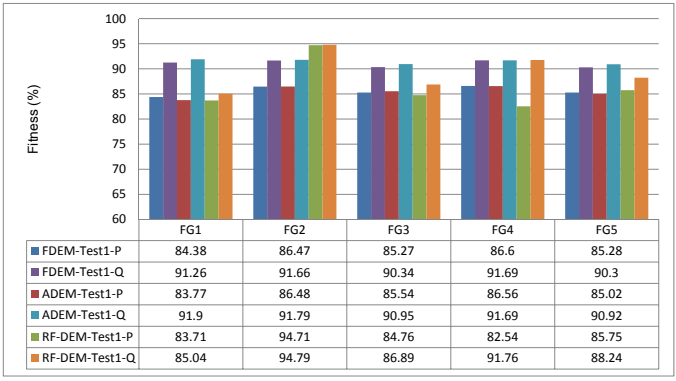

	FG1	FG2	FG3	FG4	FG5
FDEM-Test1-P	84.38	86.47	85.27	86.6	85.28
FDEM-Test1-Q	91.26	91.66	90.34	91.69	90.3
ADEM-Test1-P	83.77	86.48	85.54	86.56	85.02
ADEM-Test1-Q	91.9	91.79	90.95	91.69	90.92
RF-DEM-Test1-P	83.71	94.71	84.76	82.54	85.75
RF-DEM-Test1-Q	85.04	94.79	86.89	91.76	88.24

Figure 6.3: Performance of the proposed models in Test1.

measured data from disturbances at TL6, TL6, TL6, TL5, TL3 for FG1, FG2, FG3, FG4, FG5, respectively.

As it can be seen in Fig. 6.4, 6.4 and 6.5, most of the testing results can be considered good. Except in the Test2 and Test3, the performance of the RF-DEM in the group of FG1 and FG2 is not acceptable. Specifically, the tests of TL5 and TL6 do not match well for the identified RF-DEM. The reason is that the training data does not contain the dynamics from disturbances at TL5, 6, where are much stronger than the other data since the disturbance locations at TL5, 6 are close to the measured point. Without these strong dynamic data in the training, the RF-DEM cannot learn the right relationship between inputs and outputs, consequentially cannot predict well the outputs.

The following is the demonstration of the importance of "sufficient" data for RF-DEM. In Fig. 6.4 and 6.5, the performance of RF-DEM is poor since the training data does not contain right information of the system dynamics under disturbances occurred at TL5, 6. In FG1, substitute the training date under disturbance at TL2 with TL5, the testing data stay disturbances at TL4, 5, 6, then the smallest Fitness value under disturbances at TL5, 6 is as much as 86.16 %, which improves from 67.49 %. In FG2, substitute the training set under disturbance at TL4 with TL6, the testing data remain disturbances at TL2, 5, 6, then the smallest Fitness value under disturbances at TL5, 6 improves from 70.77 % to 85.32 %. Fig. 6.6 shows that it is important to obtain suitable training

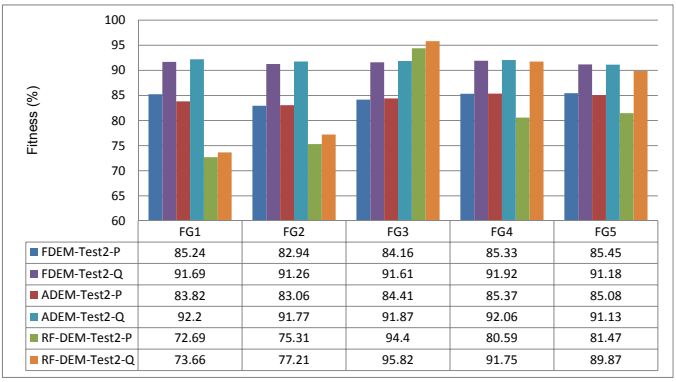

	FG1	FG2	FG3	FG4	FG5
FDEM-Test2-P	85.24	82.94	84.16	85.33	85.45
FDEM-Test2-Q	91.69	91.26	91.61	91.92	91.18
ADEM-Test2-P	83.82	83.06	84.41	85.37	85.08
ADEM-Test2-Q	92.2	91.77	91.87	92.06	91.13
RF-DEM-Test2-P	72.69	75.31	94.4	80.59	81.47
RF-DEM-Test2-Q	73.66	77.21	95.82	91.75	89.87

Figure 6.4: Performance of the proposed models in Test2.

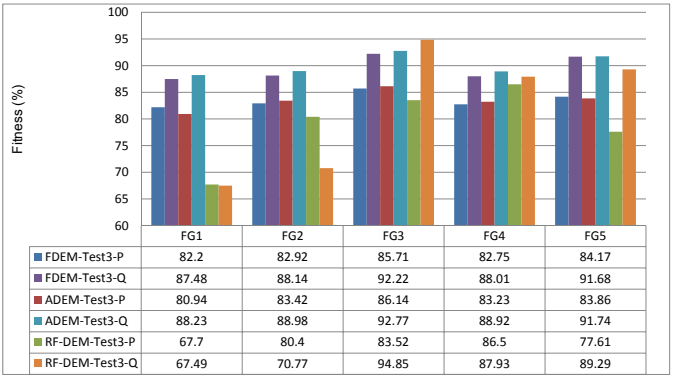

	FG1	FG2	FG3	FG4	FG5
FDEM-Test3-P	82.2	82.92	85.71	82.75	84.17
FDEM-Test3-Q	87.48	88.14	92.22	88.01	91.68
ADEM-Test3-P	80.94	83.42	86.14	83.23	83.86
ADEM-Test3-Q	88.23	88.98	92.77	88.92	91.74
RF-DEM-Test3-P	67.7	80.4	83.52	86.5	77.61
RF-DEM-Test3-Q	67.49	70.77	94.85	87.93	89.29

Figure 6.5: Performance of the proposed models in Test3.

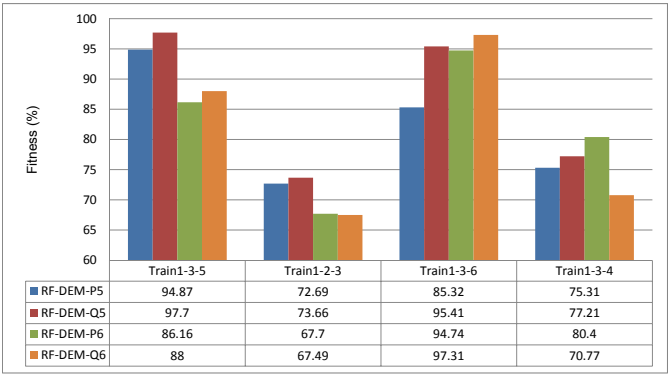

	Train1-3-5	Train1-2-3	Train1-3-6	Train1-3-4
RF-DEM-P5	94.87	72.69	85.32	75.31
RF-DEM-Q5	97.7	73.66	95.41	77.21
RF-DEM-P6	86.16	67.7	94.74	80.4
RF-DEM-Q6	88	67.49	97.31	70.77

Figure 6.6: Performance of the RF-DEM with new training data.

sets. This algorithm may also be modified to check whether measured data is sufficient since the RF-DEM performs poor when there is lack of appropriate data.

6.2.3 Different Penetration Levels

In the penetration level scenario, the PLs of DGs are set as 10 %, 30 % and 50 %, which are the same settings as in Section 3.6.3. The training data are the responses when the disturbances occur in TL1, 3, 5. The testing data are the responses when the disturbances occur in TL2, 6, where are far away and close to the measured PCC. The performance of the proposed FDEM, ADEM, and RF-DEM is shown in Fig. 6.7 and 6.8.

As it can be seen from Fig. 6.7 and 6.8, with an increasing penetration level, the performance of the derived models is becoming worse, however, these results can still be considered as good since all the Fitness values are above 80 %.

According to the results in Fig. 6.1, 6.2, 6.3, 6.4, 6.5, 6.6, 6.7 and 6.8, all estimated outputs of the proposed models match well with the measured outputs. The FDEM, ADEM and RF-DEM have sufficient performance for ADNs in the above test cases.

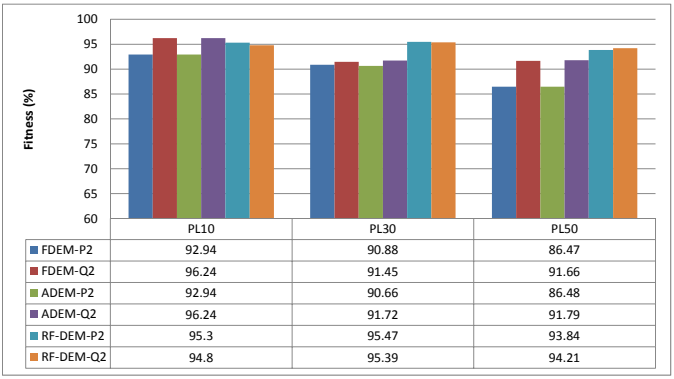

	PL10	PL30	PL50
FDEM-P2	92.94	90.88	86.47
FDEM-Q2	96.24	91.45	91.66
ADEM-P2	92.94	90.66	86.48
ADEM-Q2	96.24	91.72	91.79
RF-DEM-P2	95.3	95.47	93.84
RF-DEM-Q2	94.8	95.39	94.21

Figure 6.7: Performance of the proposed models in penetration scenario with fault at TL2.

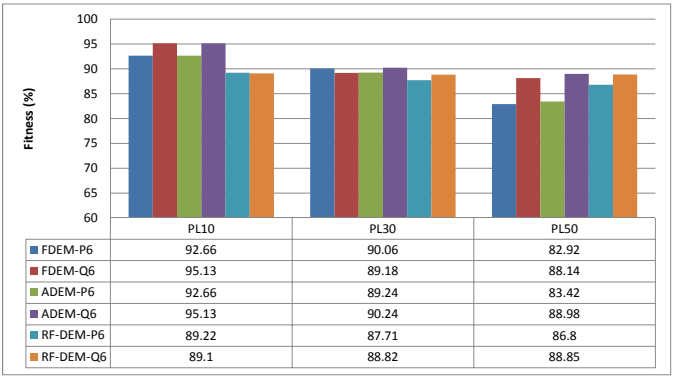

	PL10	PL30	PL50
FDEM-P6	92.66	90.06	82.92
FDEM-Q6	95.13	89.18	88.14
ADEM-P6	92.66	89.24	83.42
ADEM-Q6	95.13	90.24	88.98
RF-DEM-P6	89.22	87.71	86.8
RF-DEM-Q6	89.1	88.82	88.85

Figure 6.8: Performance of the proposed models in penetration scenario with fault at TL6.

6.3 Validations and Applications

The indicators for validation include different fault durations, fault levels and operating points. The electrical system for validation is the same as CG1 in Section 3.6.1.1. The identified ADEM model by combination of SM, EC and static power load is used for validation, which is represented in Equation 6.1. The values of the ADEM parameters are shown in Table 6.2, where only the non-zero parameters are listed. The ADEM is implemented as a module model with identified parameters in PowerFactory. The disturbances occur at the middle of TL5, which is close to the measured PCC point.

$$\begin{cases} \dot{X} = \begin{bmatrix} p_3 & 0 & 0 \\ 0 & 0 & 1 \\ p_4 & 0 & p_5 \end{bmatrix} X + \begin{bmatrix} p_8 \\ 0 \\ 0 \end{bmatrix} U + \begin{bmatrix} p_{17} \\ 0 \\ 0 \end{bmatrix} \\ Y = \begin{bmatrix} p_9 & 0 & 0 \\ p_{10} & 0 & 0 \end{bmatrix} X + \begin{bmatrix} p_{13} \\ p_{14} \end{bmatrix} U + \begin{bmatrix} p_{15} \\ p_{16} \end{bmatrix} \end{cases} \tag{6.1}$$

Table 6.2: Parameters of the identified ADEM

Parameters	Value
p3	-1.2734
p4	-0.08
p5	-1.984
p8	-11.1871
p11	0.0001
p12	0.0008
p13	19.3597
p14	23.2315
p15	-10.6759
p16	-14.9467
p17	-227.9298

6.3.1 Comparison with Static Power Load

The first validation is the comparison between the original and equivalent system, as well as the conventional equivalent system which uses a static constant power load to substitute the ADN. In the three test cases, the disturbances occur at the middle of TL5, which is close to the measured PCC point.

Response of PCC The corresponding responses of the PCC are shown in Fig. 6.9, where "Full, Equi, Pload" denotes the original, equivalent, and conventional equivalent systems, respectively. The responses of voltage, active and reactive power are compared.

As it can be seen from Fig. 6.9, the responses of proposed ADEM model and the original detailed distribution network have a good agreement, but the responses of the static equivalent model show a divergence.

Response of the generator G3 In the literature on dynamic equivalent [20], machine rotor angle dynamics, active and reactive power are often compared for validation, which is important for stability analysis and operation in transmission systems. The responses of generator G3 is chosen for comparison, since G3 is close to the disturbance at TL5 and has a strong reaction to the disturbance. The results are shown in Fig. 6.10, where the responses of the rotor angle, active and reactive power are compared. In Fig. 6.10,

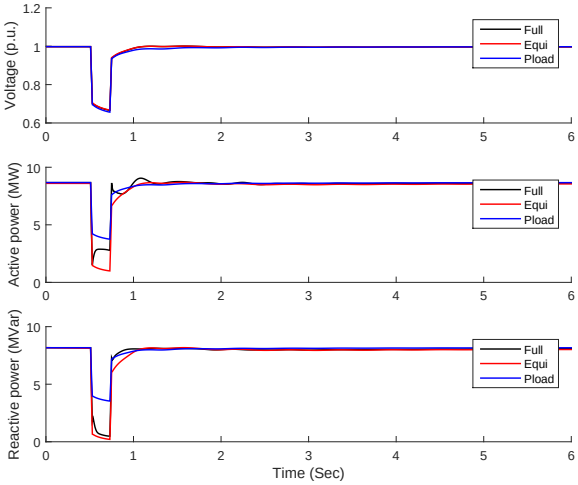

Figure 6.9: Response of PCC in original, equivalent and conventional system.

the rotor angle of G3 is going to be stable again after 6 second in all three cases. Compared to the responses of the static constant power load, the responses of the proposed equivalent model have a better agreement with the original distribution system.

According to the simulation results in Fig. 6.9 and 6.10, the ADEM has a better performance of matching the original system dynamics than a static constant power equivalent model.

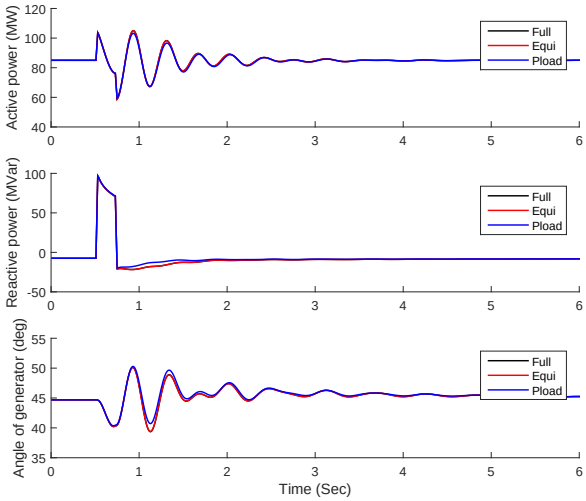

Figure 6.10: Response of G3 in original, equivalent and conventional system.

6.3.2 Fault Durations

Critical clearing time is the maximum fault clearing time for which the generator remains in synchronism, which is an important indicator for power system transient stability [88]. To investigate the critical clearing time, usually the process of trial and error has to be applied in simulation, where the test conditions have to be changed in each simulation [89]. Fault duration and level are the potential conditions that should be changed. In the fault duration case, the clearing fault duration is set as 0.1, 0.2 and 0.5 second, which corresponding responses of PCC are shown in Fig. 6.11, 6.12 and 6.13.

As it can be seen from Fig. 6.11, 6.12 and 6.13, the responses of the PCCs between original system and equivalent system match well. For the sake of simplicity, only responses of angle of generator G3 are compared. The results are shown in Fig. 6.14, 6.15 and 6.16, where the upper subplots are the comparison of rotor angle, the lower subplots are the difference value of rotor angle between the original and equivalent system. As it can be seen in Fig. 6.14, 6.15 and 6.16, the largest difference value of the rotor angle is around 0.1 degree.

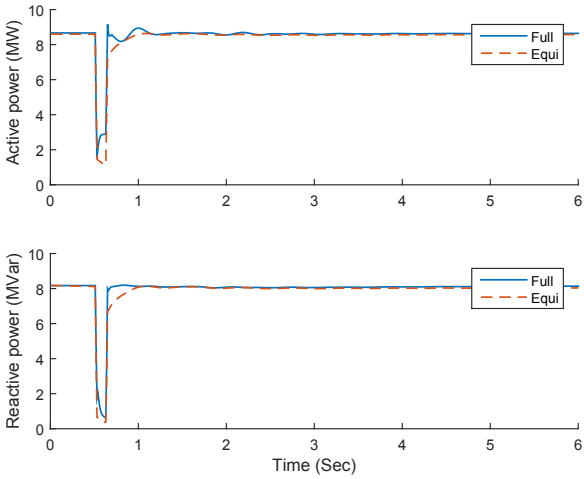

Figure 6.11: Response of PCC with 0.1 second fault duration.

The dynamic behaviors at the PCCs during the transient term match well since this identified ADEM captured the main dynamics for different fault durations. It means that the obtained ADEM has the right performance for fault duration between 0.1 and 0.5 second, which is the common range of fault duration in the grid code [67].

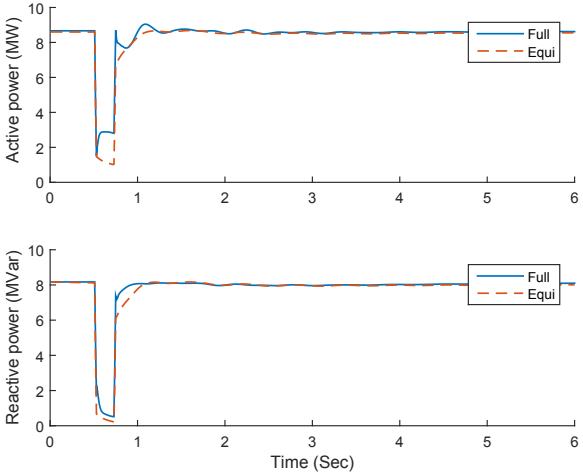

Figure 6.12: Response of PCC with 0.2 second fault duration.

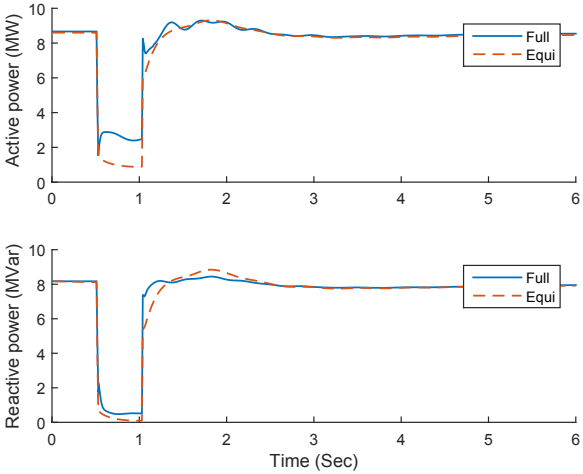

Figure 6.13: Response of PCC with 0.5 second fault duration.

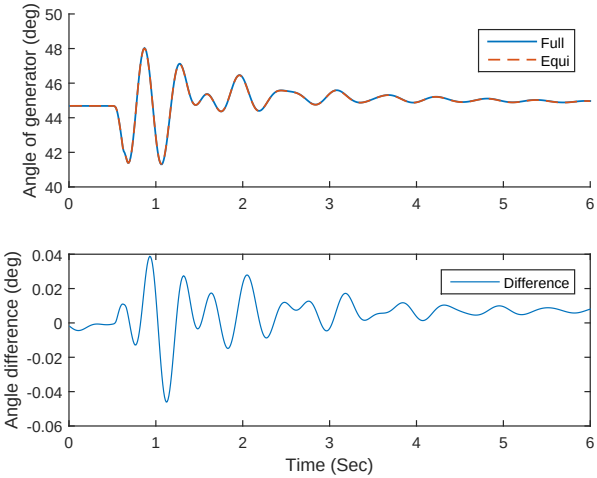

Figure 6.14: Response of G3 with 0.1 second fault duration.

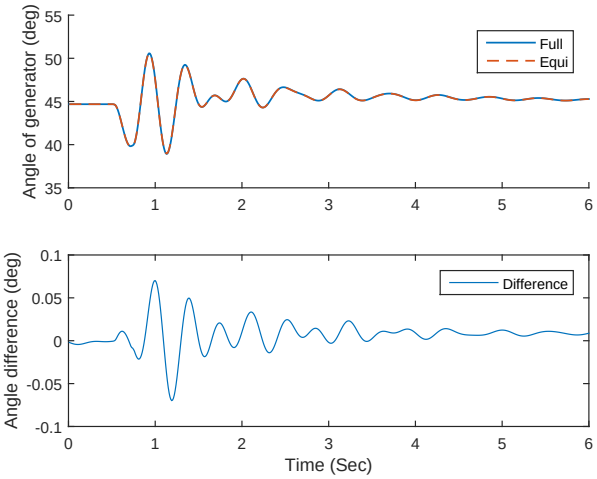

Figure 6.15: Response of G3 with 0.2 second fault duration.

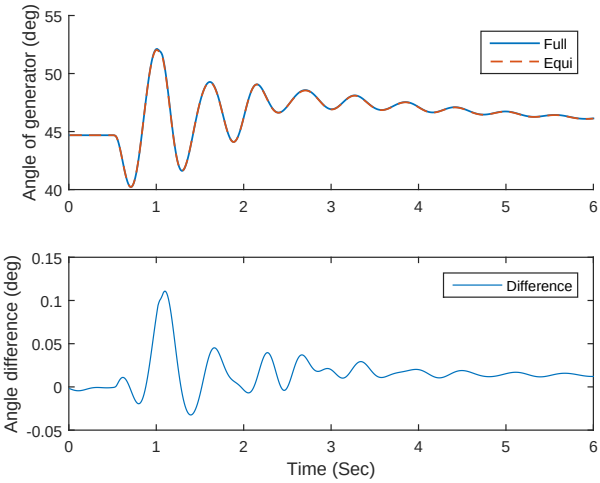

Figure 6.16: Response of G3 with 0.5 second fault duration.

6.3.3 Fault Levels

The fault level scenario is to demonstrate the performance of ADEMs under the condition of different fault levels. The locations of the disturbances remain the same as in the fault duration scenario, and the configurations of electrical system retain the same as CG1 in Section 3.6.1.1.

The fault levels are set as 750 MVA, 1000 MVA and 1250 MVA [33, 34, 68]. The responses of the PCCs at the three fault levels are shown in Fig. 6.17, 6.18 and 6.19, respectively. The responses of active and reactive power at the PCCs match well in the three test cases. Fig. 6.17 shows that there is a bigger difference gap of active and reactive power than in Fig. 6.18 and 6.19 during fault term. The reason is that the measured data used for training did not cover the dynamics of the lower fault level well. Its performance can be improved by adding the lower fault level response data into the training data to obtain the final ADEM.

Fig. 6.20, 6.21 and 6.22 show the responses of generator G3 during the three fault levels, respectively. With the increasing fault levels, the oscillation of rotor angle is bigger, which is an expected response. The difference value of the rotor

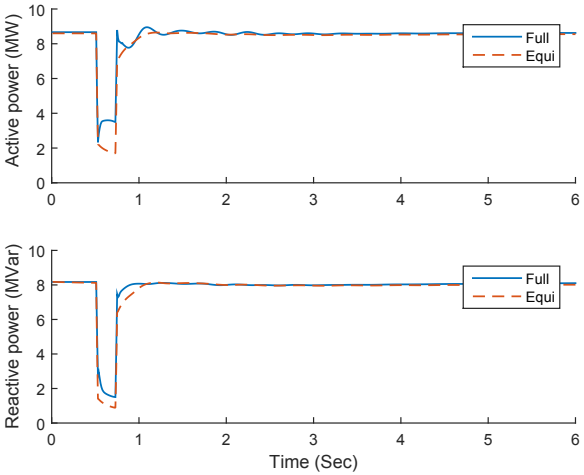

Figure 6.17: Response of PCC at 750 MVA fault level.

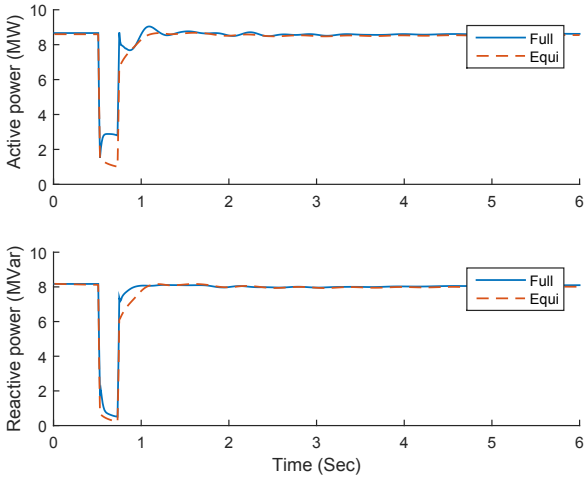

Figure 6.18: Response of PCC at 1000 MVA fault level.

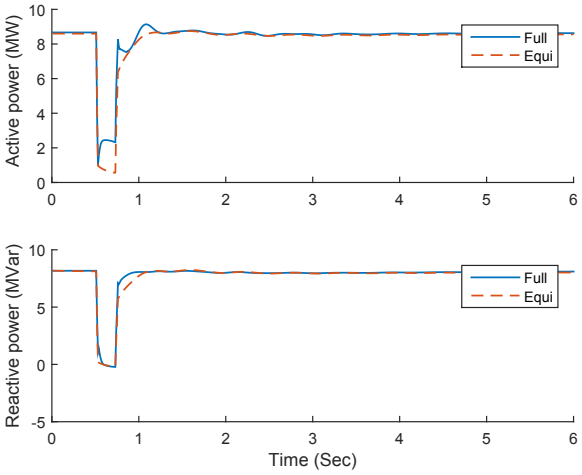

Figure 6.19: Response of PCC at 1250 MVA fault level.

angle is similar, the absolute difference value is around 0.05 degree. It can be considered the dynamic equivalent model captures the dynamic of rotor angle well.

In conclusion, the obtained third-order ADEM is suitable to substitute the original ADN for the investigated fault levels. Note that there is a limitation for the fault levels, the lower fault level may cause worse agreement between the equivalent and original systems. In these situations, measured data from lower fault levels should include into the training data.

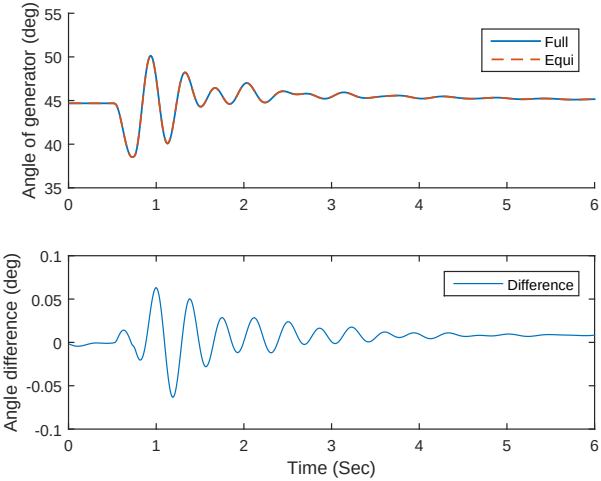

Figure 6.20: Response of G3 at 750 MVA fault level.

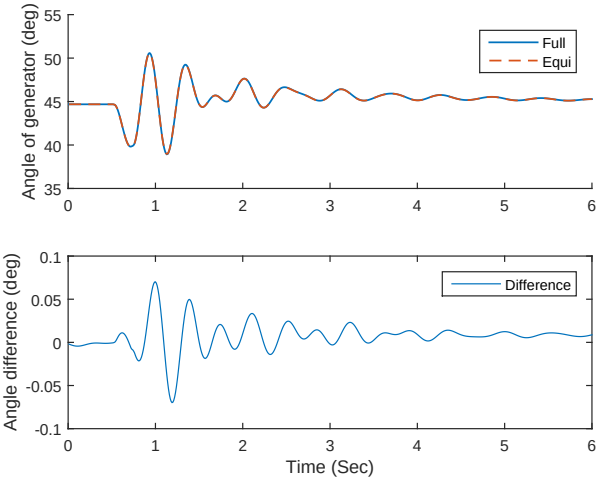

Figure 6.21: Response of G3 at 1000 MVA fault level.

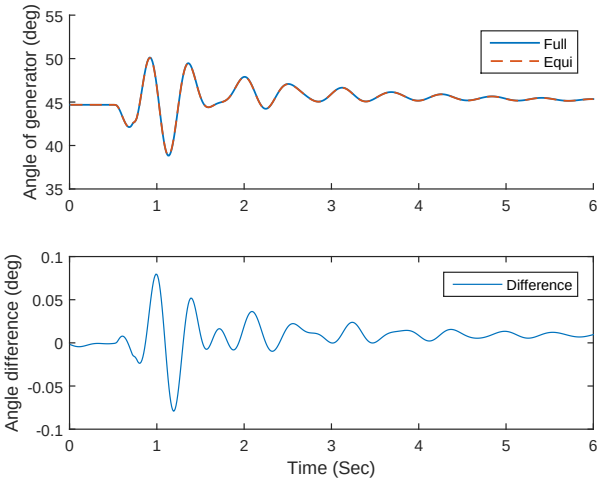

Figure 6.22: Response of G3 at 1250 MVA fault level.

6.3.4 Operating Points

Considering that the transmission system may have different operation points during different times, this scenario is designed to represent the fitness of ADEM between different operating points. Three test cases are set up by changing active and reactive power in the range between 10 % and 20 %. The first case is changing active and reactive power of Load 3 from 100 MW and 35 MVar to 120 MW and 45 MVar, respectively. The second case is changing active and reactive power of Load 1 from 125 MW and 50 MVar to 115 MW and 45 MVar, respectively. The third case is combining the changes of the first and second cases. The responses of the PCCs for the three cases are shown in Fig. 6.23, 6.24 and 6.25. The responses of the generator rotor angle are presented in Fig. 6.26, 6.27, 6.28.

According to the results in Fig. 6.23, 6.24, 6.25, 6.26, 6.27 and 6.28, the responses of the active and reactive power, as well as the rotor angle behavior are closed to each other, respectively. The only difference is the value of the steady rotor angles. The change of operating points in the transmission system has a small influence on the dynamics of the active distribution network. However, if a

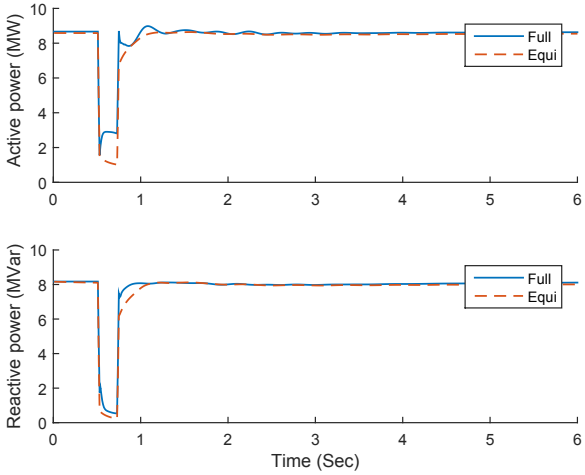

Figure 6.23: Response of PCC in Case1.

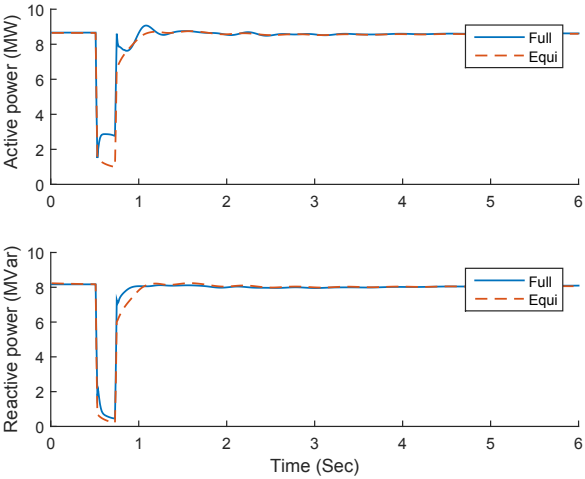

Figure 6.24: Response of PCC in Case2.

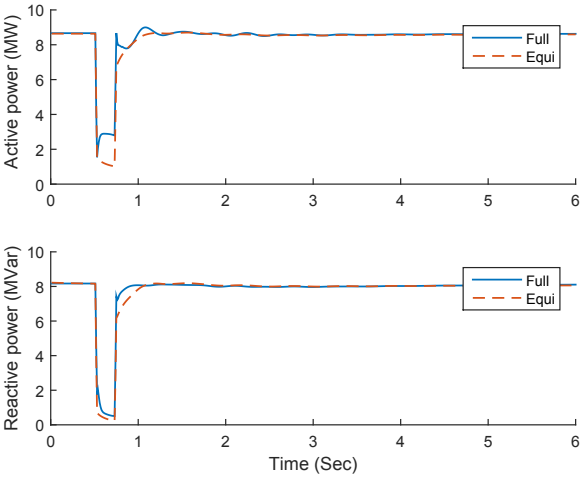

Figure 6.25: Response of PCC in Case3.

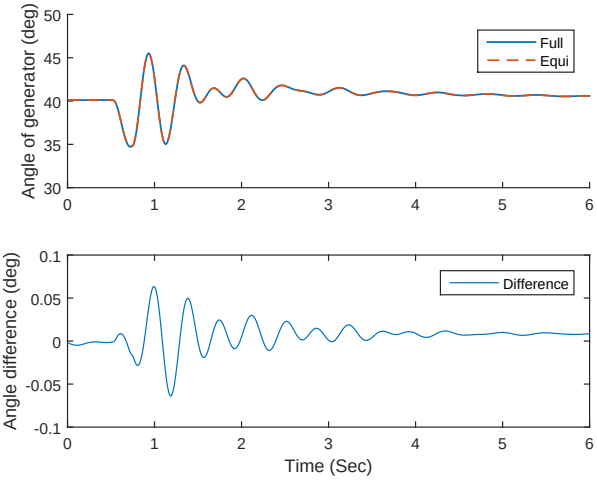

Figure 6.26: Response of G3 in Case1.

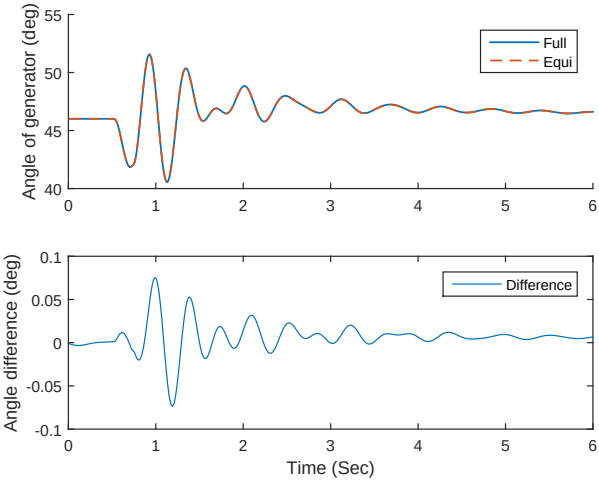

Figure 6.27: Response of G3 in Case2.

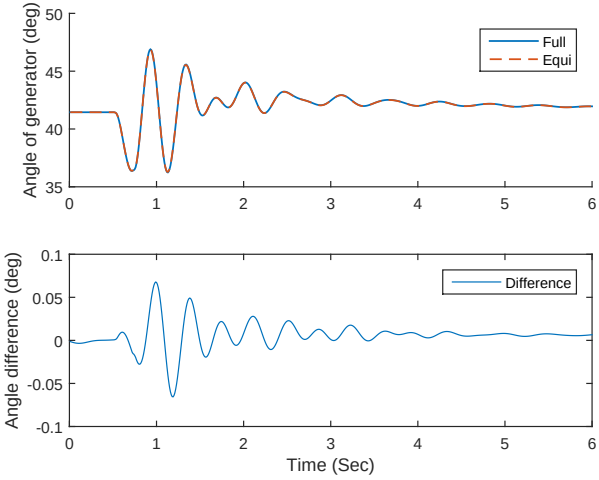

Figure 6.28: Response of G3 in Case3.

significant change of the operation points happens, the steady voltage value and the voltage dynamics at the PCC change a lot, the obtained ADEM may not be suitable anymore. In this situation, the equivalent models should be identified again with new measured data.

6.3.5 Small Disturbance Analysis

Concerning the performance of the proposed dynamic equivalent models during small disturbance, the critical Eigenvalues can be taken into account for comparison [34]. The Eigenvalues provide the dynamic behavior information of a power system under small disturbance. The closer the location of the Eigenvalues of original and equivalent system in the s-plane, the better equivalent system matches to the responses of original system during small disturbance. The Eigenvalues plotted in S-plane are shown in Fig. 6.29, where the "circle" is the Eigenvalue of the original system and the "star" is the eigenvalue of the equivalent system.

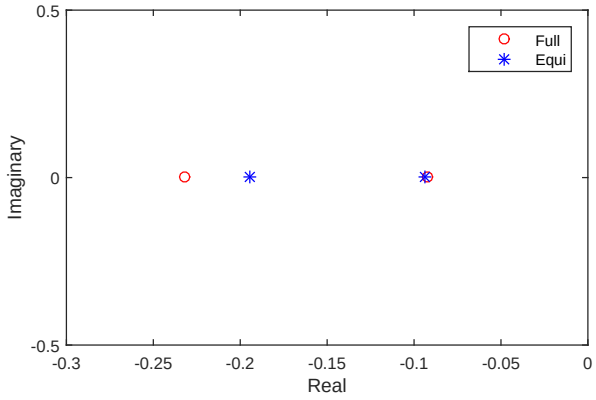

Figure 6.29: Critical eigenvalues of the original and equivalent system.

As it can be seen in Fig. 6.29, both original and equivalent systems have similar eigenvalues. Hence it can be concluded that both systems have similar dynamic behaviors during small disturbance.

Table 6.3: Summary of the proposed dynamic equivalent models

	Strength	Preferred case
FDEM	Simple and low order model, easy to integrate with other tools as a module component	Simple form of equivalent model is required
ADEM	Adaptive structure of equivalent model, simple and low order model, easy to integrate with other tools as a module component	Simple form of equivalent model and further simplification are required
RF-DEM	Easy to implement, variable importance analysis	Difficult to derive equivalent from physical models

6.4 Summary

This chapter compares the performance of the proposed dynamic equivalent models: FDEM, ADEM and RF-DEM. Suitable situations for their application are also provided. The obtained ADEM dynamic equivalent model in CG1 is used for validation in scenarios with different fault durations, fault levels and operation points. The performance of the ADEM for small disturbances is analyzed by calculating Eigenvalues between the original and equivalent systems. According to the results shown in the test cases, a general conclusion is the three proposed dynamic equivalent models can substitute the ADNs well for transient analysis in the investigated scenarios.

A summary of the developed dynamic equivalent models is provided in Table 6.3. From a practical point of view, ADEM is considered as the first choice of the presented dynamic equivalent models, since it covers the features of FDEM and it is simpler than RF-DEM.

Chapter 7

Conclusion and Future Work

7.1 Conclusion

Three new dynamic equivalent models for active distribution networks: fixed-structure dynamic equivalent model, adaptive dynamic equivalent model, and random forest-based dynamic equivalent model, were presented in this dissertation. They were compared by taking into account of different distributed generator combinations, fault locations, and penetration levels. In the end, they were validated by the application of different fault durations, fault levels, as well as operation points. According to the presented results, the proposed models matched the original systems well, they were successful in substituting the external part of the sub-systems.

In Chapter 1, the background of the electrical system and the impacts of increasing penetration of DGs on power system were presented. To address the challenges of the complexity and large size of power systems, the equivalent technique for ADNs is important and necessary. The detailed challenges and motivations were presented and the history of equivalent technique was introduced. The description of the challenges and motivations, as well as the summary of the equivalent technique history forms the first contribution of the dissertation work.

In Chapter 2, from equivalent model and method point of view, the dynamic equivalent models of ADNs were classified into three types: modal-based, model-free, and model-based approaches. The modal-based approach derives the equivalent model from linearized system models with model-reduction methods

that have a strict mathematical basis. The model-free approach derives the equivalent model from measured data with machine learning methods that train the hidden relationships between inputs and outputs. The model-based approach firstly derives a fixed-structure equivalent model, then identifies the unknown parameters with measured data and optimization methods. The classifications and descriptions of the modal-based, model-based and model-free approaches, and also the summary of their advantages and disadvantages of the three approaches represent the second contribution.

In Chapter 3, a fixed-structure dynamic equivalent model was proposed. It was assumed that the dynamics of a system can be represented by significant component models with unknown parameters. The approximation models of individual physical models were derived and the physical components were introduced as induction machines, synchronous machines, electric converters and static power loads. The FDEM is represented by the combination of the derived four individual equivalent models. Finally it is a six-order state space model as in Equation 3.22, which can be easily integrated as a standard components with to-be-edited parameters in power system tools. The optimization algorithm and the identification procedure were also introduced. The scenarios of different DG combinations, fault locations, and penetration levels were taken into account for comparison. The derivation of the FDEM represents the fourth contribution and this model is also the first new dynamic equivalent model.

In practice, different active distribution networks may have different dynamic behaviors with different orders of equivalent models. In Chapter 4, the adaptive dynamic equivalent models were represented as flexible structure equivalent models, which are adapted to measurement data. In this work, the equivalent model problem was formulated to the form of Markov decision process problem, which includes five tuples state, action, transition probability, reward, and reward discount. Based on analysis of the different features between the learning algorithms, modified Q-learning was selected to solve the MDP problem since the algorithm does not require the exact transition and reward models. The transformation from equivalence problem to MDP problem and the representation of the ADEM are considered as the fifth contribution and ADEM is the second new dynamic equivalent model.

When proper knowledge about the structure of ADNs is missing, a model-free equivalent model based on Random Forest was provided in Chapter 5. The

random forest-based dynamic equivalent model applied voltage variable as well as delayed active and reactive power as inputs. The outputs were defined as active and reactive power. An analysis procedure, which includes number of trees and subsets as well as variable importance and combination of input variables, was designed for an optimal RF-DEM, the test results were presented. The derivation of the RF-DEM and the analysis of its features are the sixth contribution and RF-DEM is the third new dynamic equivalent model.

In Chapter 6, further analysis and investigations were carried out on the developed dynamic equivalent models. The investigated scenarios include different DG combinations, fault locations, and penetration levels. It can be concluded that the proposed models are suitable for building equivalent model of active distribution networks.

The applications of the developed equivalent models were also presented in this dissertation work, specifically different fault clear times, fault levels, and operation points. The full and equivalent electrical system were developed in PowerFactory and the equivalent model was developed as module component with parameters to be edited. The results show that the equivalent system with the derived equivalent model matches well with the original full systems. The comparison and analysis work is the seventh contribution in this dissertation.

The main features of the proposed dynamic equivalent models are shown in Table 7.1. Generally, ADEM is the preferred one, the reason was described in Section 6.4.

Table 7.1: Main features of the proposed dynamic equivalent models

	Advantages	Disadvantages
FDEM	Explicit and simple	Constraints from model equations Fixed-structure Require measurement data
ADEM	Explicit and simple Flexible structure	Constraints from model equations Require measurement data
RF-DEM	Easy implementation	No identical model structure between different trainings Require measurement data

7.2 Future Work

This dissertation proposes three new dynamic equivalent models for active distribution networks. There are several aspects that deserve further investigation and improvement in future research.

The three dynamic equivalent models are designed for medium term transient analysis, but they do not cover the fast transient analysis. An interesting direction could be further development of dynamic equivalent models for wide term transient analysis, such as electromechanical transient together with electromagnetic transients. The general approach is combing electromechanical and electromagnetic equivalent models together, the related literature can be found in [24, 90, 91].

Another interesting direction is deriving new individual equivalent models for the ADEM. A further investigation of worst cases for the proposed models is also interesting.

Furthermore the integration of the proposed dynamic equivalent models into a real monitoring and control platform for electrical system represents an interesting advancement of this dissertation work.

Appendix A

Parameters of transmission system

Table A.1: Generator parameters

Generator	G1	G2	G3	Unit	Description
Active Power	247.5	163	85	MW	
Reactive Power	0	6.7	-10.9	MVar	
Power Factor	1	0.85	0.85		
Nominal voltage	16.5	18	13.8	kV	
Voltage	1.04	1.025	1.025	p.u.	
Inertia	9.55	4.165	2.765	s	Acceleration time constant
Xl	0.083	0.141	0.0949	p.u.	Leakage reactance
Xd	0.36	1.172	1.68	p.u.	Synchronous reactance
Xq	0.24	1.66	1.61	p.u.	Synchronous reactance
Xd'	0.15	0.23	0.23	p.u.	Transient reactance
Td'	3.37	0.8	0.806	s	Transient time constant
Controller					avr IEEEX1

Table A.2: Transformer parameters

Transformer	T1	T2	T3	Unit
Rate Power	250	200	150	MVA
High voltage side	230	230	230	kV
Low voltage side	16.5	18	13.8	kV
Short circuit	14	12.50	8.79	%

Table A.3: Transmission line parameters

Line	Resistance [Ohm]	Reactance [Ohm]
TL1	5.29	44.965
TL2	16.928	85.169
TL3	4.4965	38.088
TL4	6.2951	53.3232
TL5	20.631	89.93
TL6	8.993	48.668

Table A.4: Transmission load parameters

Load	Active power [MW]	Reactive Power [MVar]
L5	125	50
L6	90	30
L8	100	35

Table A.5: Generator controller parameters

Controller	G1	G2	G3	Unit	Description
K	0.001	400	0.001	p.u.	Controller gain
T	0.2	0.05	0.2	p.u.	Controller time constant
Te	0.5	0.95	0.5	p.u.	Exciter time constant
Ke	-0.044	-0.17	-0.044	p.u.	Exciter constant
Vmin	-1	-3	-1	p.u.	Controller minimum output
Vmax	1	3	1	p.u.	Controller maximum output

Appendix B

Parameters of distribution system

Table B.1: Parameters of distribution loads

Loads	Active power [MW]	Reactive power [MVar]
L11	3.28	1.59
DG1	-(1 ∼ 5)	-2 ∼ 1
L22	0.10	0.05
L23	0.06	0.03
L24	1.66	0.81
L25	0.26	0.13
DG2	-(1 ∼ 5)	-2 ∼ 1
L31	3.12	1.5
DG3	-(1 ∼ 5)	-2 ∼ 1
L41	0.85	0.42
L51	2.22	1.07
L52	0.08	0.04
DG5	-(1 ∼ 5)	-2 ∼ 1
L61	3.24	1.57
L71	2.13	1.03

Table B.2: Parameters of distribution feeders

Feeders	Resistance [Ohm]	Reactance [Ohm]
F10	0.37	0.19
F20	0.74	0.38
F21	0.41	0.21
F22	3.64	1.85
F23	0.81	0.41
F25	0.23	0.12
F30	1.51	0.77
F40	0.22	0.11
F50	0.2	0.1
F51	0.33	0.17
F60	0.38	0.19
F70	0.32	0.16

Table B.3: Parameters of distribution transformers

Connected component	Powr rating [MVA]	Related voltage [kV]	Short circuit impedance [%]
CWTG 1.0 MW	1.12	20/0.4	6
CWTG 1.5 MW	1.67	20/0.4	6
DFIG 2.0 MW	2.23	20/0.69	6
DFIG 2.5 MW	2.78	20/0.69	6
DFIG 3.5 MW	4.0	20/0.69	6
FSIG 2.0 MW	2.5	20/0.96	8
SG 2.0 MW	2.5	20/0.69	8
PV 2.0 MW	2.2	20/0.4	8
PV 2.5 MW	2.6	20/0.4	8
PV 3.0 MW	3.2	20/0.4	8
TF	180	230/20	14

Table B.4: Parameters of SG

Parameter	Value	Unit	Description
Active Power	2	MW	
Reactive Power	0.67	MVar	
Power Factor	0.8		
Nominal voltage	0.69	kV	
Voltage	1	p.u.	
Inertia	3.6	s	Acceleration time constant
Xl	0.1	p.u.	Leakage reactance
Xd	2	p.u.	Synchronous reactance
Xq	2	p.u.	Synchronous reactance
Xd'	0.3	p.u.	Transient reactance
Xq'	0.3	p.u.	Transient reactance
Td'	1	s	Transient time constant

Table B.5: Parameters of DFIG and FSIG

Parameters	DFIG	FSIG	Unit	Description
Rs	0.01	0.01	p.u.	Stator resistance
Xs	0.1	0.1	p.u.	Stator reactance
Xm	3.5	3	p.u.	Magnetization reactance
Rr	0.01	0.01	p.u.	Rotor resistance
Xr	0.1	0.1	p.u.	Rotor reactance
H	75	100	kgmˆ2	Single cage

Table B.6: Parameters of PV and CWTG

	PV	CWTG	Unit	Description
X	0.1	0.1	p.u.	Short circuit impedance

Table B.7: Parameters of DG controllers

DG Type	Controller gain K	Controller time constant T
SG	200	0.05
PV	0.005	0.03
DFIG	4	0.1
CWTG	0.5	0.02

Bibliography

[1] J. A. P. Lopes, N. Hatziargyriou, J. Mutale, P. Djapic, and N. Jenkins. Integrating distributed generation into electric power systems: A review of drivers, challenges and opportunities. *Electric power systems research*, 77(9):1189–1203, 2007.

[2] A. Ishchenko, J. M. A. Myrzik, and W. L. Kling. Dynamic equivalencing of distribution networks with dispersed generation using krylov methods. In *Power Tech, 2007 IEEE Lausanne*, pages 2023–2028, July 2007.

[3] Overview renewable energy sources act. `http://www.germanenergyblog.de/?page_id=283`. Accessed: 06-Apr-2016.

[4] J. Mahseredjian, V. Dinavahi, and J. A. Martinez. Simulation tools for electromagnetic transients in power systems: Overview and challenges. *IEEE Transactions on Power Delivery*, 24(3):1657–1669, Jul 2009.

[5] A. M. Azmy and I. Erlich. Impact of distributed generation on the stability of electrical power system. In *IEEE Power Engineering Society General Meeting, 2005*, volume 2, pages 1056–1063, Jun 2005.

[6] V. Calderaro, J.V. Milanovic, M. Kayikci, and A. Piccolo. The impact of distributed synchronous generators on quality of electricity supply and transient stability of real distribution network. *Electric Power Systems Research*, 79(1):134–143, 2009.

[7] J. C. Boemer, M. Gibescu, and W. L. Kling. Dynamic models for transient stability analysis of transmission and distribution systems with distributed

generation: An overview. In *PowerTech, 2009 IEEE Bucharest*, pages 1–8, Jun 2009.

[8] E. N. Azadani, C. Canizares, and K. Bhattacharya. Modeling and stability analysis of distributed generation. In *2012 IEEE Power and Energy Society General Meeting*, pages 1–8, Jul 2012.

[9] P. Kundur, J. Paserba, V. Ajjarapu, G. Andersson, A. Bose, C. Canizares, N. Hatziargyriou, D. Hill, A. Stankovic, C. Taylor, T. Van Cutsem, and V. Vittal. Definition and classification of power system stability ieee/cigre joint task force on stability terms and definitions. *IEEE Transactions on Power Systems*, 19(3):1387–1401, Aug 2004.

[10] Y. A. Kazachkov, J. W. Feltes, and R. Zavadil. Modeling wind farms for power system stability studies. In *Power Engineering Society General Meeting, 2003, IEEE*, volume 3, pages 1526–1533, Jul 2003.

[11] M. Reza, P. H. Schavemaker, J. G. Slootweg, W. L. Kling, and L. van der Sluis. Impacts of distributed generation penetration levels on power systems transient stability. In *Power Engineering Society General Meeting, 2004. IEEE*, volume 2, pages 2150–2155, June 2004.

[12] Y. Xu, Z. Y. Dong, K. Meng, R. Zhang, and K. P. Wong. Real-time transient stability assessment model using extreme learning machine. *IET Generation, Transmission Distribution*, 5(3):314–322, March 2011.

[13] S. C. Savulescu. *Real-time stability assessment in modern power system control centers*, volume 42. John Wiley & Sons, 2009.

[14] Smart Grid Task Force. Regulatory recommendations for the deployment of flexibility, 2015.

[15] J. B. Ward. Equivalent circuits for power-flow studies. *Transactions of the American Institute of Electrical Engineers*, 68(1):373–382, July 1949.

[16] T. L. Baldwin, L. Mili, and A. G. Phadke. Dynamic ward equivalents for transient stability analysis. *IEEE Transactions on Power Systems*, 9(1):59–67, Feb 1994.

[17] P. Dimo. *Nodal analysis of power systems*. International Scholarly Book Services, Inc.,Forest Grove, OR, Jan 1975.

[18] R.W. de Mello, R. Podmore, and K.N. Stanton. Coherency-based dynamic equivalents: applications in transient stability studies. In *Proc. PICA Conf*, pages 23–31, 1975.

[19] R. Podmore. Identification of coherent generators for dynamic equivalents. *IEEE Transactions on Power Apparatus and Systems*, PAS-97(4):1344–1354, July 1978.

[20] J. H. Chow, R. Galarza, P. Accari, and W. W. Price. Inertial and slow coherency aggregation algorithms for power system dynamic model reduction. *IEEE Transactions on Power Systems*, 10(2):680–685, May 1995.

[21] N. R. Watson and J. Arrillaga. Frequency-dependent ac system equivalents for harmonic studies and transient convertor simulation. *IEEE Transactions on Power Delivery*, 3(3):1196–1203, Jul 1988.

[22] B. Gustavsen and A. Semlyen. Rational approximation of frequency domain responses by vector fitting. *IEEE Transactions on Power Delivery*, 14(3):1052–1061, Jul 1999.

[23] F. Milano and K. Srivastava. Dynamic rei equivalents for short circuit and transient stability analyses. *Electric Power Systems Research*, 79(6):878–887, 2009.

[24] Y. Liang, X. Lin, A. M. Gole, and M. Yu. Improved coherency-based wide-band equivalents for real-time digital simulators. *IEEE Transactions on Power Systems*, 26(3):1410–1417, Aug 2011.

[25] A. M. Stankovic, A. T. Saric, and M. Milosevic. Identification of nonparametric dynamic power system equivalents with artificial neural networks. *IEEE Transactions on Power Systems*, 18(4):1478–1486, Nov 2003.

[26] A. M. Stankovic and A. T. Saric. Transient power system analysis with measurement-based gray box and hybrid dynamic equivalents. *IEEE Transactions on Power Systems*, 19(1):455–462, Feb 2004.

[27] A. M. Azmy, I. Erlich, and P. Sowa. Artificial neural network-based dynamic equivalents for distribution systems containing active sources. *IEE Proceedings - Generation, Transmission and Distribution*, 151(6):681–688, Nov 2004.

[28] F. D. Kanellos and N. D. Hatziargyriou. Dynamic equivalents of distribution networks with embedded wind parks. In *Power Tech Conference Proceedings, 2003 IEEE Bologna*, volume 2, page 8 pp., Jun 2003.

[29] X. Feng, Z. Lubosny, and J. Bialek. Dynamic equivalencing of distribution network with high penetration of distributed generation. In *Proceedings of the 41st International Universities Power Engineering Conference*, volume 2, pages 467–471, Sept 2006.

[30] X. Feng, Z. Lubosny, and J. W. Bialek. Identification based dynamic equivalencing. In *Power Tech, 2007 IEEE Lausanne*, pages 267–272, July 2007.

[31] Ishchenko, A., Myrzik, J. M. A., and W. L. Kling. Dynamic equivalencing of distribution networks with dispersed generation using hankel norm approximation. *Transmission Distribution IET Generation*, 1(5):818–825, Sept 2007.

[32] M. Dehghani and S.K.Y. Nikravesh. Nonlinear state space model identification of synchronous generators. *Electric Power Systems Research*, 78(5):926–940, 2008.

[33] S. M. Zali and J. V. Milanovic. Modelling of distribution network cell based on grey-box approach. In *Power Generation, Transmission, Distribution and Energy Conversion (MedPower 2010), 7th Mediterranean Conference and Exhibition on*, pages 1–6, Nov 2010.

[34] S. M. Zali and J. V. Milanovic. Generic model of active distribution network for large power system stability studies. *IEEE Transactions on Power Systems*, 28(3):3126–3133, Aug 2013.

[35] K. Nojiri, S. Suzaki, K. Takenaka, and M. Goto. Modal reduced dynamic equivalent model for analog type power system simulator. *IEEE Transactions on Power Systems*, 12(4):1518–1523, Nov 1997.

[36] A. Ishchenko. *Dynamics and stability of distribution networks with dispersed generation*. PhD thesis, Technical University of Eindhoven, 2008.

[37] A. C. Antoulas, D. C. Sorensen, and S. Gugercin. A survey of model reduction methods for large-scale systems. *Contemporary Mathematics*, 280:193–219, 2001.

[38] A. C. Antoulas and D. C. Sorensen. Approximation of large-scale dynamical systems: an overview. *International Journal of Applied Mathematics and Computer Science*, 11(5):1093–1121, 2001.

[39] A. Megretski. Model reduction by projection: General properties. University Lecture, 2004.

[40] S. Gugercin. An iterative SVD-Krylov based method for model reduction of large-scale dynamical systems. In *Proceedings of the 44th IEEE Conference on Decision and Control*, pages 5905–5910, Dec 2005.

[41] I. A. Basheer and M. Hajmeer. Artificial neural networks: fundamentals, computing, design, and application. *Journal of Microbiological Methods*, 43(1):3–31, 2000. Neural Computting in Micrbiology.

[42] Basic concepts for neural networks. `http://www.cheshireeng.com/Neuralyst/nnbg.htm`. Accessed: 14-Apr-2016.

[43] D. Hunter, H. Yu, M. S. Pukish III, J. Kolbusz, and B. M. Wilamowski. Selection of proper neural network sizes and architectures - a comparative study. *IEEE Transactions on Industrial Informatics*, 8(2):228–240, May 2012.

[44] L. Ljung. *System identification-Theory for the user*. Prentice-Hall, 1999.

[45] X. S. Feng. *Dynamic equivalencing of distribution network with embedded generation*. PhD thesis, University of Edinburgh, 2012.

[46] M. Dehghani and S. K. Y. Nikravesh. State-space model parameter identification in large-scale power systems. *IEEE Transactions on Power Systems*, 23(3):1449–1457, Aug 2008.

[47] Tesla powerwall. `https://www.teslamotors.com/powerwall`. Accessed: 10-Apr-2016.

[48] O. Erdinc and M. Uzunoglu. Optimum design of hybrid renewable energy systems: Overview of different approaches. *Renewable and Sustainable Energy Reviews*, 16(3):1412–1425, 2012.

[49] Joan Rocabert, Alvaro Luna, Frede Blaabjerg, and Pedro Rodriguez. Control of power converters in ac microgrids. *IEEE Transactions on Power Electronics*, 27(11):4734–4749, Nov 2012.

[50] T. Thiringer and J. Luomi. Comparison of reduced-order dynamic models of induction machines. *IEEE Transactions on Power Systems*, 16(1):119–126, Feb 2001.

[51] S. M. Zaid and M. Taleb. Structural modeling of small and large induction machines using integral manifolds. *IEEE Transactions on Energy Conversion*, 6(3):529–535, Sept 1991.

[52] E. Ghahremani, M. Karrari, and O. P. Malik. Synchronous generator third-order model parameter estimation using online experimental data. *IET Generation, Transmission Distribution*, 2(5):708–719, Sept 2008.

[53] J. V. Milanovic, K. Yamashita, S. Martinez Villanueva, S. Z. Djokic, and L. M. Korunovic. International industry practice on power system load modeling. *IEEE Transactions on Power Systems*, 28(3):3038–3046, Aug 2013.

[54] Y. Li, H. d. Chiang, B. k. Choi, Y. t. Chen, D. h. Huang, and M. G. Lauby. Representative static load models for transient stability analysis: development and examination. *IET Generation, Transmission Distribution*, 1(3):422–431, May 2007.

[55] J. H. Chow, R. Galarza, P. Accari, and W. W. Pric. Inertial and slow coherency aggregation algorithms for power system dynamic model reduction. *IEEE Transactions on Power Systems*, 10(2):680–685, May 1995.

[56] L. M. Fernandez, F. Jurado, and J. R. Saenz. Aggregated dynamic model for wind farms with doubly fed induction generator wind turbines. *Renewable Energy*, 33(1):129–140, 2008.

[57] J. Nocedal and S. J. Wright. *Numerical optimization*. Springer series in operations research. Springer, New York, 1999.

[58] Y. Yuan. A review of trust region algorithms for optimization. In *ICIAM*, volume 99, pages 271–282, 2000.

[59] A. Wachter and T. L. Biegler. On the implementation of an interior-point filter line-search algorithm for large-scale nonlinear programming. *Mathematical Programming*, 106(1):25–57, 2006.

[60] Choosing a solver - matlab simulink. `http://nl.mathworks.com/help/optim/ug/choosing-a-solver.html`. Accessed: 08-Jan-2016.

[61] Creating idnlgrey model files - matlab simulink. `http://nl.mathworks.com/help/optim/ug/choosing-a-solver.html`. Accessed: 08-Jan-2016.

[62] Estimating nonlinear grey-box models - matlab simulink. `http://nl.mathworks.com/help/ident/ug/estimating-nonlinear-grey-box-models.html`. Accessed: 08-Jan-2016.

[63] Compare model output and measured output - matlab compare. `http://de.mathworks.com/help/ident/ref/compare.html`. Accessed: 11-Apr-2016.

[64] PowerFactory 14.1.3. *Nine bus system, User Manual*, Apr 2015.

[65] A. Bracale, R. Caldon, M. Coppo, D. Dal Canto, R. Langella, G. Petretto, F. Pilo, G. Pisano, D. Proto, S. Ruggeri, S. Scalari, and R. Turri. Active management of distribution networks with the atlantide models. In *Power Generation, Transmission, Distribution and Energy Conversion (MEDPOWER 2012), 8th Mediterranean Conference on*, pages 1–7, Oct 2012.

[66] Digsilent. PowerFactory information. `http://www.digsilent.de/index.php/products-powerfactory.html`. Accessed: 26-Dec-2015.

[67] M. Tsili and S. Papathanassiou. A review of grid code technical requirements for wind farms. *IET Renewable Power Generation*, 3(3):308–332, Sept 2009.

[68] System earthing and fault levels. `http://www.enwl.co.uk/about-us/long-term-development-statement/policies-and-technical-references/system-earthing-and-fault-levels`. Accessed: 14-Apr-2016.

[69] M. Reza, P. H. Schavemaker, J. G. Slootweg, W. L. Kling, and L. van der Sluis. Impacts of distributed generation penetration levels on power systems transient stability. In *Power Engineering Society General Meeting, 2004. IEEE*, pages 2150–2155 Vol.2, June 2004.

[70] S. M. Zali. *Equivalent dynamic model of distribution network with distributed generation*. Ph.D., University of Manchester, 2012.

[71] Wikipedia. Markov decision process. `https://en.wikipedia.org/wiki/Markov_decision_process`. Accessed: 14-Apr-2016.

[72] R. S. Sutton and A. G. Sutton. Reinforcement learning: An introduction, 2015.

[73] L. Busoniu, D. Ernst, B. De Schutter, and R. Babuska. Approximate reinforcement learning: An overview. In *2011 IEEE Symposium on Adaptive Dynamic Programming and Reinforcement Learning (ADPRL)*, pages 1–8, April 2011.

[74] C. J. Watkins and P. Dayan. Technical note: Q-learning. *Machine Learning*, 8(3):279–292, 1992.

[75] D. L. Poole and A. K. Mackworth. *Artificial intelligence: foundations of computational agents*. Cambridge University Press, New York, NY, USA, 2010.

[76] F. S. Melo, S. P. Meyn, and M. I. Ribeiro. An analysis of reinforcement learning with function approximation. In *Proceedings of the 25th international conference on Machine learning*, pages 664–671. ACM, 2008.

[77] J. Baxter and P. L. Bartlett. Infinite-horizon policy-gradient estimation. *J. Artif. Int. Res.*, 15(1):319–350, November 2001.

[78] J. V. Tu. Advantages and disadvantages of using artificial neural networks versus logistic regression for predicting medical outcomes. *Journal of Clinical Epidemiology*, 49(11):1225–1231, 1996.

[79] L. Breiman. Random forests. *Machine Learning*, 45(1):5–32, Oct 2001.

[80] Decision tree. `https://en.wikipedia.org/wiki/Decision_tree`. Accessed: 14-Apr-2016.

[81] A. Liaw and M. Wiene. Classification and regression by randomForest. *R news*, 2(3):18–22, 2002.

[82] L. Rokach and O. Maimon. Top-down induction of decision trees classifiers - a survey. *IEEE Transactions on Systems, Man, and Cybernetics, Part C (Applications and Reviews)*, 35(4):476–487, Nov 2005.

[83] M. LeBlanc and J. Crowley. Survival trees by goodness of split. *Journal of the American Statistical Association*, 88(422):457–467, 1993.

[84] Manual-setting up, using and understanding random forests v4.0. `https://www.stat.berkeley.edu/~breiman/Using_random_forests_v4.0.pdf`. Accessed: 14-Apr-2016.

[85] R. Genuer, J. M. Poggi, and C. T. Malot. Variable selection using random forests. *Pattern Recognition Letters*, 31(14):2225–2236, 2010.

[86] U. Gromping. Variable importance assessment in regression: Linear regression versus random forest. *The American Statistician*, 63(4):308–319, 2009.

[87] P. Geurts. Regression tree package. `http://www.montefiore.ulg.ac.be/~geurts/Software.html`. Accessed: 25-Apr-2016.

[88] J. Machowski, J. Bialek, and J. R. Bumby. *Power system dynamics and stability*. John Wiley & Sons, Oct 1997.

[89] S. K. Salman and A. L. J. Teo. Investigation into the estimation of the critical clearing time of a grid connected wind power based embedded generator. In *Transmission and Distribution Conference and Exhibition 2002: Asia Pacific. IEEE/PES*, volume 2, pages 975–980, Oct 2002.

[90] Y. Zhang, A. M. Gole, W. Wu, B. Zhang, and H. Sun. Development and analysis of applicability of a hybrid transient simulation platform combining TSA and EMT elements. *IEEE Transactions on Power Systems*, 28(1):357–366, Feb 2013.

[91] D. N. Hussein, M. Matar, and R. Iravani. A type-4 wind power plant equivalent model for the analysis of electromagnetic transients in power systems. *IEEE Transactions on Power Systems*, 28(3):3096–3104, Aug 2013.

E.ON ERC Band 1
Streblow, R.
Thermal Sensation and Comfort Model for Inhomogeneous Indoor Environments
1. Auflage 2011
ISBN 978-3-942789-00-4

E.ON ERC Band 2
Naderi, A.
Multi-phase, multi-species reactive transport modeling as a tool for system analysis in geological carbon dioxide storage
1. Auflage 2011
ISBN 978-3-942789-01-1

E.ON ERC Band 3
Westner, G.
Four Essays related to Energy Economic Aspects of Combined Heat and Power Generation
1. Auflage 2012
ISBN 978-3-942789-02-8

E.ON ERC Band 4
Lohwasser, R.
Impact of Carbon Capture and Storage (CCS) on the European Electricity Market
1. Auflage 2012
ISBN 978-3-942789-03-5

E.ON ERC Band 5
Dick, C.
Multi-Resonant Converters as Photovoltaic Module-Integrated Maximum Power Point Tracker
1. Auflage 2012
ISBN 978-3-942789-04-2

E.ON ERC Band 6
Lenke, R.
A Contribution to the Design of Isolated DC-DC Converters for Utility Applications
1. Auflage 2012
ISBN 978-3-942789-05-9

E.ON ERC Band 7
Brännström, F.
Einsatz hybrider RANS-LES-Turbulenzmodelle in der Fahrzeugklimatisierung
1. Auflage 2012
ISBN 978-3-942789-06-6

E.ON ERC Band 8
Bragard, M.
The Integrated Emitter Turn-Off Thyristor - An Innovative MOS-Gated High-Power Device
1. Auflage 2012
ISBN 978-3-942789-07-3

E.ON ERC Band 9
Hoh, A.
Exergiebasierte Bewertung gebäudetechnischer Anlagen
1. Auflage 2013
ISBN 978-3-942789-08-0

E.ON ERC Band 10
Köllensperger, P.
The Internally Commutated Thyristor - Concept, Design and Application
1. Auflage 2013
ISBN 978-3-942789-09-7

E.ON ERC Band 11
Achtnicht, M.
Essays on Consumer Choices Relevant to Climate Change: Stated Preference Evidence from Germany
1. Auflage 2013
ISBN 978-3-942789-10-3

E.ON ERC Band 12
Panašková, J.
Olfaktorische Bewertung von Emissionen aus Bauprodukten
1. Auflage 2013
ISBN 978-3-942789-11-0

E.ON ERC Band 13
Vogt, C.
Optimization of Geothermal Energy Reservoir Modeling using Advanced Numerical Tools for Stochastic Parameter Estimation and Quantifying Uncertainties
1. Auflage 2013
ISBN 978-3-942789-12-7

E.ON ERC Band 14
Benigni, A.
Latency exploitation for parallelization of power systems simulation
1. Auflage 2013
ISBN 978-3-942789-13-4

E.ON ERC Band 15
Butschen, T.
Dual-ICT – A Clever Way to Unite Conduction and Switching Optimized Properties in a Single Wafer
1. Auflage 2013
ISBN 978-3-942789-14-1

E.ON ERC Band 16
Li, W.
Fault Detection and Protection inMedium Voltage DC Shipboard Power Systems
1. Auflage 2013
ISBN 978-3-942789-15-8

E.ON ERC Band 17
Shen, J.
Modeling Methodologies for Analysis and Synthesis of Controls and Modulation Schemes for High-Power Converters with Low Pulse Ratios
1. Auflage 2014
ISBN 978-3-942789-16-5

E.ON ERC Band 18
Flieger, B.
Innenraummodellierung einer Fahrzeugkabine
in der Programmiersprache Modelica
1. Auflage 2014
ISBN 978-3-942789-17-2

E.ON ERC Band 19
Liu, J.
Measurement System and Technique for Future Active Distribution Grids
1. Auflage 2014
ISBN 978-3-942789-18-9

E.ON ERC Band 20
Kandzia, C.
Experimentelle Untersuchung der Strömungsstrukturen in einer Mischlüftung
1. Auflage 2014
ISBN 978-3-942789-19-6

E.ON ERC Band 21
Thomas, S.
A Medium-Voltage Multi-Level DC/DC Converter with High Voltage Transformation Ratio
1. Auflage 2014
ISBN 978-3-942789-20-2

E.ON ERC Band 22
Tang, J.
Probabilistic Analysis and Stability Assessment for Power Systems with Integration of Wind Generation and Synchrophasor Measurement
1. Auflage 2014
ISBN 978-3-942789-21-9

E.ON ERC Band 23
Sorda, G.
The Diffusion of Selected Renewable Energy Technologies: Modeling, Economic Impacts, and Policy Implications
1. Auflage 2014
ISBN 978-3-942789-22-6

E.ON ERC Band 24
Rosen, C.
Design considerations and functional analysis of local reserve energy markets for distributed generation
1. Auflage 2014
ISBN 978-3-942789-23-3

E.ON ERC Band 25
Ni, F.
Applications of Arbitrary Polynomial Chaos in Electrical Systems
1. Auflage 2015
ISBN 978-3-942789-24-0

E.ON ERC Band 26
Michelsen, C. C.
The *Energiewende* in the German Residential Sector: Empirical Essays on Homeowners' Choices of Space Heating Technologies
1. Auflage 2015
ISBN 978-3-942789-25-7

E.ON ERC Band 27
Rolfs, W.
Decision-Making under Multi-Dimensional Price Uncertainty for Long-Lived Energy Investments
1. Auflage 2015
ISBN 978-3-942789-26-4

E.ON ERC Band 28
Wang, J.
Design of Novel Control algorithms of Power Converters for Distributed Generation
1. Auflage 2015
ISBN 978-3-942789-27-1

E.ON ERC Band 29
Helmedag, A.
System-Level Multi-Physics Power Hardware in the Loop Testing for Wind Energy Converters
1. Auflage 2015
ISBN 978-3-942789-28-8

E.ON ERC Band 30
Togawa, K.
Stochastics-based Methods Enabling Testing of Grid-related Algorithms through Simulation
1. Auflage 2015
ISBN 978-3-942789-29-5

E.ON ERC Band 31
Huchtemann, K.
Supply Temperature Control Concepts in Heat Pump Heating Systems
1. Auflage 2015
ISBN 978-3-942789-30-1

E.ON ERC Band 32
Molitor, C.
Residential City Districts as Flexibility Resource: Analysis, Simulation, and Decentralized Coordination Algorithms
1. Auflage 2015
ISBN 978-3-942789-31-8

E.ON ERC Band 33
Sunak, Y.
Spatial Perspectives on the Economics of Renewable Energy Technologies
1. Auflage 2015
ISBN 978-3-942789-32-5

E.ON ERC Band 34
Cupelli, M.
Advanced Control Methods for Robust Stability of MVDC Systems
1. Auflage 2015
ISBN 978-3-942789-33-2

E.ON ERC Band 35
Chen, K.
Active Thermal Management for Residential Air Source Heat Pump Systems
1. Auflage 2015
ISBN 978-3-942789-34-9

E.ON ERC Band 36
Pâques, G.
Development of SiC GTO Thyristors with Etched Junction Termination
1. Auflage 2016
ISBN 978-3-942789-35-6

E.ON ERC Band 37
Garnier, E.
Distributed Energy Resources and Virtual Power Plants: Economics of Investment and Operation
1. Auflage 2016
ISBN 978-3-942789-37-0

E.ON ERC Band 38
Calì, D.
Occupants' Behavior and its Impact upon the Energy Performance of Buildings
1. Auflage 2016
ISBN 978-3-942789-36-3

E.ON ERC Band 39
Isermann, T.
A Multi-Agent-based Component Control and Energy Management System for Electric Vehicles
1. Auflage 2016
ISBN 978-3-942789-38-7